

MR3522: Remote Sensing of the Atmosphere and Ocean

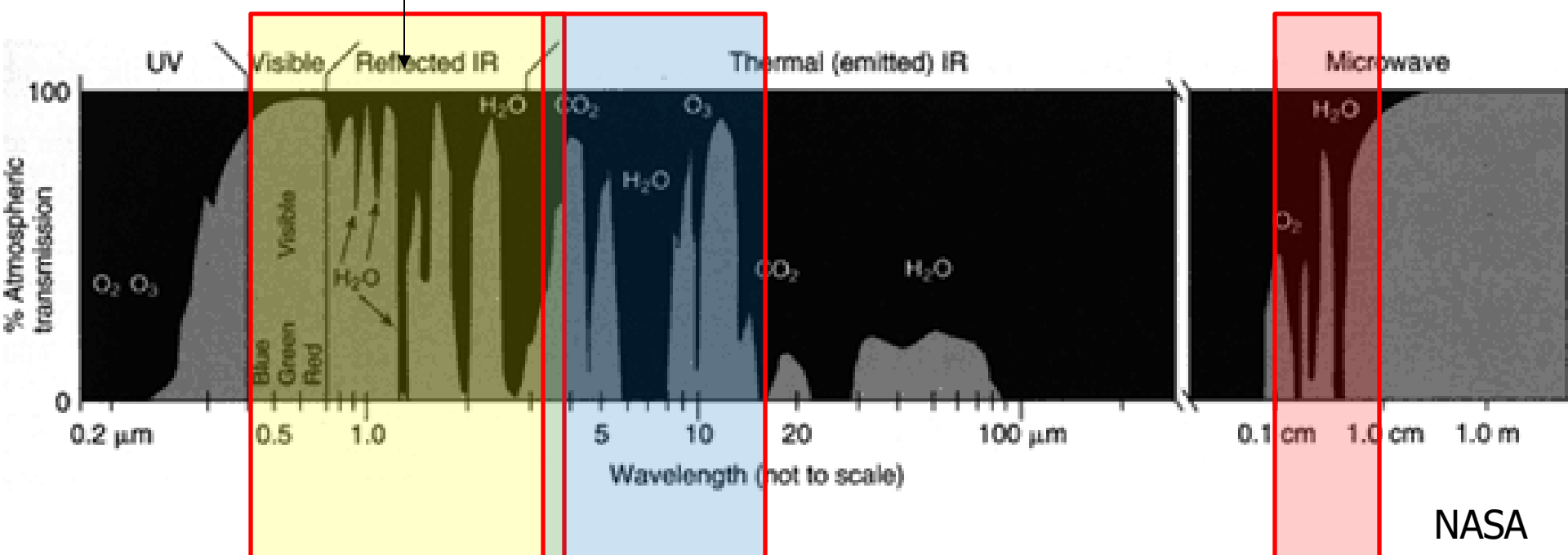
Introduction to Microwave Radiative Transfer

Main Topics

- Frequency vs wavelength
- Simplifying Planck's Law
- Ocean emissivity
- Absorption and scattering of microwaves

Atmospheric Absorption Spectra

Solar radiation a.k.a
shortwave radiation
(reflection)



Infrared radiation
a.k.a longwave
radiation (emission)

Microwaves
(reflection and
emission)

IR vs. Microwave (MW) Remote Sensing

- Microwave radiation can penetrate clouds, air molecules, aerosols, rain, vegetation, and limited layers of liquid water (like the sea surface), and soil (especially dry soil). IR is scattered/absorbed by hydrometeors.
- However, emittance at MW is much less than at IR (think of the Planck curve at 300 K), so a larger aperture sensor is required to achieve the same spatial resolution at MW as in IR. Therefore, MW must be in LEO to achieve acceptable spatial resolution. (Although GEO MW sensors may be on the way soon!)
- Consequently, temporal resolution at MW for a single instrument is 1–2 days. Passive IR sensors in geostationary can provide up to 30 second temporal resolution.

In the microwave part of the EM spectrum...

we typically work with frequency (ν)
rather than wavelength as the spectral variable

the frequencies are small enough (or wavelengths long enough)
so that the Planck function can be simplified into a linear function:

$$B_\lambda(T) = \frac{2\hbar c^2 \lambda^{-5}}{e^{\frac{\hbar c}{\lambda kT}} - 1} \quad \text{if } \hbar c/\lambda kT \ll 1, \text{ then use } e^x \approx 1+x \text{ (for small } x\text{)}$$

true for $\lambda > 0.5 \text{ cm}$ or $\nu < 60 \text{ GHz}$, when $T \sim 300 \text{ K}$

$$\left. \begin{aligned} B(\lambda, T) &\sim (2ck/\lambda^4) T \\ B(\nu, T) &= c/\nu^2 B(\lambda, T) = (2kv^2/c^2) T \end{aligned} \right\} \text{Linear with } T$$

How does this help our interpretation of radiative transfer at MW frequencies?

Our simplest solution: $L = \varepsilon_s B(\nu, T) = (2kv^2/c^2) \varepsilon_s T$

Let's define Brightness Temperature, $T_B = L c^2/2kv^2$

Then, $T_B = \varepsilon_s T$ (temperature of the sfc if a blackbody)

... so in RT solution can substitute T_B for radiance, and T for $B(\nu, T)$ everywhere

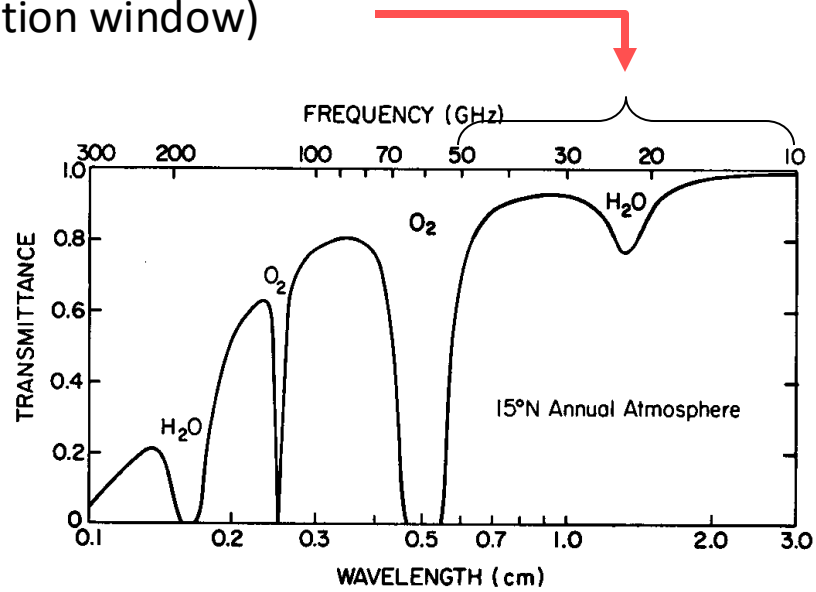
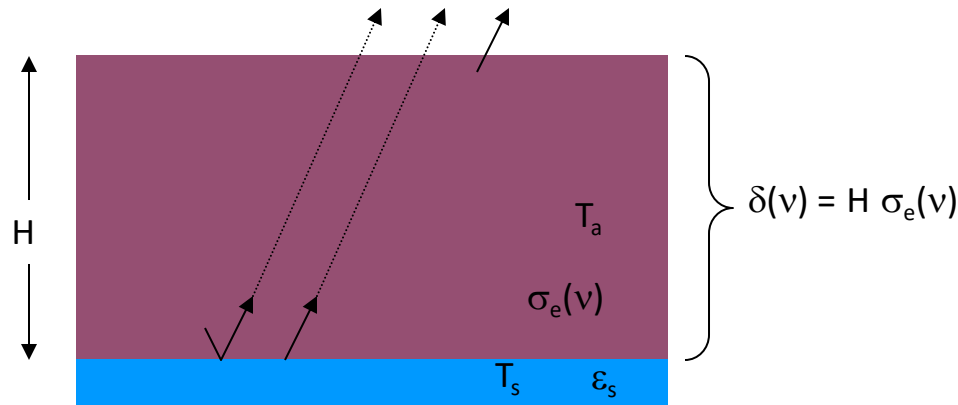
Idealized Case #4

$\nu < 50\text{GHz}$ (relative absorption window)

optically thin **homogeneous** atmosphere

$$\sigma_e(\nu, z) = \sigma_e(\nu) = \sigma_a(\nu) + \sigma_s(\nu)$$

$$T(z) = T_{\text{air}}$$



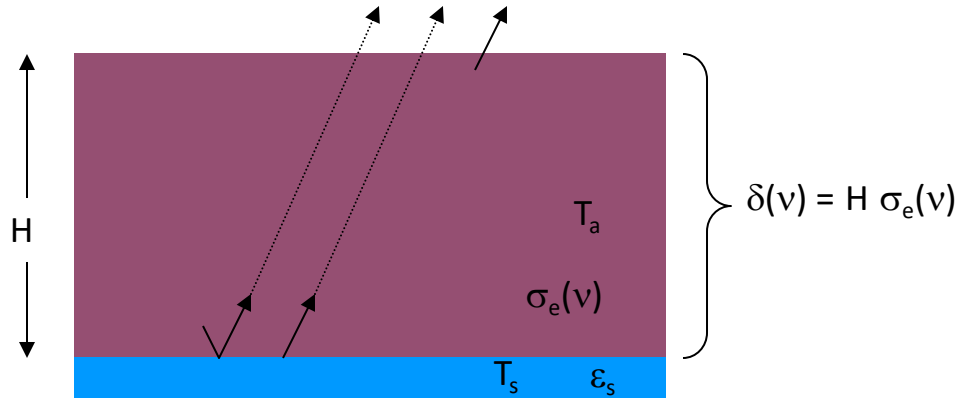
Surface radiance = **emission** + **reflectance**

Sources (path radiance) by **emission** only

$$L_t(v, \theta, \phi) = L_0(v, \theta, \phi)\tau_d(v) + \int_{\tau_0}^t B(v, T(p)) d\tau_d$$

Radiance emitted by the atmosphere out the top (path radiance):

$$\int_{\tau_0}^t B(v, T(p)) d\tau_d = B(v, T_a)[1 - \tau_d(v)]$$



$$1 - \tau_d(v) = \sigma_a(v) \text{ (since there is no atmospheric reflectance)} \\ = \epsilon_a(v)$$

(note this is also the radiance emitted by the atmosphere out the bottom)

The total radiance at the top of the atmosphere then becomes:

$$L_t(v, \theta, \phi) = \epsilon_s(v, \theta, T_s, S)B(v, T_s)\tau_d(v) + \quad \text{Radiance emitted by the surface, transmitted to top}$$

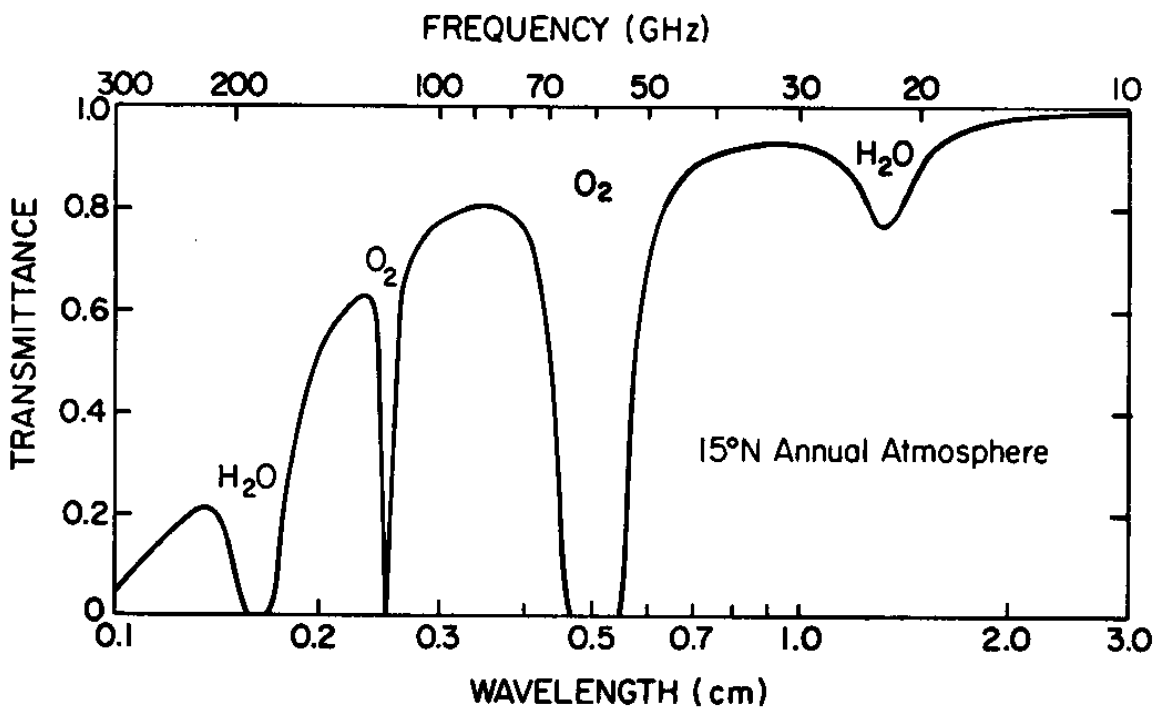
$$[1 - \epsilon_s(v, \theta, T_s, S)]B(v, T_a)[1 - \tau_d(v)]\tau_d(v) + \quad \text{Radiance emitted by the atmosphere out the bottom, reflected off surface, transmitted to top}$$

$$B(v, T_a)[1 - \tau_d(v)] \quad \text{Radiance emitted by the atmosphere out the top}$$

(notice **surface emittance** depends on **temperature** and **salinity, S** - more on this later)

If we multiply by $c^2/2kv^2$...

$$T_B(v, \theta, \phi) = \varepsilon_s(v, \theta, T_s, S) T_s \tau_d(v) + \\ [1 - \varepsilon_s(v, \theta, T_s, S)] T_a [1 - \tau_d(v)] \tau_d(v) + \\ T_a [1 - \tau_d(v)]$$

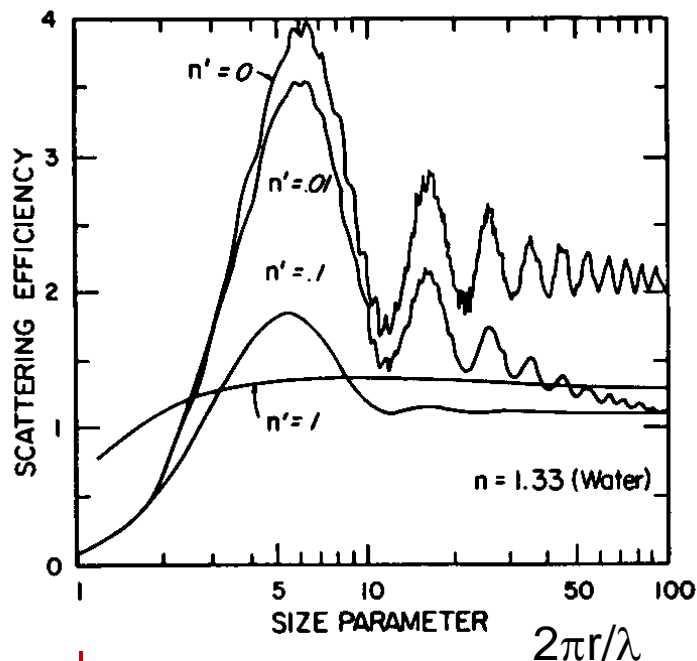


Two gases contribute to the atmospheric Absorption in MW part of spectrum:

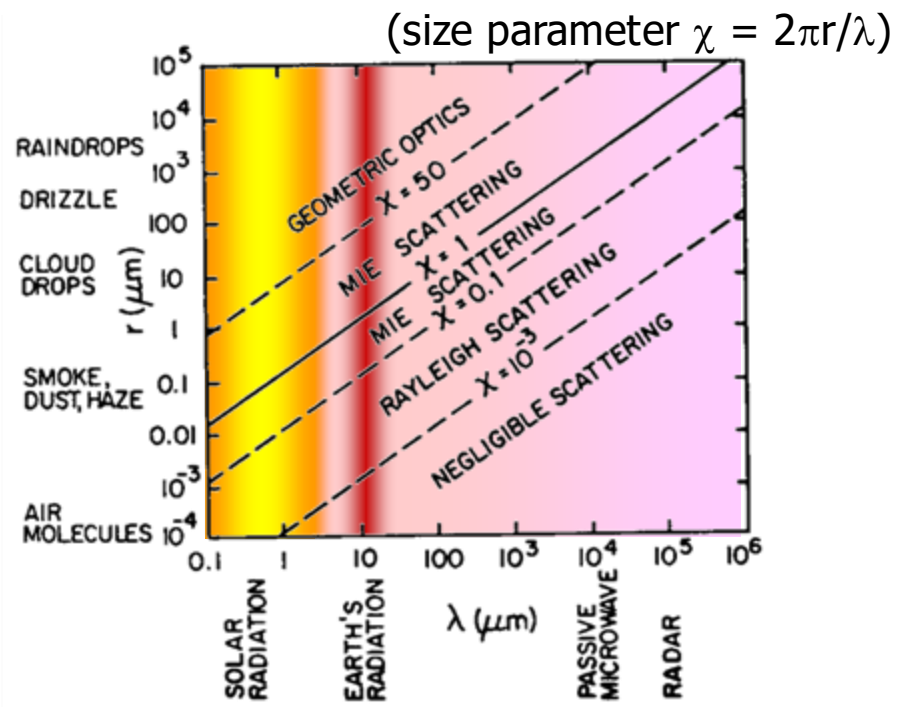
$\text{H}_2\text{O}_{(v)}$ and O_2

$$\sigma_s(\lambda, z) = \int_0^{\infty} \pi r^2 Q_s(\lambda, m, r) n(r) dr \longleftrightarrow \text{See Chapter 3 in text.}$$

$n(r) = 10^3/\text{cm}$ for cloud drops
 $10^{19}/\text{cm}$ for molecules



Drops $r = 0.1 \text{ cm}$ for $\lambda = 0.6 \text{ cm}$
 Air $r = 0.1 \mu\text{m}$ for $\lambda = 0.6 \mu\text{m}$



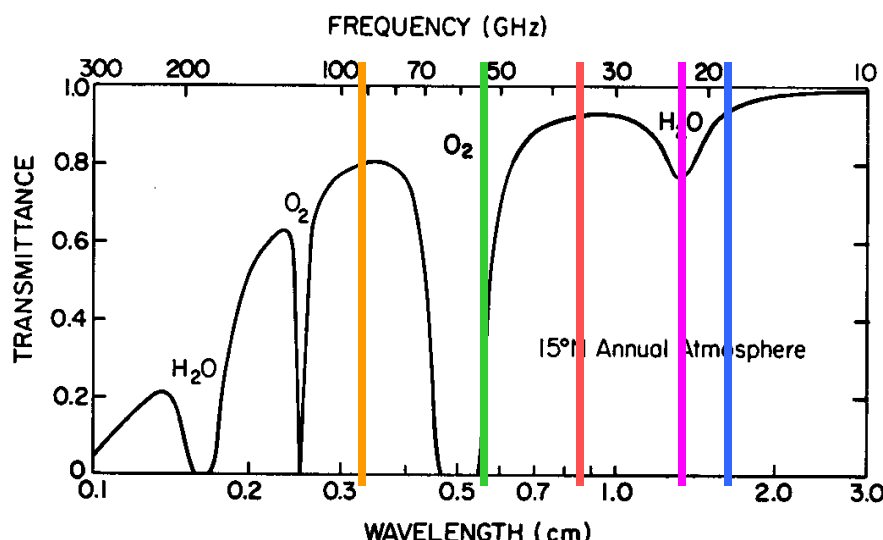
$r = 10 \mu\text{m} = 10^{-3} \text{cm}$ for cloud drops
 $10^{-4} \mu\text{m}$ for molecules

What is the influence of **clouds**?

Interactions with particles in the atmosphere are controlled by their size
therefore molecules and aerosol particles
have negligible interaction with MW photons

Interactions with cloud drops depend on their size. For Mie scattering the critical radius (needed for significant interaction) can be defined as $r_c = \lambda/2\pi$

| | <u>ν (GHz)</u> | <u>λ (cm)</u> | <u>$r_c (= \lambda/2\pi)$ (cm)</u> |
|---------------|-------------------------------|----------------------------------|---|
| SSMI channels | 91 | 0.33 | 0.052 (0.52 mm) |
| | 37 | 0.81 | 0.13 |
| | 22 | 1.36 | 0.22 |
| | 19 | 1.58 | 0.25 |
| Oxygen band | 55 | 0.55 | 0.08 |



(typical cloud droplet is 10µm)
(typical raindrop is 1mm)

Non-precipitating clouds
have weak interactions

Precipitating clouds can have
strong interactions

Precipitation

As cloud droplets grow to precipitation size, optical depth increases.

Does T_B increase or decrease?

$$T_B(v, \theta, \varphi) = \varepsilon_s(v, \theta, T_s, S) T_s \tau_d(v) + \\ [1 - \varepsilon_s(v, \theta, T_s, S)] T_a [1 - \tau_d(v)] \tau_d(v) + \\ T_a [1 - \tau_d(v)]$$

$$T_B = 0.4(280).9 + \\ 0.6(260)0.1(0.9) \\ 260(0.1) \\ = 100.8 + 14 + 26 = \mathbf{140.8\text{K}}$$

$$T_B = 0.4(280)0 + \\ 0.6(260)1(0) \\ 260(1) \\ = \mathbf{260\text{K}}$$

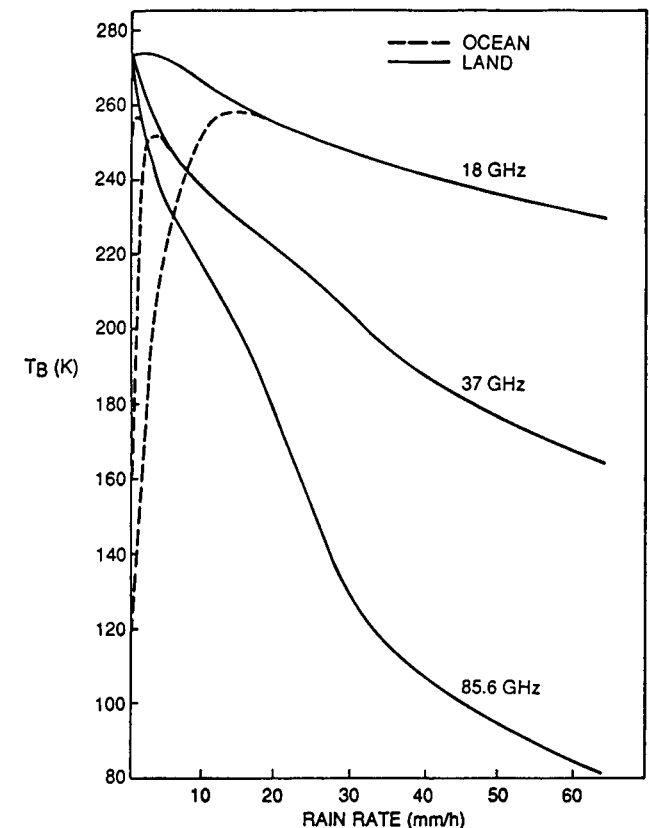
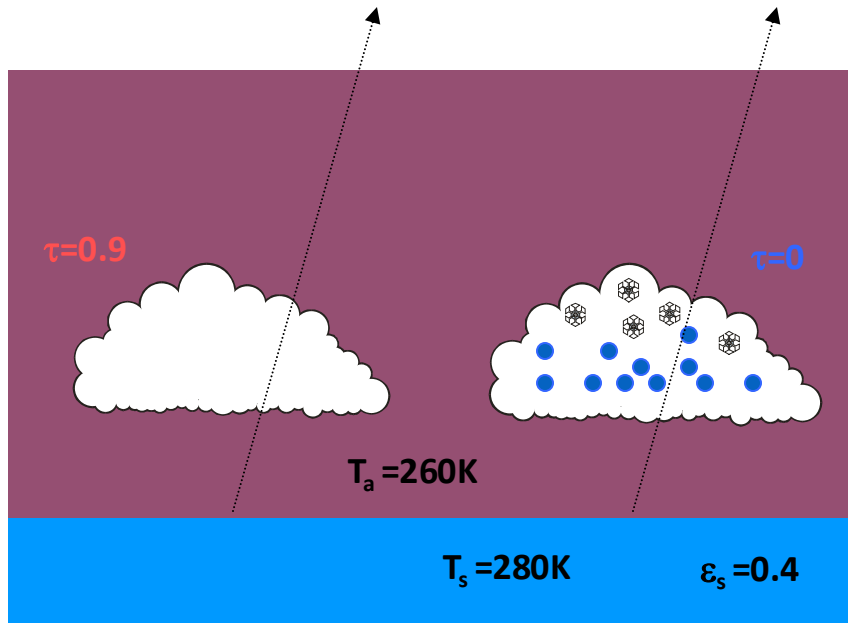
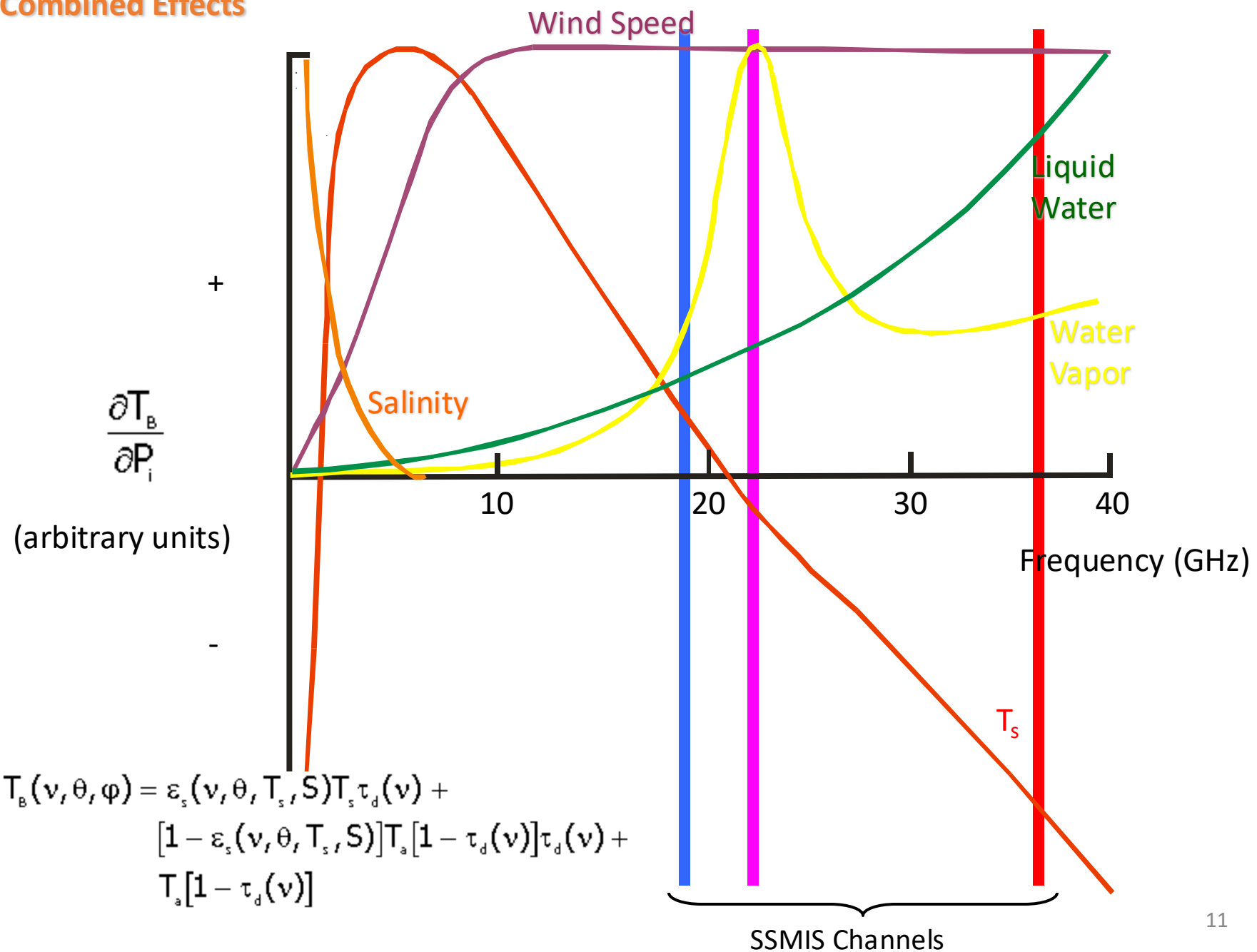


FIGURE 9.16. Brightness temperature versus rain rate for three frequencies. [After Spencer *et al.* (1989).]

Combined Effects



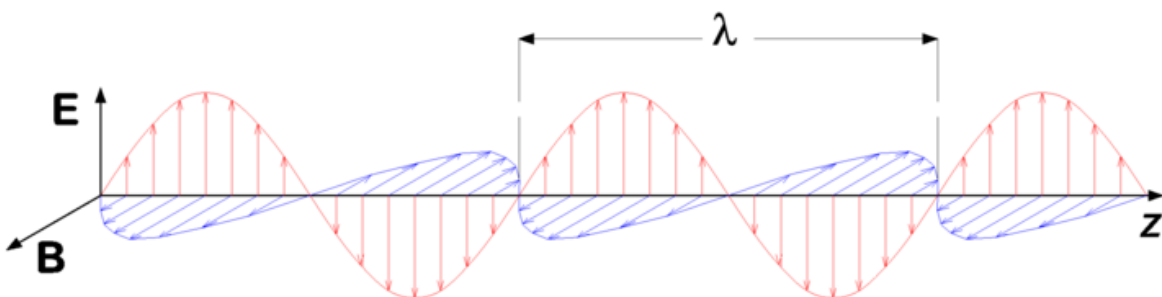
MR3522: Remote Sensing of the Atmosphere and Ocean

Microwave polarization and SSMIS

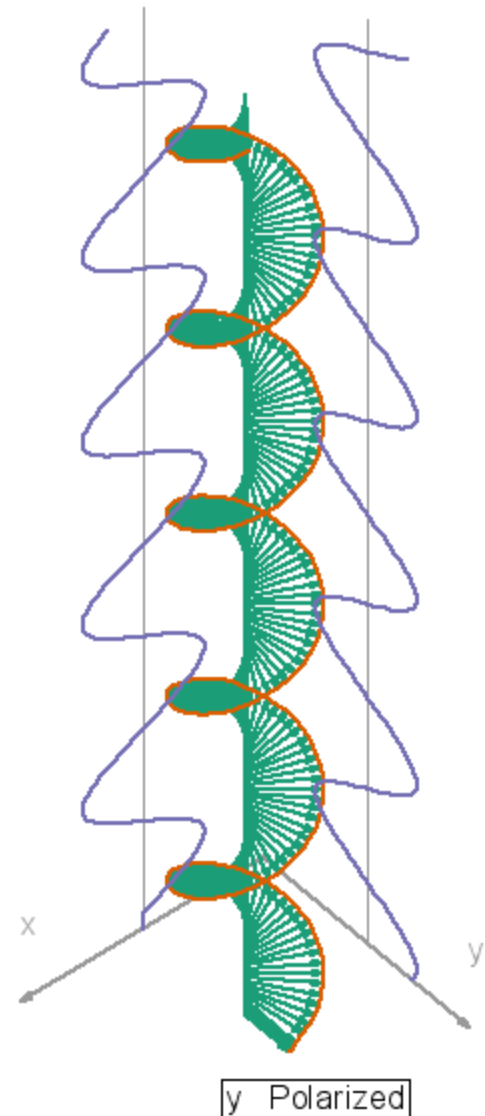
Main Topics

- Polarization of radiation
- Dependence of ocean emissivity on polarization
- SSMIS derived products
- Microwave sounder
- Spatial resolution of microwave data

Polarization of Radiation



- Polarization of radiation appears in two basic components: horizontal and vertical.
- Various linear combinations of these polarizations can lead to elliptical or circular polarizations, or other slanted linear polarizations
- Passive MW and radar take advantage of both horizontal and vertical polarization of radiation.



Emittance of ocean changes based on polarization of radiation.

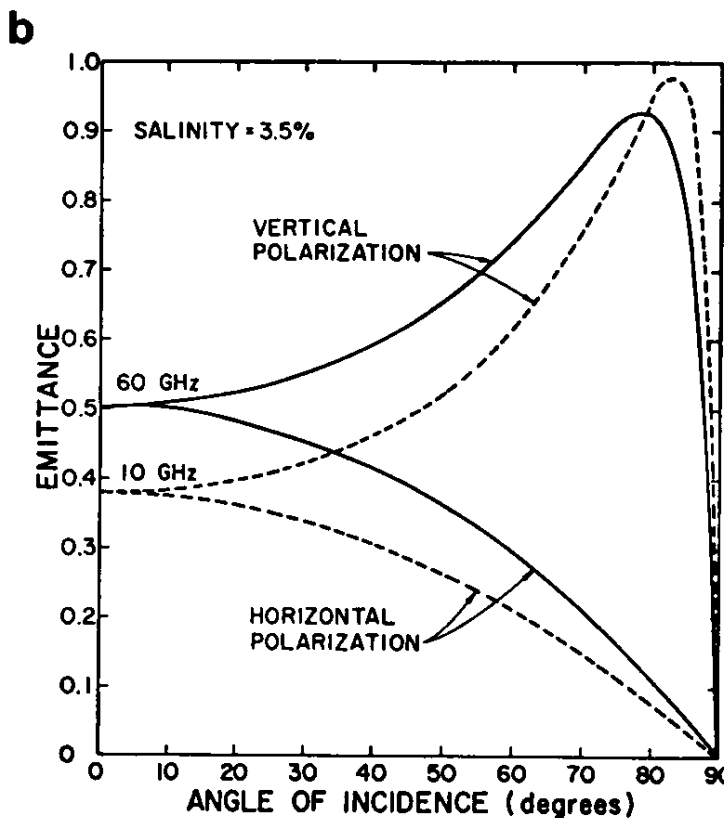
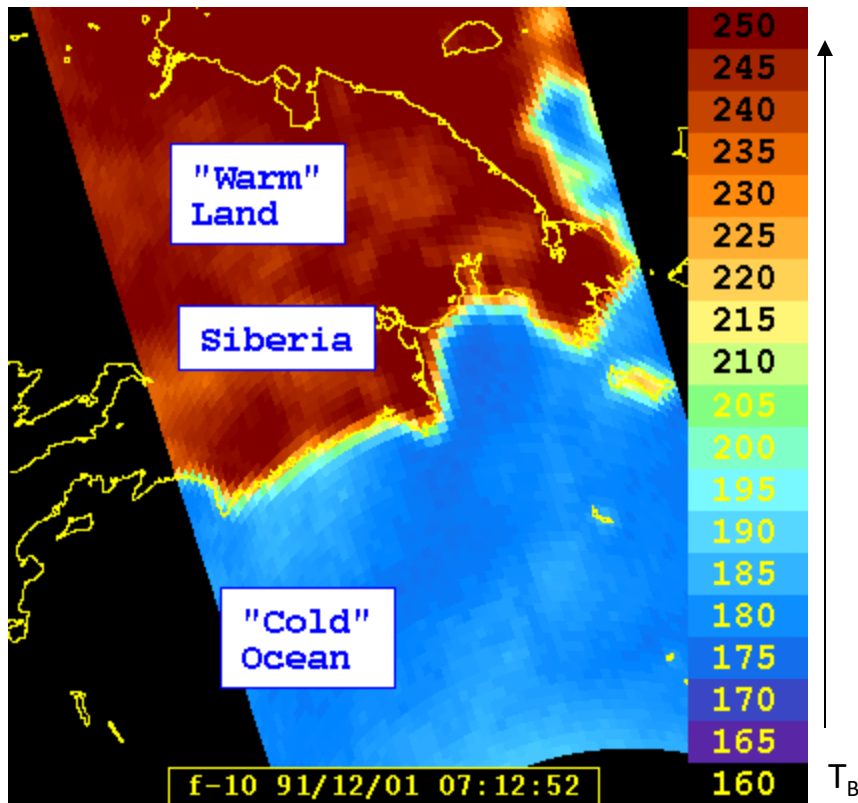
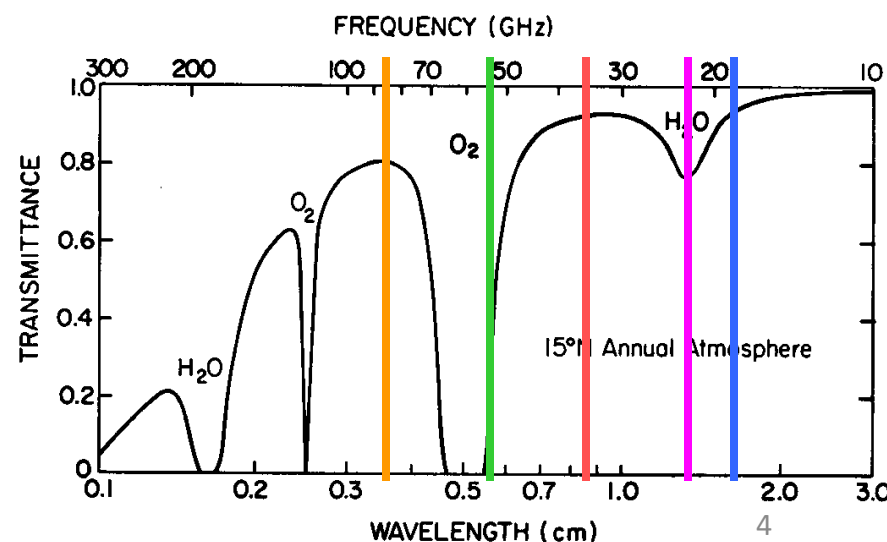


FIGURE 9.17. (a) Nadir emittance of a smooth ocean surface as a function of sea surface temperature.
(b) Emittance of a smooth ocean surface as a function of zenith angle. [After Kidder (1979).]

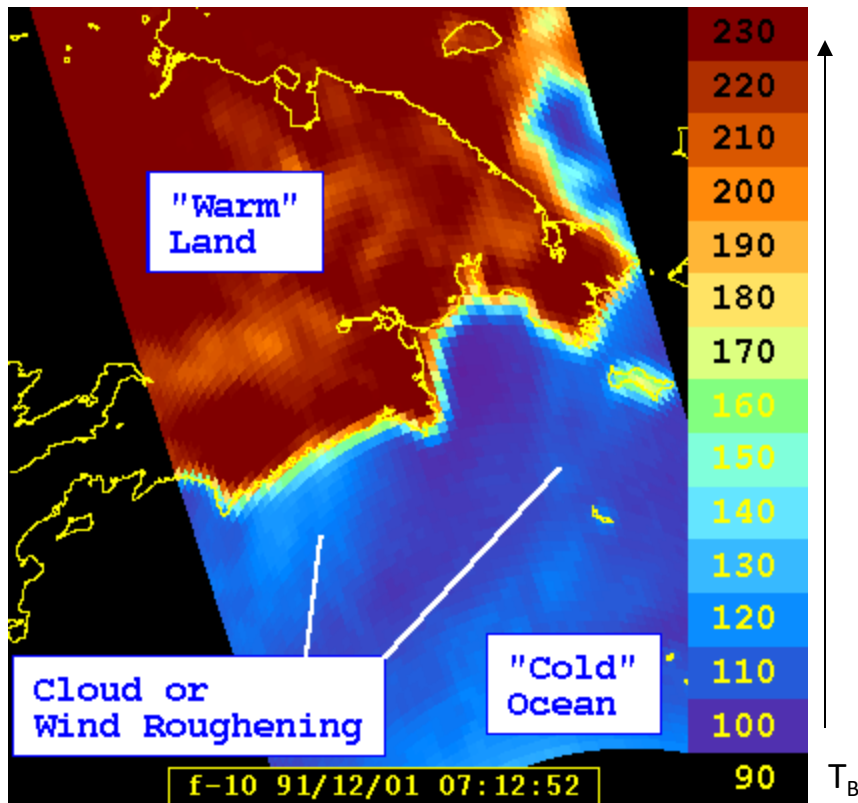
An example of “raw” SSM/I images - one for each channel



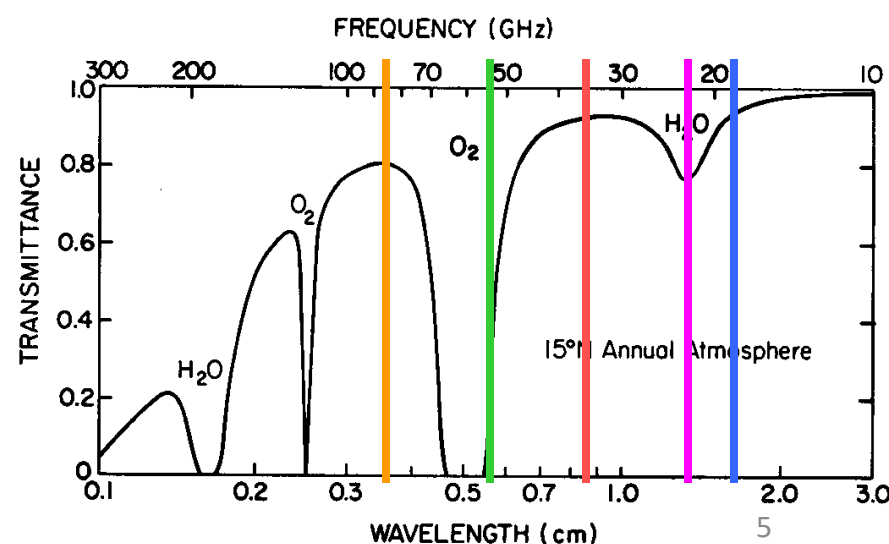
19v



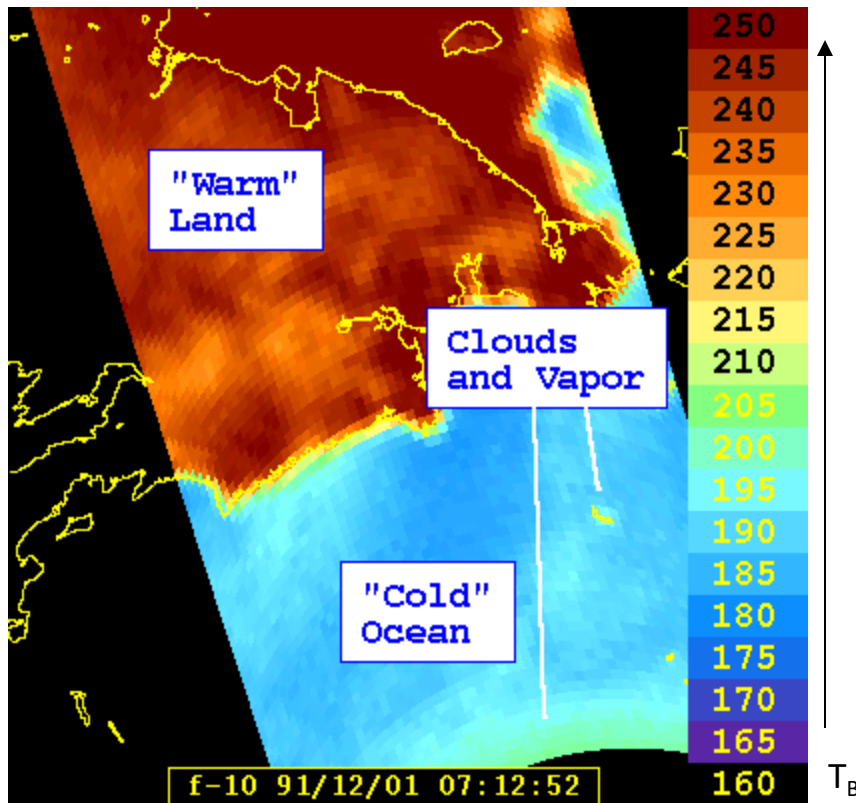
An example of “raw” SSM/I images - one for each channel



19v
19h



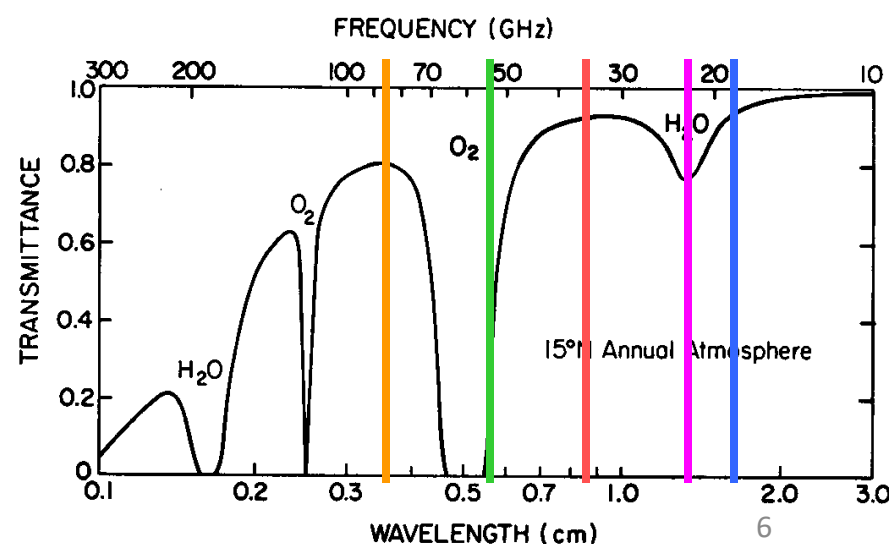
An example of “raw” SSM/I images - one for each channel



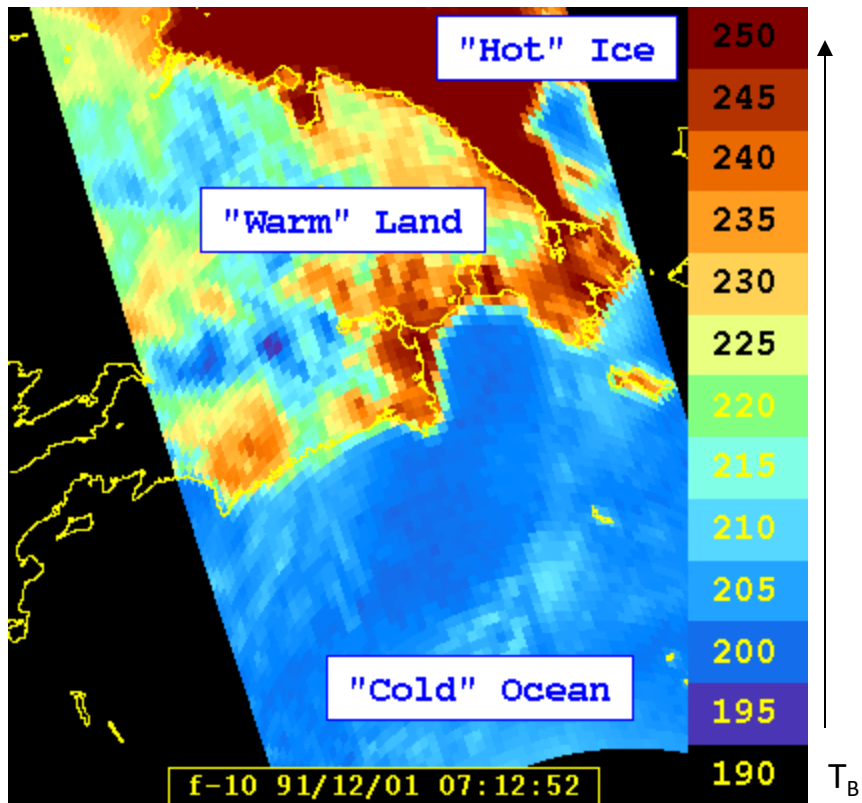
19v

19h

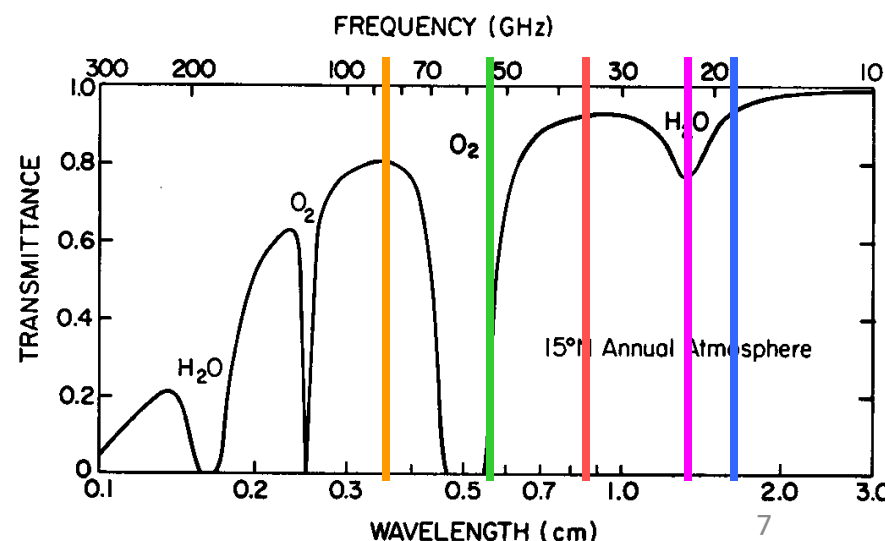
22v



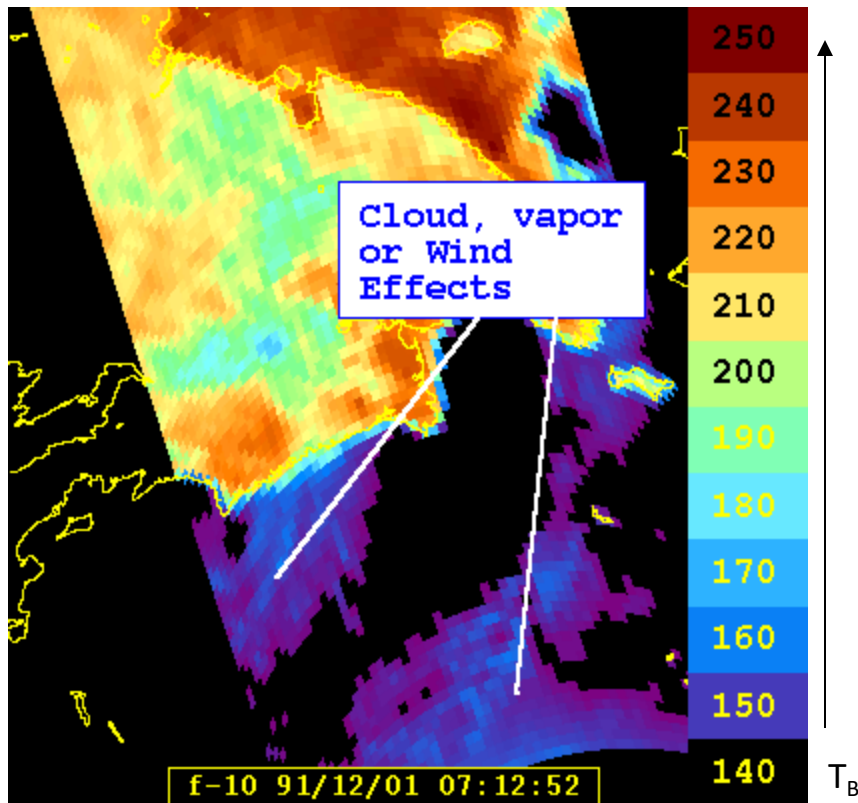
An example of “raw” SSM/I images - one for each channel



19v
19h
22v
37v



An example of “raw” SSM/I images - one for each channel



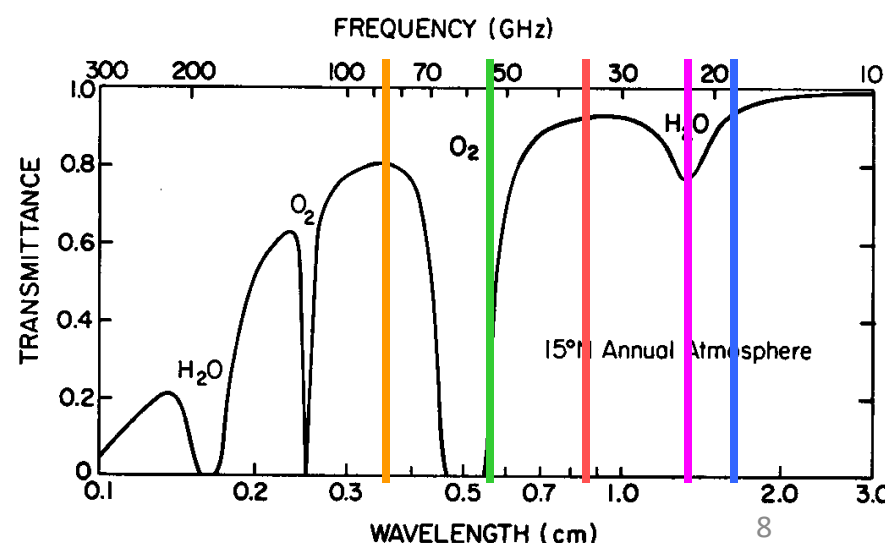
19v

19h

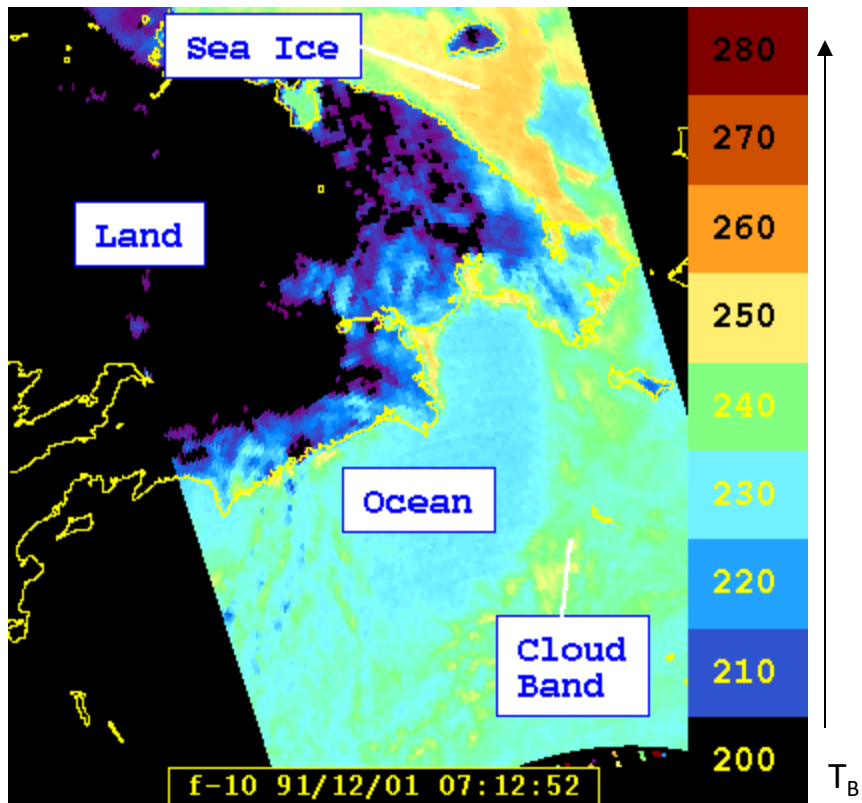
22v

37v

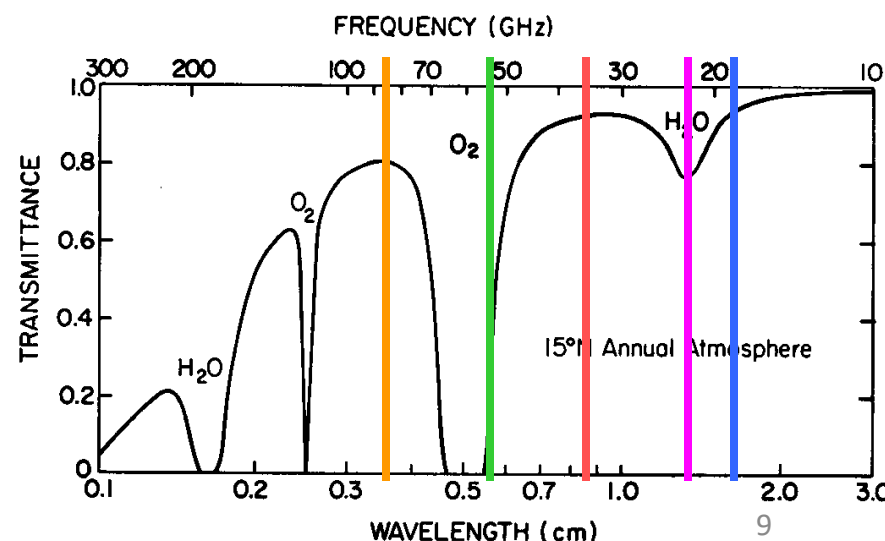
37h



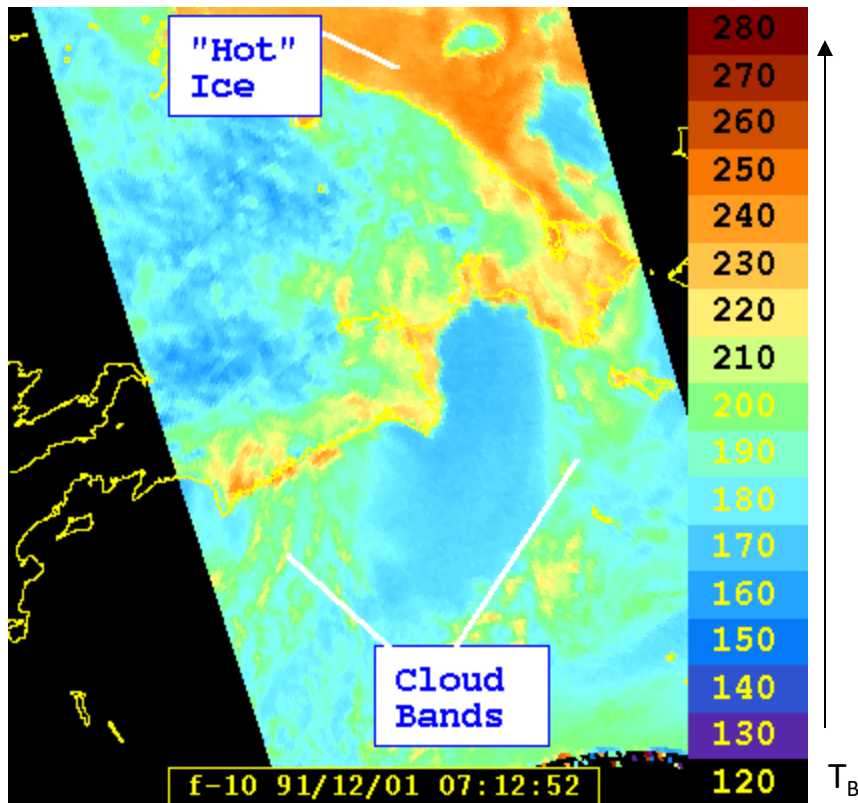
An example of “raw” SSM/I images - one for each channel



19v
19h
22v
37v
37h
85v



An example of “raw” SSM/I images - one for each channel



19v

19h

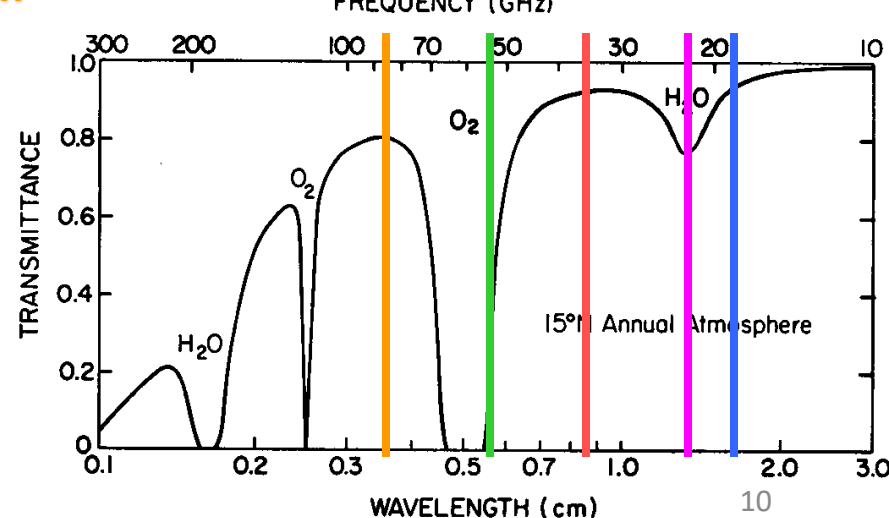
22v

37v

37h

85v

85h



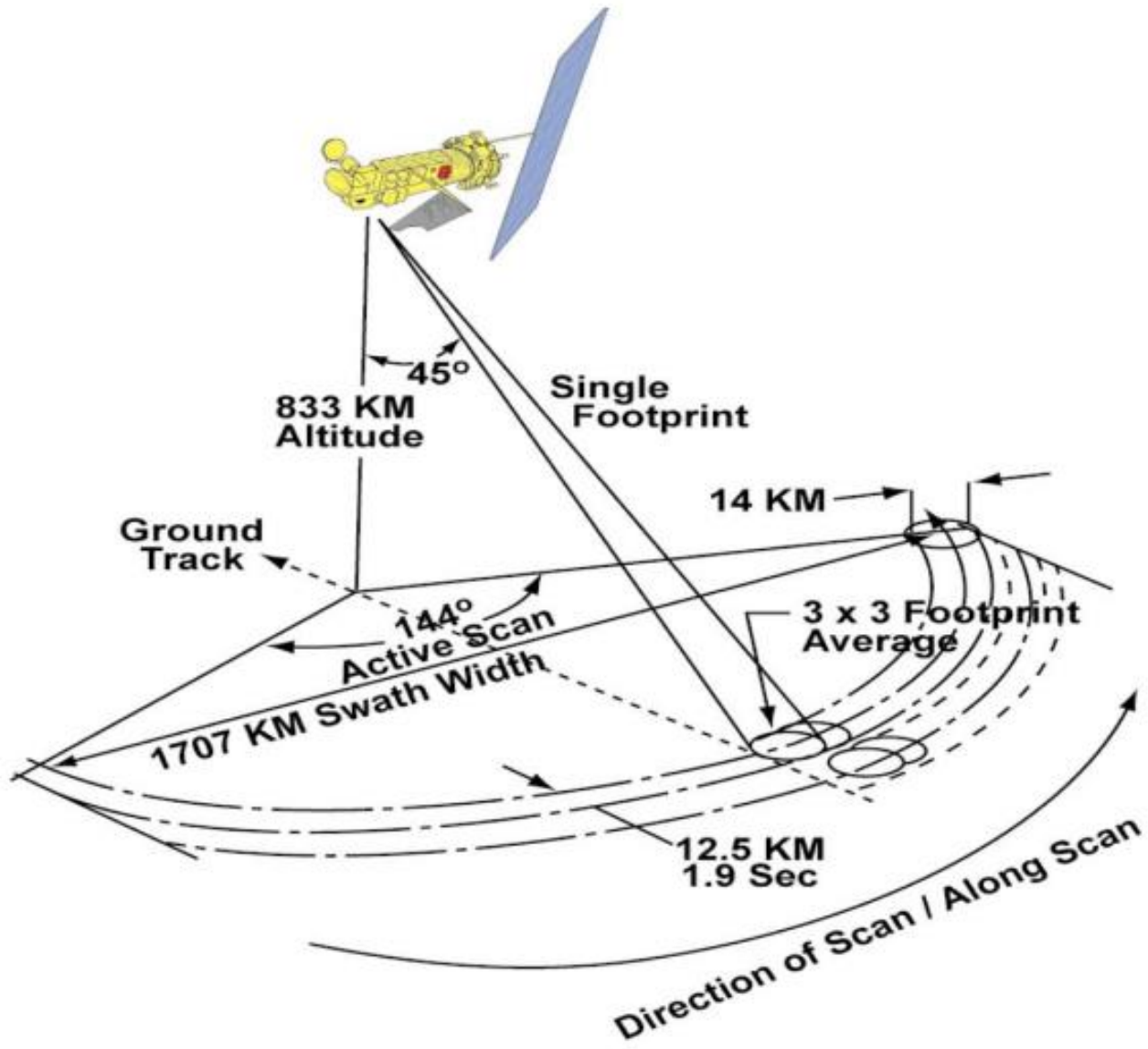
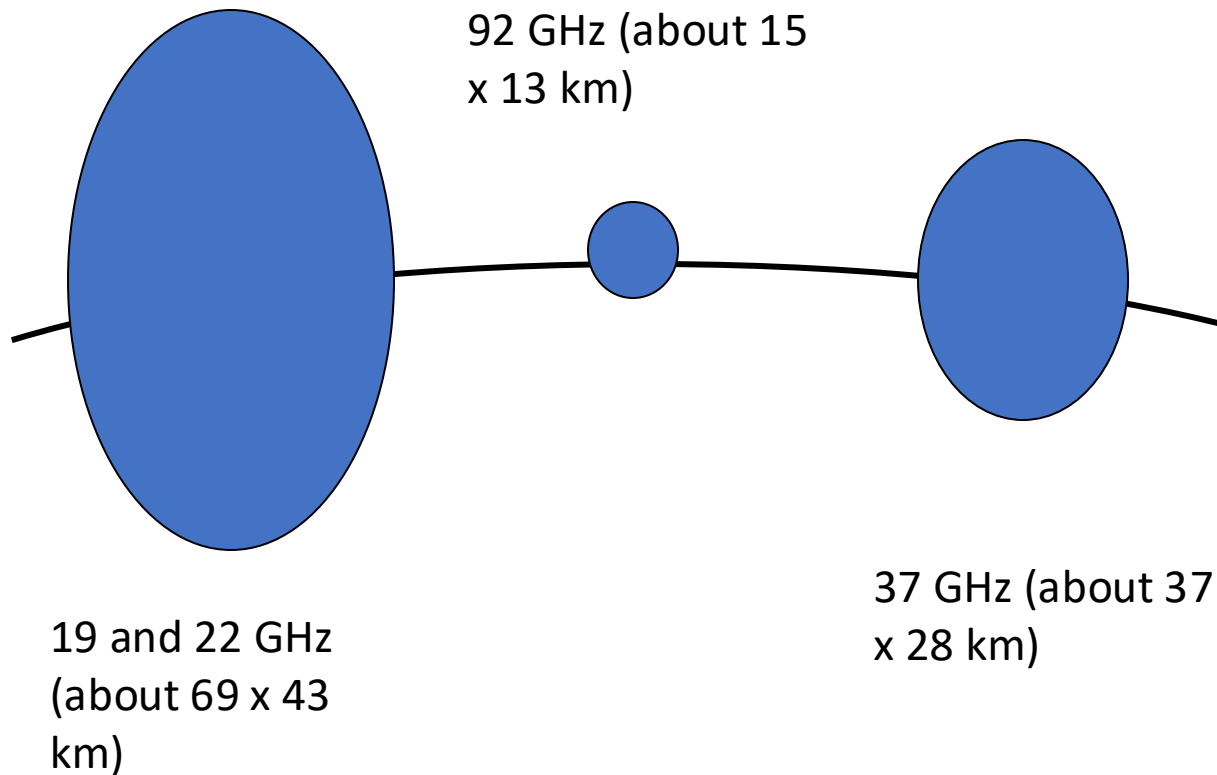


Fig. 2. SSMIS scan geometry showing direction of active scan, swath width, ground track, and footprint averages.

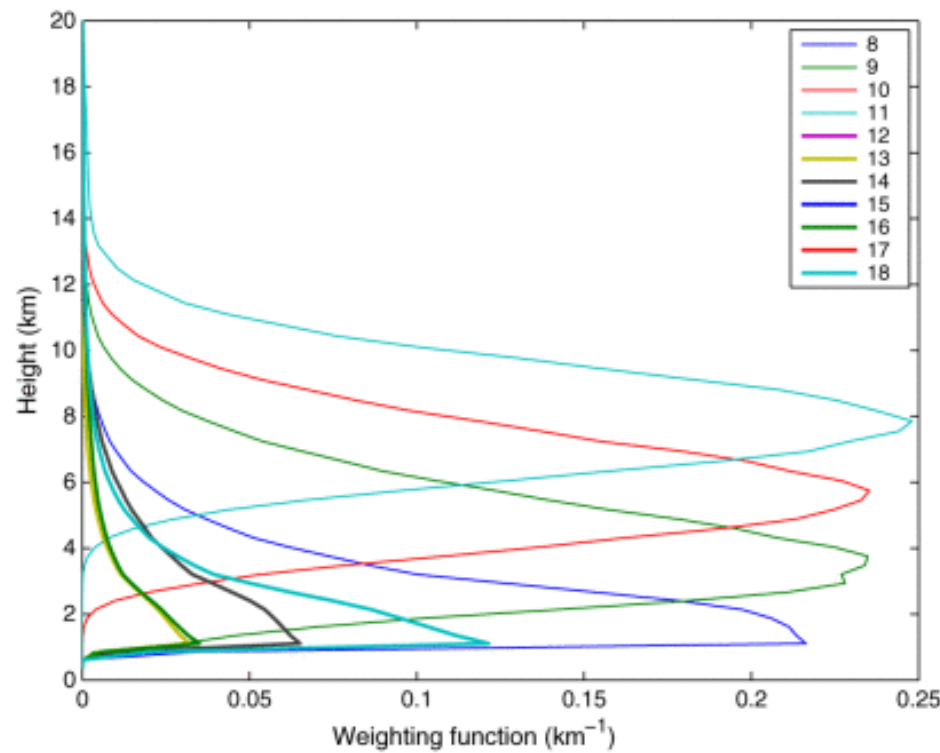
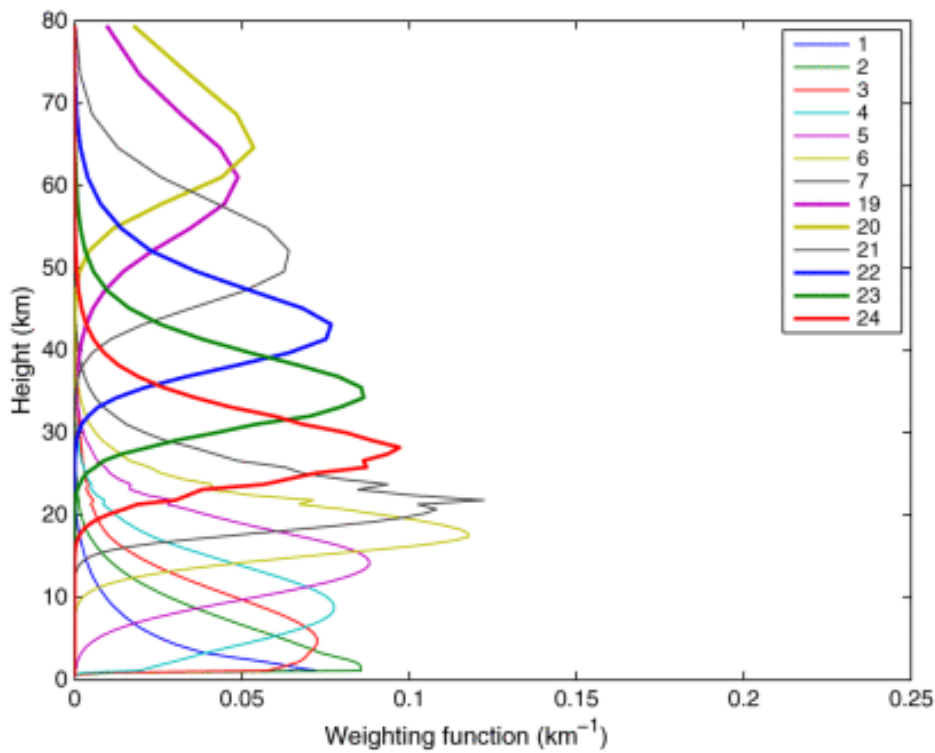
Spatial Resolution



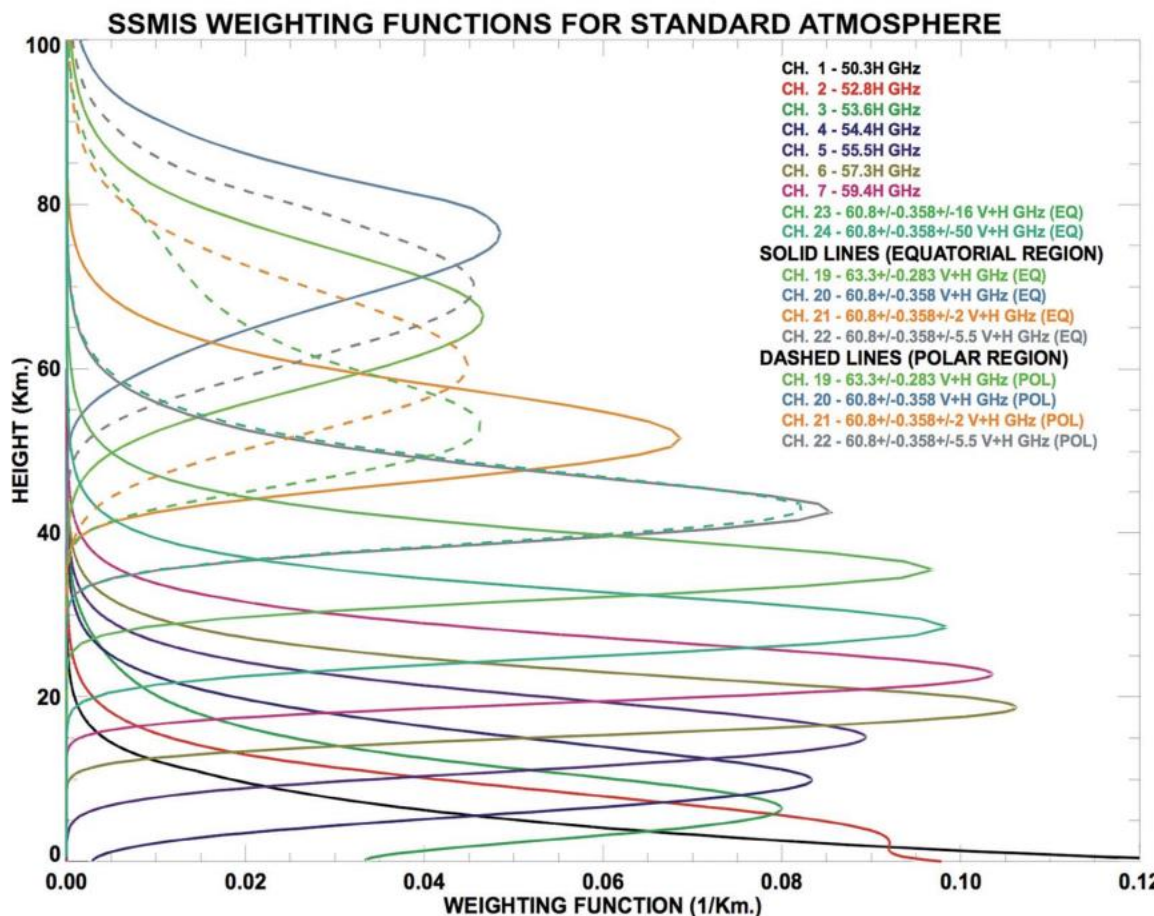
| Channel | Center Freq. (Ghz) | Passband (Mhz) | Freq. (MHz) / <u>Polarization</u> | NEDT(Max)(K) | Sampling Interval (km) | Footprint (km) |
|---------|------------------------------|----------------|--------------------------------------|--------------|---------------------------|------------------|
| 1 | 50.3 | 400 | 10 H | 0.4 | 37.5 | 38 x 38 |
| 2 | 52.8 | 400 | 10 H | 0.4 | 37.5 | 38 x 38 |
| 3 | 53.596 | 400 | 10 H | 0.4 | 37.5 | 38 x 38 |
| 4 | 54.4 | 400 | 10 H | 0.4 | 37.5 | 38 x 38 |
| 5 | 55.5 | 400 | 10 H | 0.4 | 37.5 | 38 x 38 |
| 6 | 57.29 | 350 | 10 RCP(*) | 0.5 | 37.5 | 38 x 38 |
| 7 | 59.4 | 250 | 10 RCP | 0.6 | 37.5 | 38 x 38 |
| 8 | 150 | 1500 | 200 H | 0.88 | 37.5 | 14 x 13 (imager) |
| 9 | 183.31±6.6 | 1500 | 200 H | 1.2 | 37.5 | 14 x 13 (imager) |
| 10 | 183.31±3 | 1000 | 200 H | 1.0 | 37.5 | 14 x 13 (imager) |
| 11 | 183.31±1 | 500 | 200 H | 1.25 | 37.5 | 14 x 13 (imager) |
| 12 | 19.35 | 400 | 75 H | 0.7 | 25 | 73 x 47 |
| 13 | 19.35 | 400 | 75 V | 0.7 | 25 | 73 x 47 |
| 14 | 22.235 | 400 | 75 V | 0.7 | 25 | 73 x 47 |
| 15 | 37 | 1500 | 75 H | 0.5 | 25 | 41 x 31 |
| 16 | 37 | 1500 | 75 V | 0.5 | 25 | 41 x 31 |
| 17 | 91.655 | 3000 | 100 V | 0.9 | 12.5 | 14 x 13 (imager) |
| 18 | 91.655 | 3000 | 100 H | 0.9 | 12.5 | 14 x 13 (imager) |
| 19 | 63.283248±0.2852 71 | 3 | 0.08 RCP | 2.4 | 75 | 75 x 75 |
| 20 | 60.792668±0.3578 92 | 3 | 0.08 RCP | 2.4 | 75 | 75 x 75 |
| 21 | 60.792668±0.3578 92±0.002 | 6 | 0.08 RCP | 1.8 | 75 | 75 x 75 |
| 22 | 60.792668±0.3578 92±0.006 | 12 | 0.12 RCP | 1.0 | 75 | 75 x 75 |
| 23 | 60.792668±0.3578 92±0.016 | 32 | 0.34 RCP | 0.6 | 75 | 75 x 75 |
| 24 | 60.792668±0.3578 92±0.050 | 120 | 0.84 RCP | 0.7 | 37.5 | 75 x 75 |

SSMI/S Weighting Functions

Islam et al. (2014; IEEE)

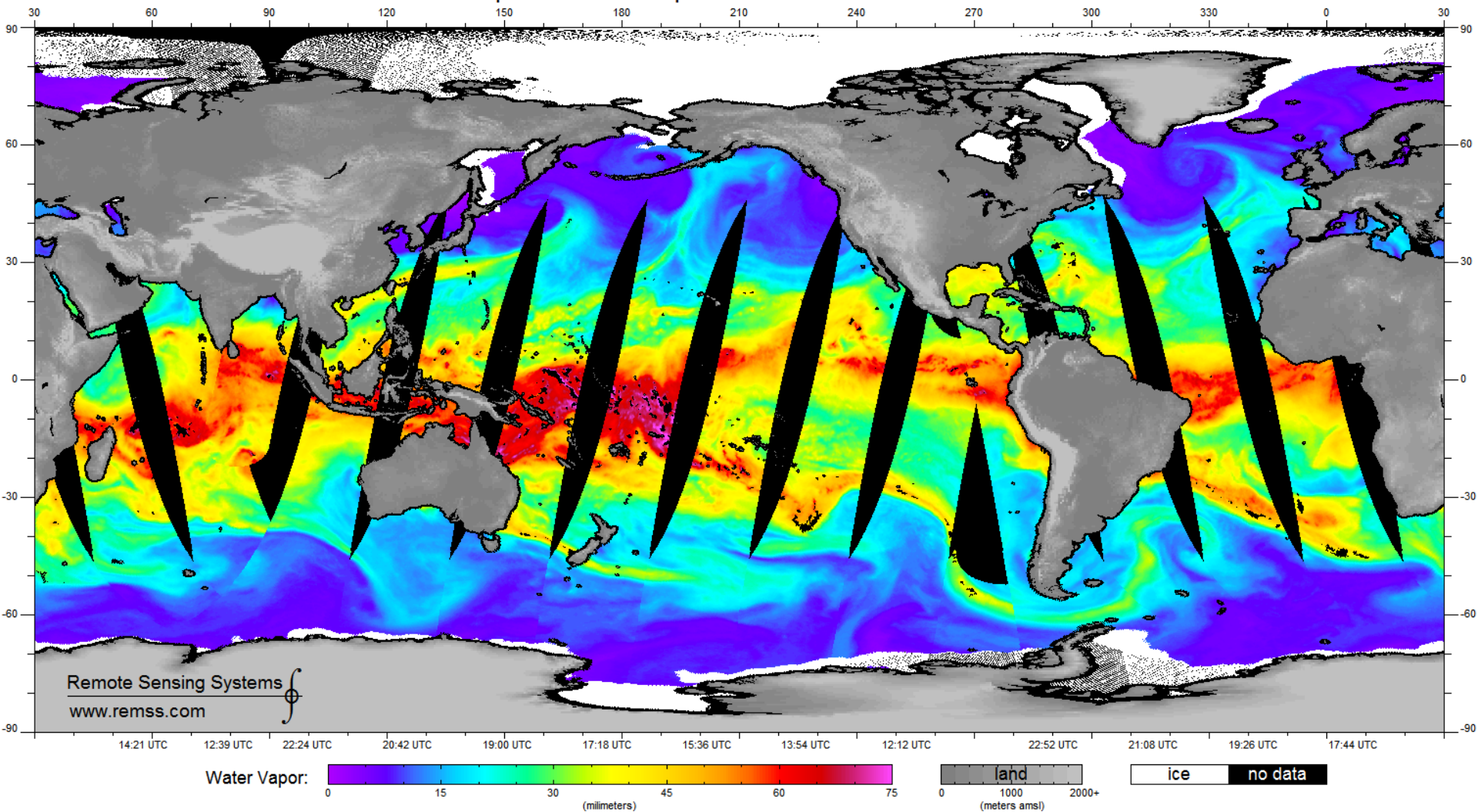


SSMI/S Weighting Functions

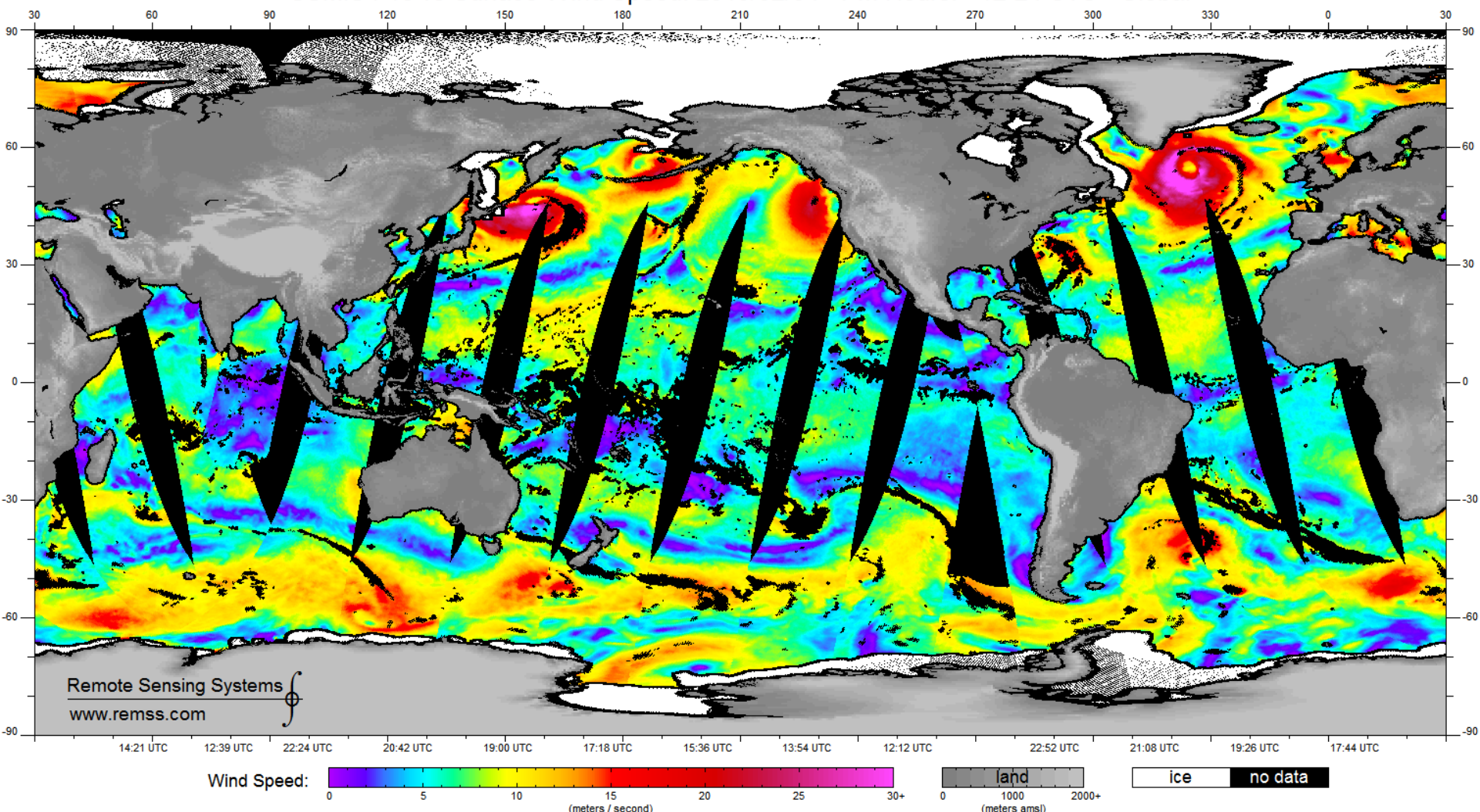


Kunkee et al. (2008)

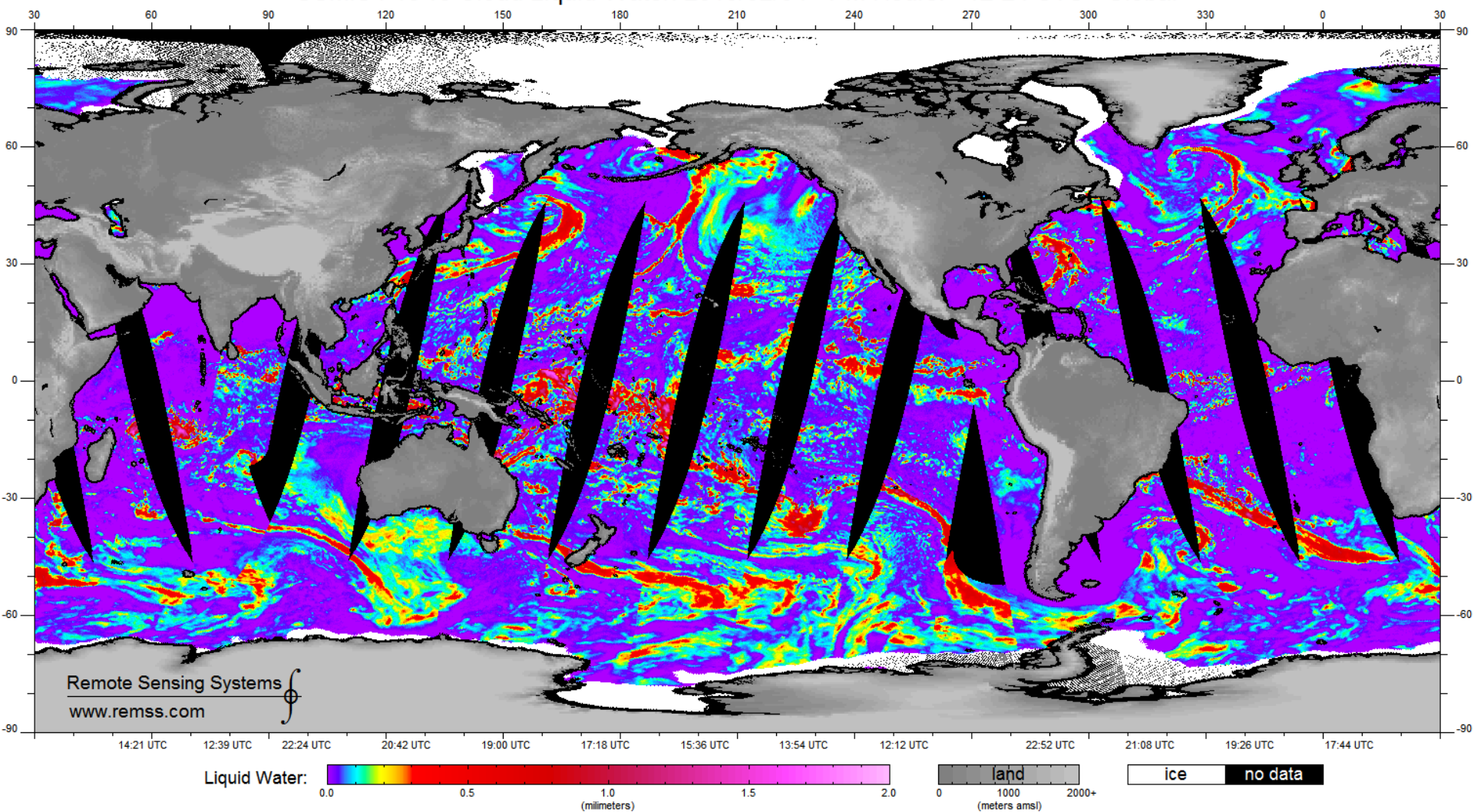
SSMIS F18 v8 Atmospheric Water Vapor: 2019/02/04 - PM Hours: ~12-24 UTC - Global



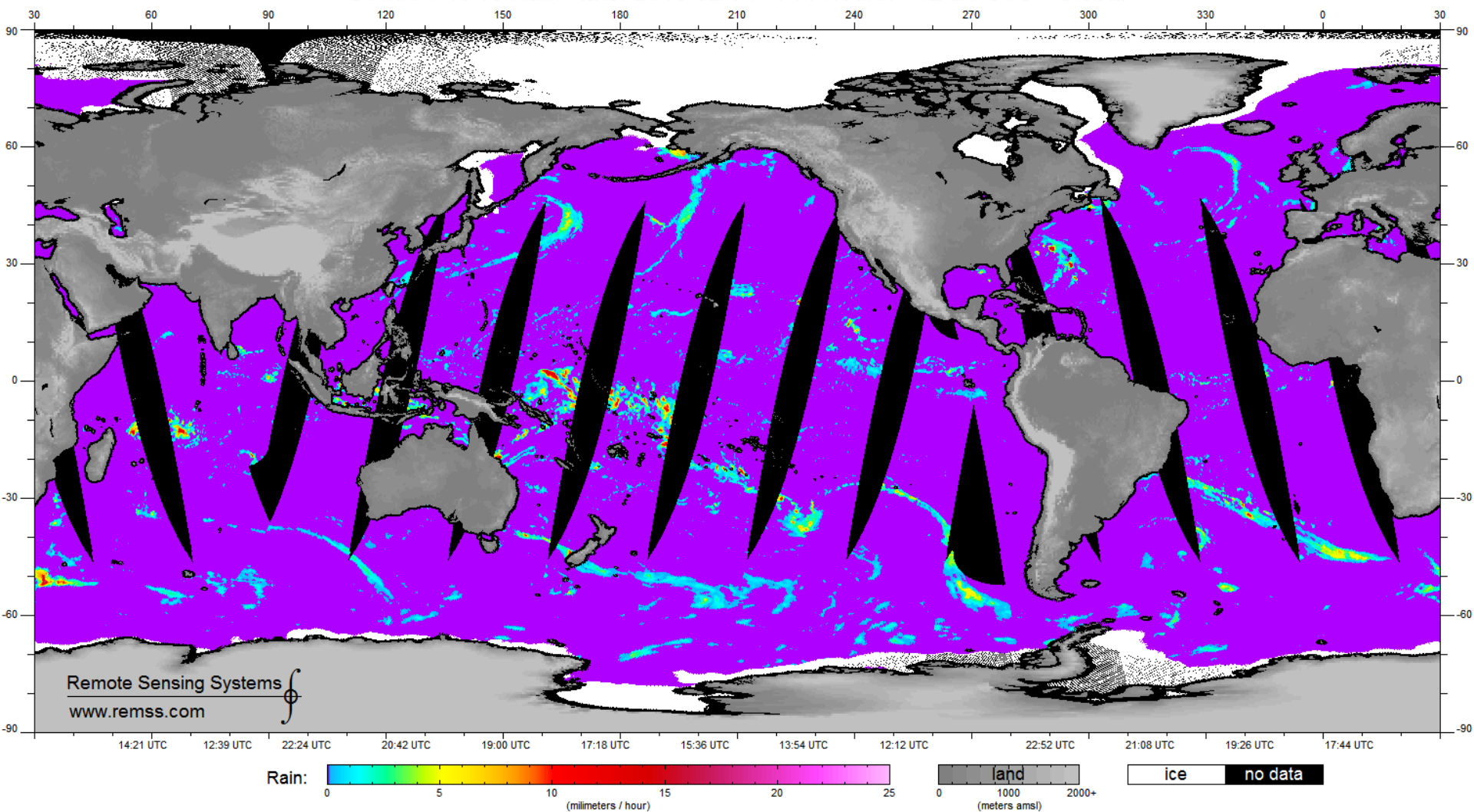
SSMIS F18 v8 Surface Wind Speed: 2019/02/04 - PM Hours: ~12-24 UTC - Global



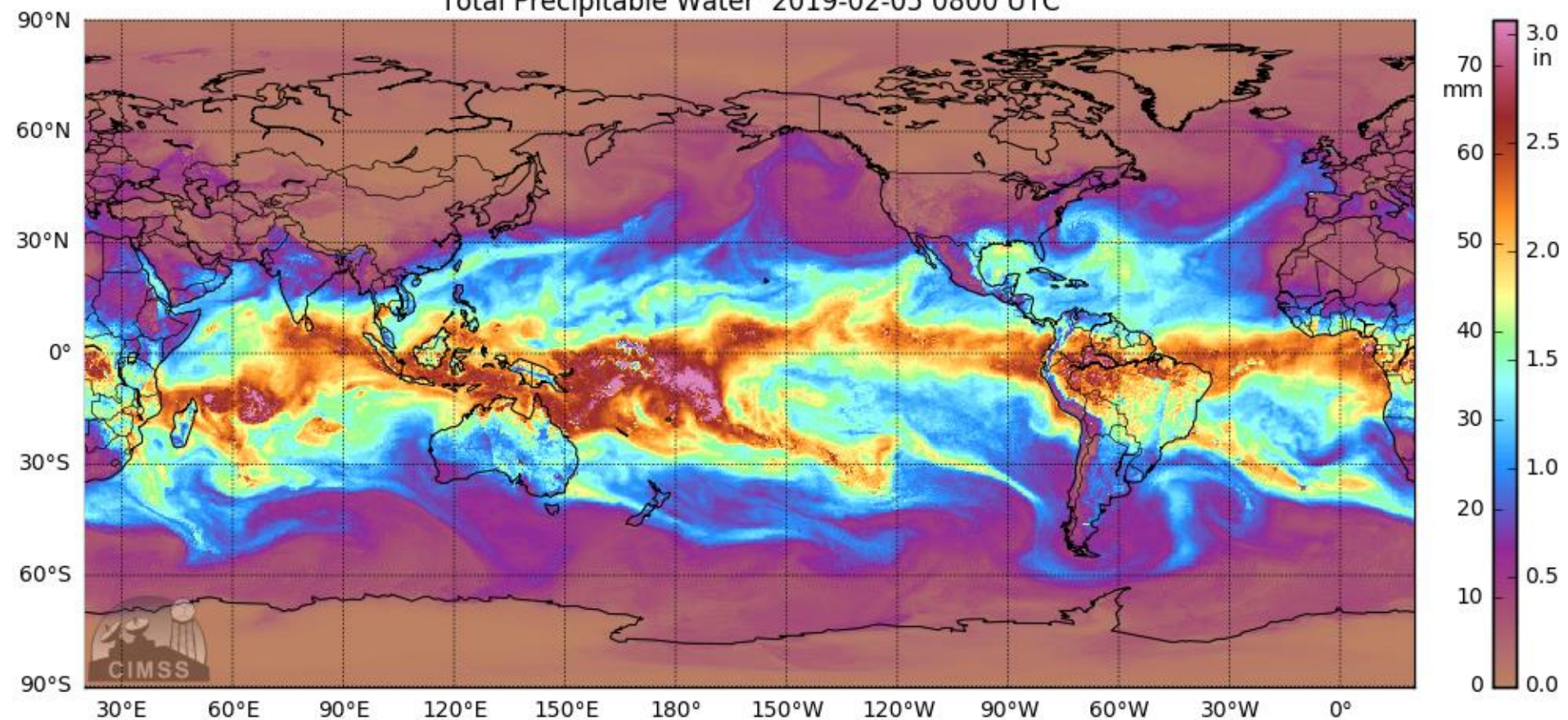
SSMIS F18 v8 Cloud Liquid Water: 2019/02/04 - PM Hours: ~12-24 UTC - Global



SSMIS F18 v8 Rain Rate: 2019/02/04 - PM Hours: ~12-24 UTC - Global

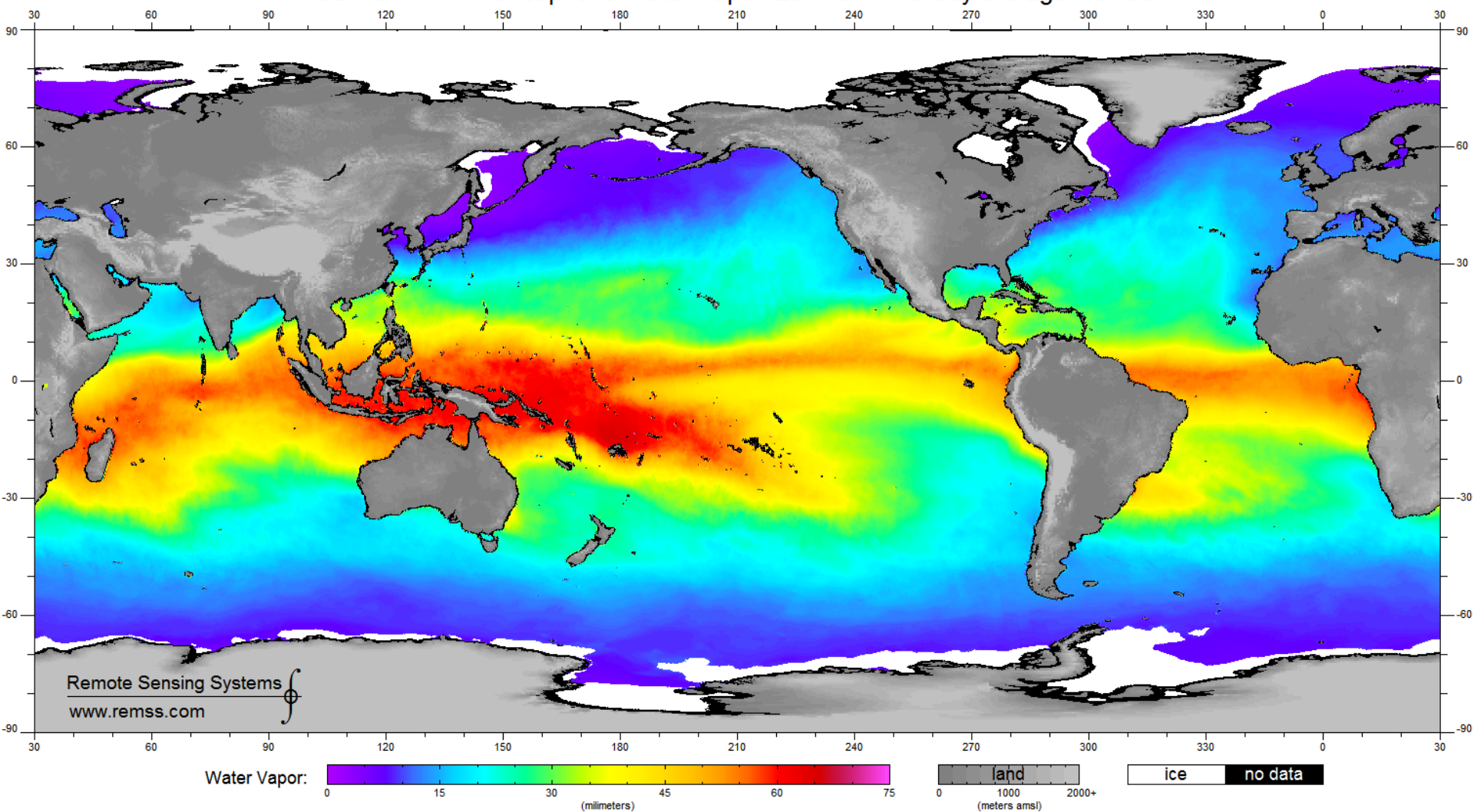


Total Precipitable Water 2019-02-05 0800 UTC

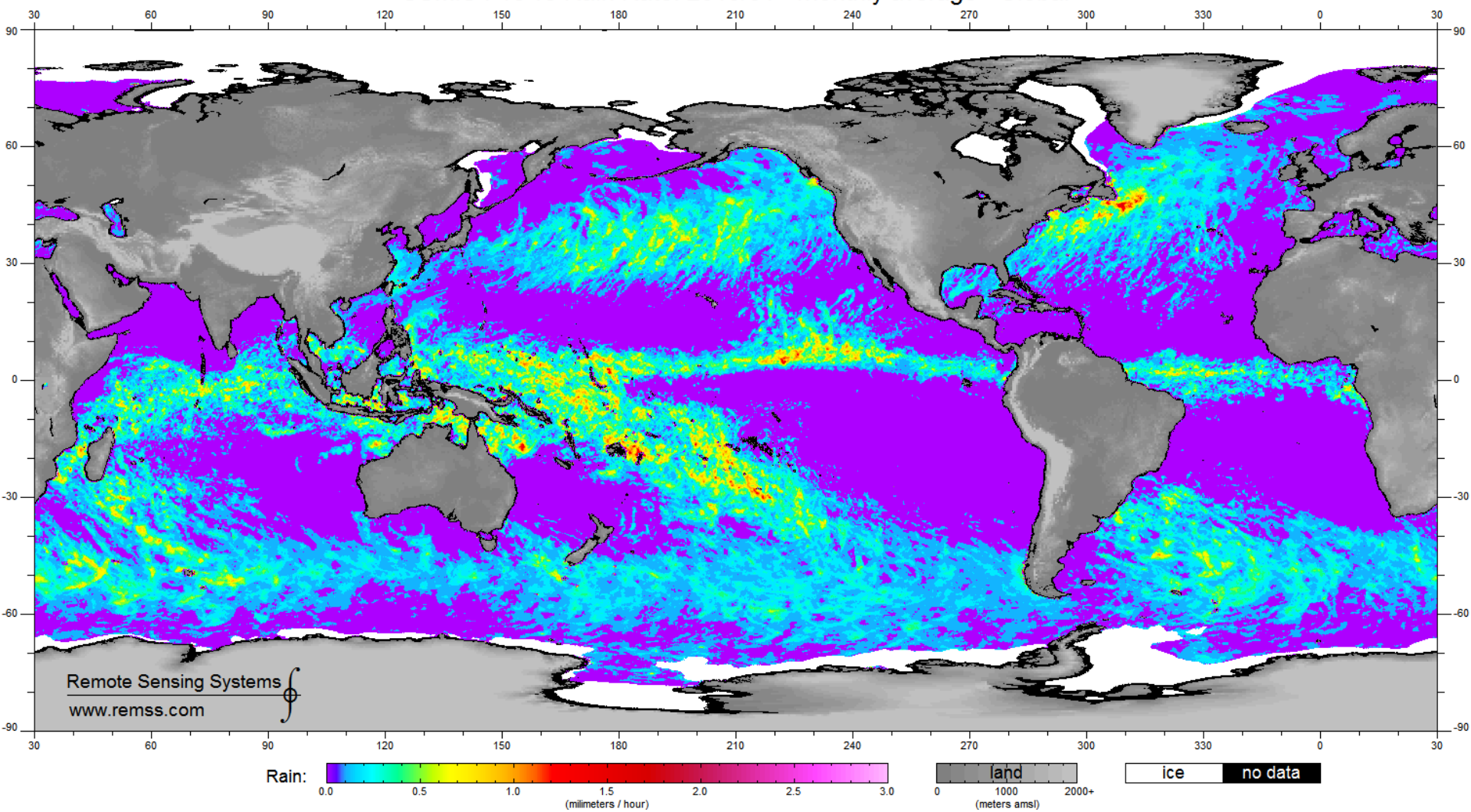


Univ. of Wisconsin CIMSS: http://tropic.ssec.wisc.edu/real-time/tpw2/product.php?color_type=tpw_nrl_colors&prod=global2×pan=24hrs&anim=html5

SSMIS F18 v8 Atmospheric Water Vapor: 2019/01 - monthly average - Global



SSMIS F18 v8 Rain Rate: 2019/01 - monthly average - Global



MR3522: Remote Sensing of the Atmosphere and Ocean

Interpreting Microwave Brightness Temperatures

Main Topics

- Locating clear-sky vs clouds
- Ambiguities in MW brightness temperature

Idealized
Homogeneous
atmosphere

$$T_{B_{19}} = \underline{\hspace{2cm}}$$

$$\underline{\hspace{2cm}}$$

$$\underline{\hspace{2cm}}$$

$$T_{B_{22}} = \underline{\hspace{2cm}}$$

$$\underline{\hspace{2cm}}$$

$$\underline{\hspace{2cm}}$$

$$T_{B_{37}} = \underline{\hspace{2cm}}$$

$$\underline{\hspace{2cm}}$$

$$\underline{\hspace{2cm}}$$

$$T_{B_{92}} = \underline{\hspace{2cm}}$$

$$\underline{\hspace{2cm}}$$

$$\underline{\hspace{2cm}}$$

ρ

$$\tau_d = 1$$

M

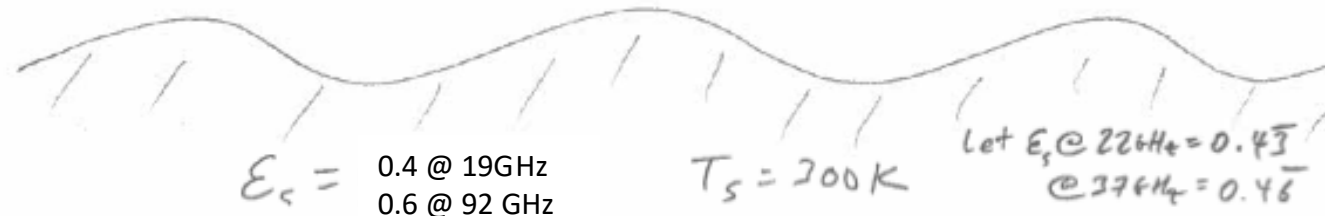
DC

CD

MD



$$T_a^{260K}$$



$$E_s = \begin{cases} 0.4 & @ 19\text{GHz} \\ 0.6 & @ 92\text{ GHz} \end{cases}$$

$$T_s = 200K$$

$$\begin{aligned} \text{Let } E_s @ 22\text{GHz} &= 0.47 \\ @ 37\text{GHz} &= 0.46 \end{aligned}$$

τ_d

| $\gamma(6\text{Hz})$ | Completely Dry (CD) | Moderately Dry (MD) | Moist (m) | Deep Convection (DC) |
|----------------------|---------------------|---------------------|-----------|----------------------|
| 19 | 1 | 0.75 | 0.65 | 0.2 |
| 22 | 1 | 0.5 | 0.15 | 0.05 |
| 37 | 1 | 0.675 | 0.5 | 0.1 |
| 92 | 1 | 0.4 | 0.1 | 0 |

 $\bar{T}_a (\text{K})$

| $\gamma(6\text{Hz})$ | CD | MD | m | DC |
|----------------------|----|----|---|----|
| 19 | | | | |
| 22 | | | | |
| 37 | | | | |
| 92 | | | | |

 $T_B(\text{K}) \sim T_c = 300\text{K}$

| $\gamma(6\text{Hz})$ | CD | MD | m | DC |
|----------------------|----|----|---|----|
| 19 | | | | |
| 22 | | | | |
| 37 | | | | |
| 92 | | | | |

Idealized
Homogeneous
atmosphere

$$T_{B_{19}} = \underline{\quad}$$

$$\underline{\quad}$$

$$\underline{\quad}$$

$$T_{B_{22}} = \underline{\quad}$$

$$\boxed{\quad}$$

$$\underline{\quad}$$

$$T_{B_{37}} = \underline{\quad}$$

$$\underline{\quad}$$

$$\underline{\quad}$$

$$T_{B_{92}} = \underline{\quad}$$

$$\underline{\quad}$$

$$\underline{\quad}$$

$$T_B(v, \theta, \phi) = \varepsilon_s(v, \theta, T_s, S) T_s \tau_d(v) + \\ [1 - \varepsilon_s(v, \theta, T_s, S)] T_s [1 - \tau_d(v)] \tau_d(v) + \\ T_s [1 - \tau_d(v)]$$

$$T_B \\ = 0.433 * 300 * 0.5 + (1 - 0.433) \\ * 260 * (1 - 0.5) * 0.5 + 260 \\ * (1 - 0.5) =$$

CD

MD

M

DC

T_a^{260K}

$\varepsilon_s = 0.4 @ 19\text{GHz}$
 $0.6 @ 92\text{ GHz}$

$T_s = 200\text{ K}$

Let $\varepsilon_s @ 22\text{GHz} = 0.43$
 $@ 37\text{GHz} = 0.46$

Idealized
Homogeneous
atmosphere

$$T_{B_{19}} = \underline{\quad}$$

$$T_{B_{22}} = \underline{\quad}$$

$$T_{B_{37}} = \underline{\quad}$$

$$T_{B_{92}} = \underline{\quad}$$

232K

$$\underline{\quad}$$

$$\underline{\quad}$$

$$\underline{\quad}$$

$$\underline{\quad}$$



$$T_B = 0.433 * 300 * 0.5 + (1 - 0.433) * 260 * (1 - 0.5) * 0.5 + 260 * (1 - 0.5) = 232K$$

CD

MD

M

DC

$$T_a^{260K}$$

$$E_s = \begin{cases} 0.4 & @ 19\text{GHz} \\ 0.6 & @ 92\text{ GHz} \end{cases}$$

$$T_s = 200K$$

$$\begin{aligned} \text{Let } E_s @ 22\text{GHz} &= 0.43 \\ @ 37\text{GHz} &= 0.46 \end{aligned}$$

Idealized
Homogeneous
atmosphere

$$T_{B_{19}} = \underline{120\text{K}}$$

$$\underline{184\text{K}}$$

$$\underline{204\text{K}}$$

$$T_{B_{22}} = \underline{130\text{K}}$$

$$\underline{232\text{K}}$$

$$\underline{259\text{K}}$$

$$T_{B_{37}} = \underline{140\text{K}}$$

$$\underline{209\text{K}}$$

$$\underline{235\text{K}}$$

$$T_{B_{92}} = \underline{180\text{K}}$$

$$\underline{253\text{K}}$$

$$\underline{261\text{K}}$$

$$\underline{257\text{K}}$$

$$\underline{260\text{K}}$$

$$\underline{261\text{K}}$$

$$\underline{260\text{K}}$$

$$T_B(v, \theta, \phi) = \varepsilon_s(v, \theta, T_s, S) T_s \tau_d(v) + \\ [1 - \varepsilon_s(v, \theta, T_s, S)] T_s [1 - \tau_d(v)] \tau_d(v) + \\ T_s [1 - \tau_d(v)]$$

$$\tau_d = 1$$

M

DC

CD

MD

$$T_a^{260\text{K}}$$

$$\varepsilon_s = 0.4 \text{ @ } 19\text{GHz} \\ 0.6 \text{ @ } 92\text{ GHz}$$

$$T_s = 200\text{K}$$

$$\text{Let } \varepsilon_s @ 22\text{GHz} = 0.43 \\ @ 37\text{GHz} = 0.46$$

Realistic
Atmosphere

$$T_{\theta 1q} = \underline{\hspace{2cm}}$$

$$T_{\theta 22} = \underline{\hspace{2cm}}$$

$$T_{\theta 33} = \underline{\hspace{2cm}}$$

$$T_{\theta 92} = \underline{\hspace{2cm}}$$

$$\begin{aligned} T_b(v, \theta, \phi) = & \varepsilon_s(v, \theta, T_s, S) T_s \tau_d(v) + \\ & [1 - \varepsilon_s(v, \theta, T_s, S)] T_s [1 - \tau_d(v)] \tau_d(v) + \\ & T_s [1 - \tau_d(v)] \end{aligned}$$

$$\tau_d = 1$$

This equation doesn't work
now because it requires a
homogenous atmosphere.
Need to integrate last two
terms over $d\tau_d$.

$$770 \quad T_a^{280k} \quad 300k$$

ε_s and T_s same as idealized.



τ_d

| ν (GHz) | Completely Dry (CD) | Moderately Dry (MD) | Moist (m) | Deep Convection (DC) |
|-------------|---------------------|---------------------|-----------|----------------------|
| 19 | 1 | 0.75 | 0.65 | 0.2 |
| 22 | 1 | 0.5 | 0.15 | 0.05 |
| 37 | 1 | 0.675 | 0.5 | 0.1 |
| 92 | 1 | 0.4 | 0.1 | 0 |

 \bar{T}_a (K)

| ν (GHz) | CD | MD | m | DC |
|-------------|----|----|-----|-----|
| 19 | | | 295 | 280 |
| 22 | | | 275 | 260 |
| 37 | | | 280 | 275 |
| 92 | | | 270 | 260 |

 T_B (k) w/ $T_c = 300$ K

| ν (GHz) | CD | MD | m | DC |
|-------------|----|----|---|----|
| 19 | | | | |
| 22 | | | | |
| 37 | | | | |
| 92 | | | | |

Realistic
Atmosphere

$$T_{\theta 1q} = \underline{120K}$$

$$\underline{196K}$$

$$\underline{214K}$$

$$T_{\theta 22} = \underline{130K}$$

$$\underline{242K}$$

$$\underline{259K}$$

$$T_{\theta 33} = \underline{140K}$$

$$\underline{218K}$$

$$\underline{244K}$$

$$T_{\theta 44} = \underline{180K}$$

$$\underline{260K}$$

$$\underline{261K}$$

$$261K$$

$$256K$$

$$261K$$

$$190K$$

$$T_b(v, \theta, \phi) = \varepsilon_s(v, \theta, T_s, S) T_s \tau_d(v) + \\ [1 - \varepsilon_s(v, \theta, T_s, S)] T_s [1 - \tau_d(v)] \tau_d(v) + \\ T_s [1 - \tau_d(v)]$$

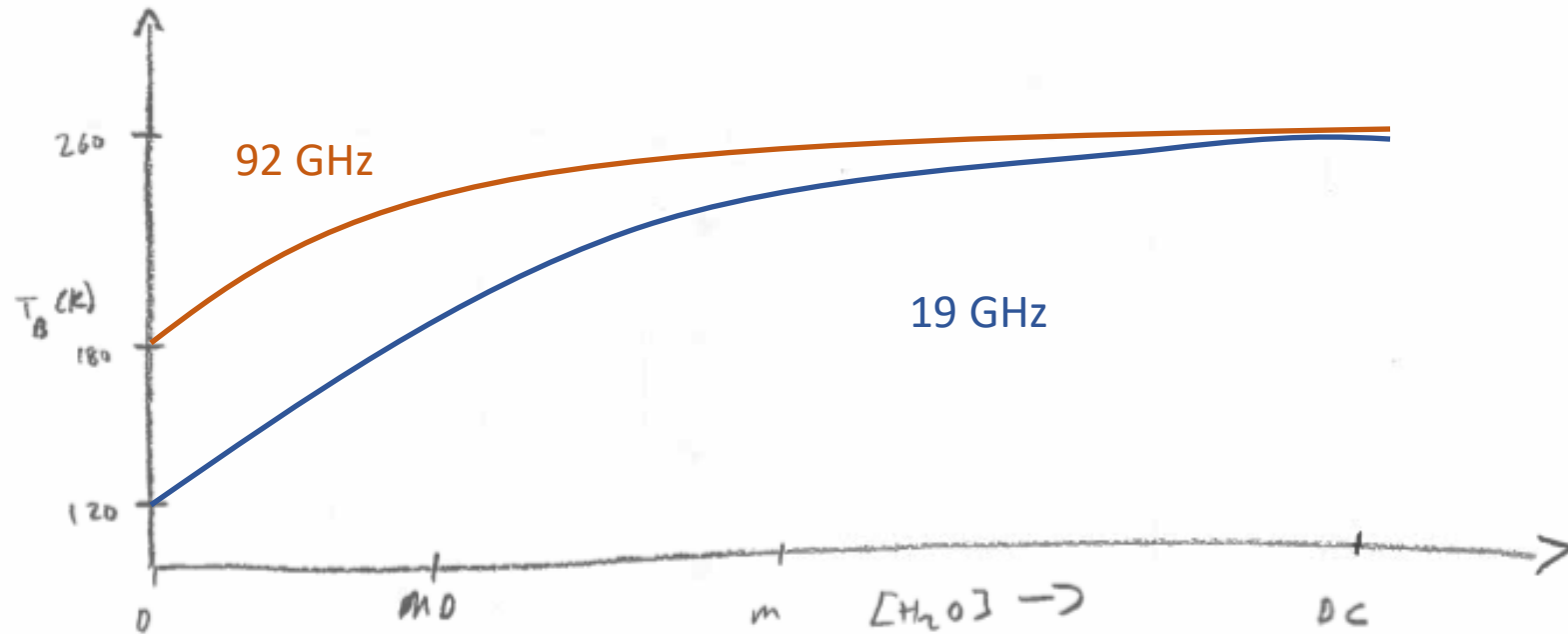
$$\tau_d = 1$$

Plugging in "estimated"
values of T_a in linear
function. Not actually
correct! But OK for
demonstration.

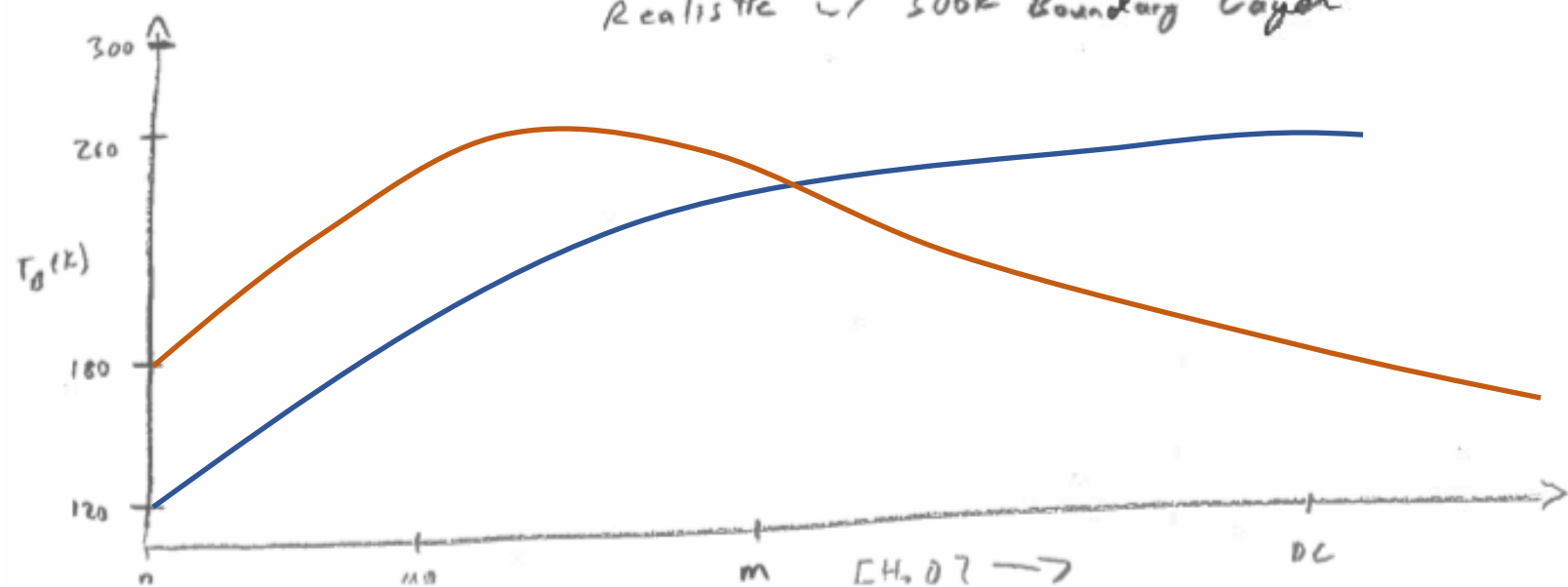
$$770 \quad T_a^{280K} \quad 300K$$

ε_s and T_s same as idealized.

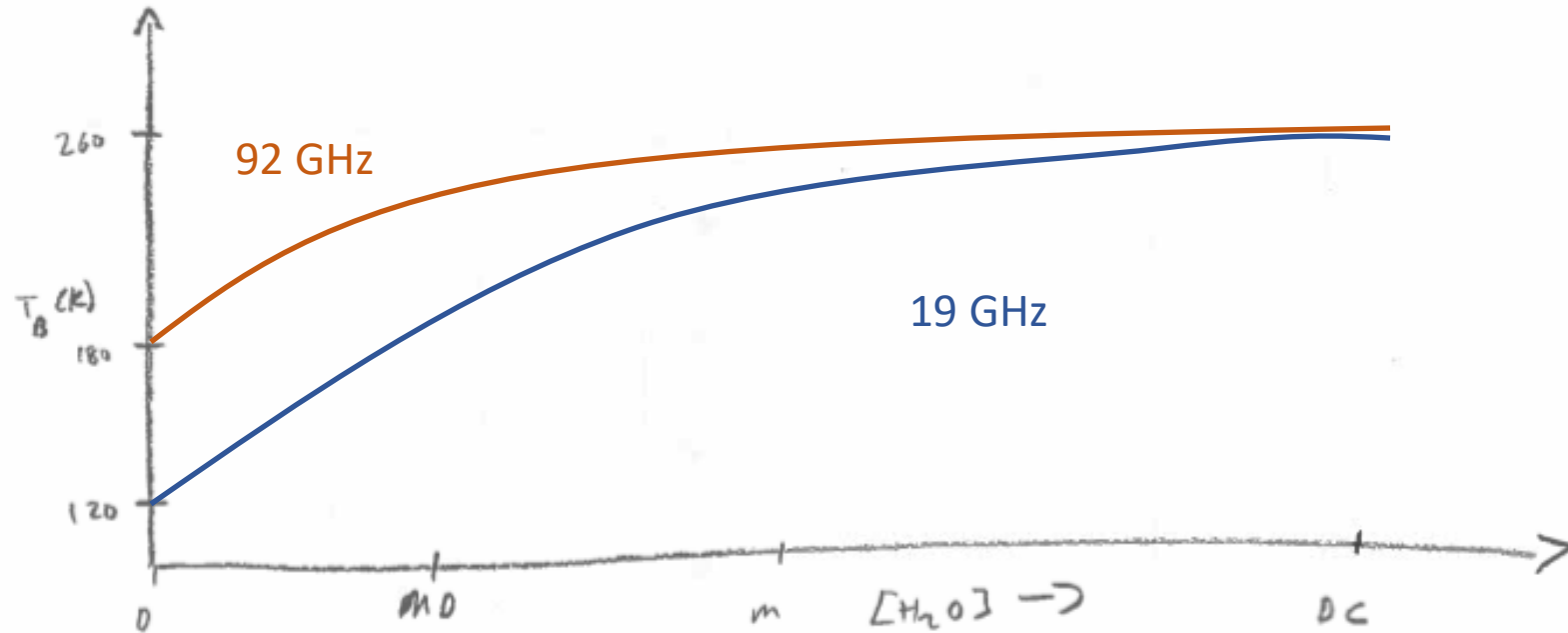
Idealized



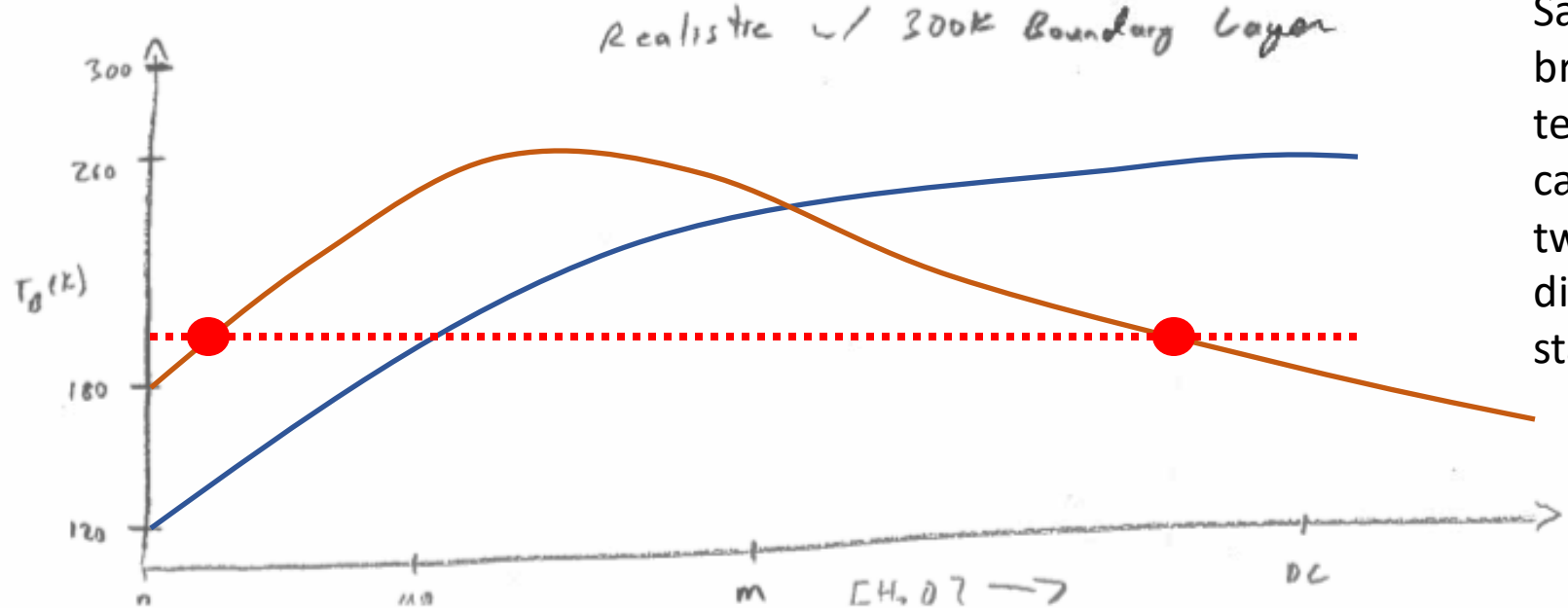
Realistic w/ 300K Boundary Layer



Idealized



Same
brightness
temperature
can represent
two very
different
states!



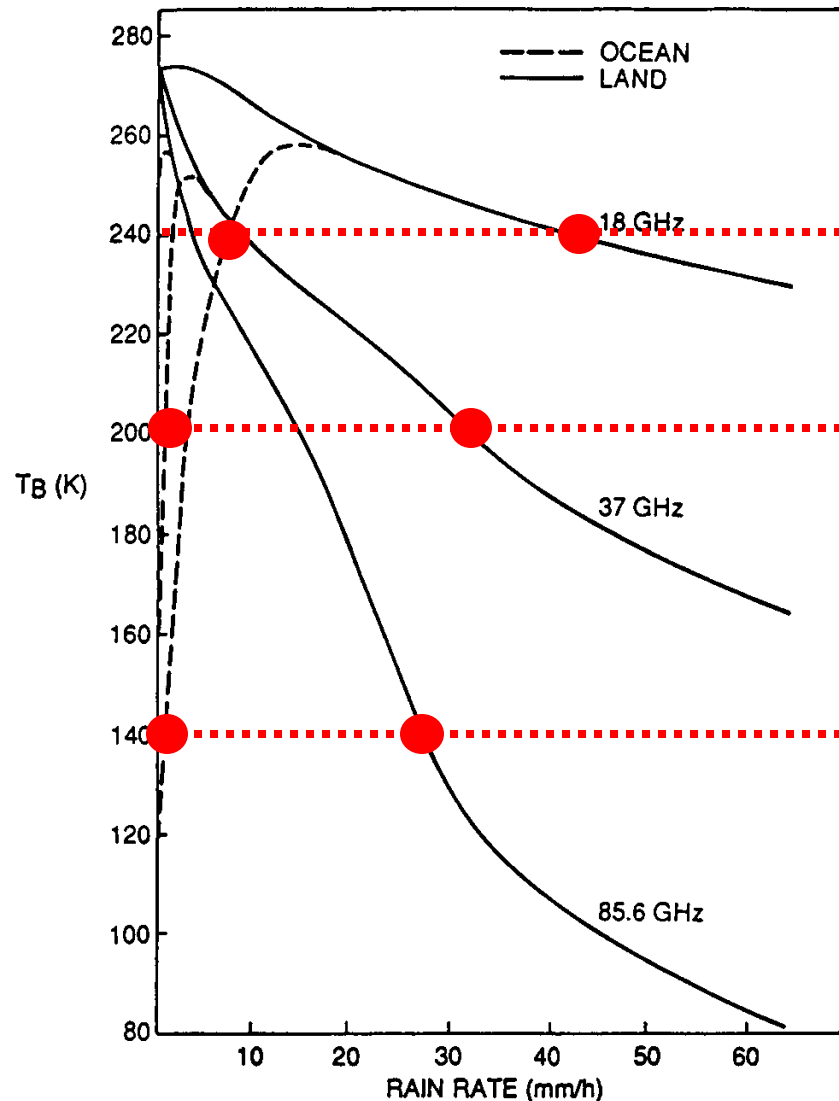
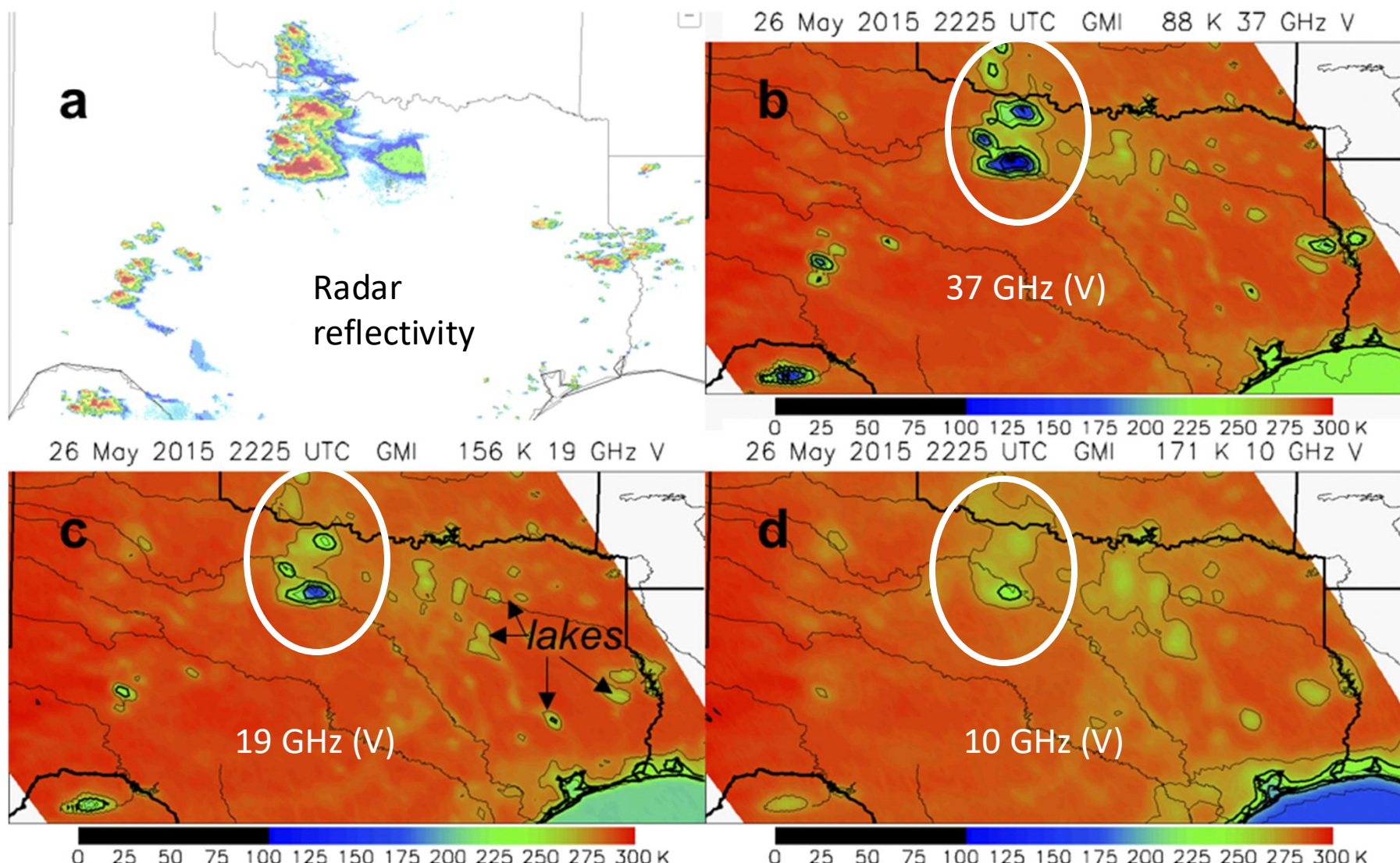
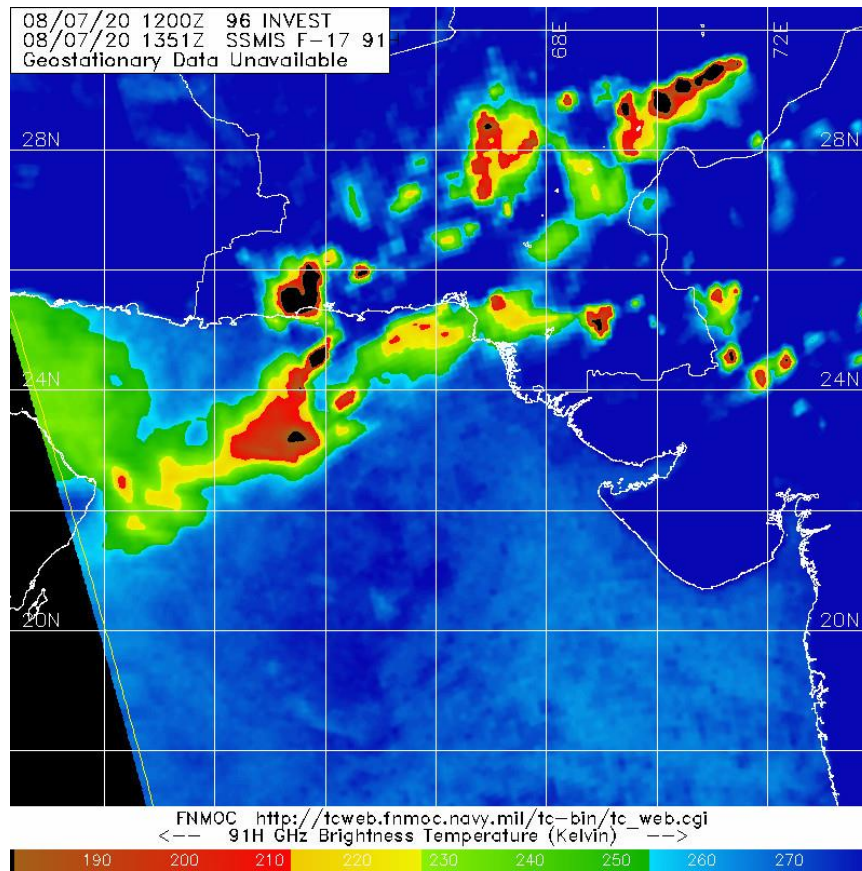


FIGURE 9.16. Brightness temperature versus rain rate for three frequencies. [After Spencer *et al.* (1989).]

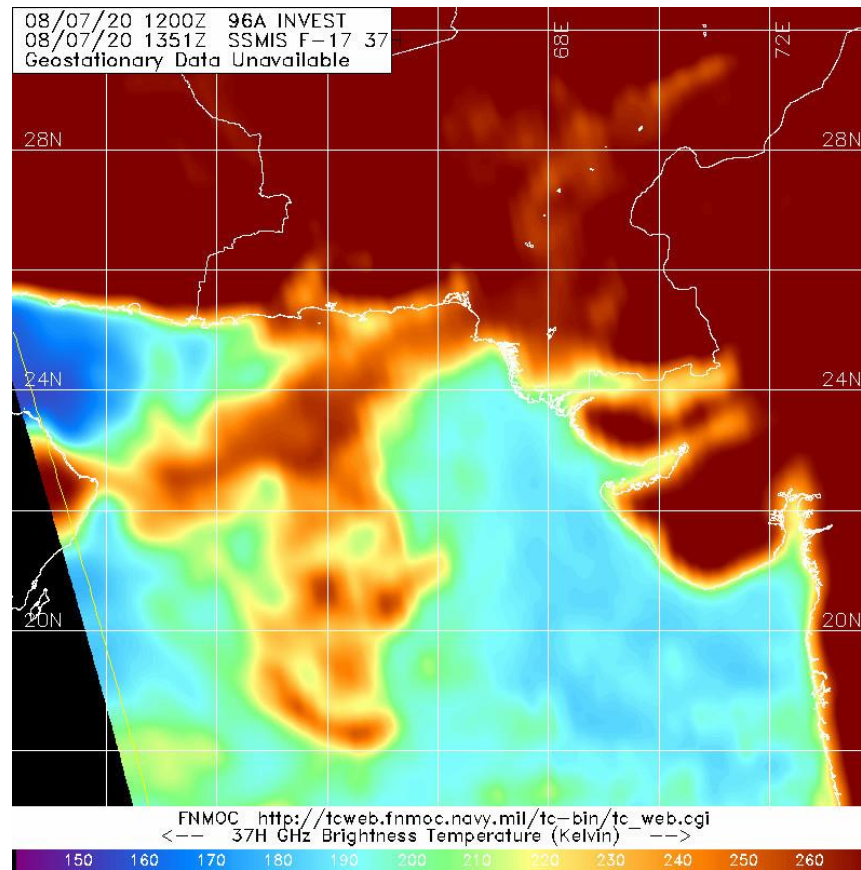


Example convective outbreak in Texas at 2225 UTC 26 May 2015. (a) Ground-based radar reflectivity mosaic. GMI (b) 37-, (c) 19-, and (d) 10-GHz vertically polarized brightness temperatures. Contour interval in (b)–(d) is 25 K, with thick contours every 50 K, and the minimum brightness temperature in the domain is printed in the panel title.

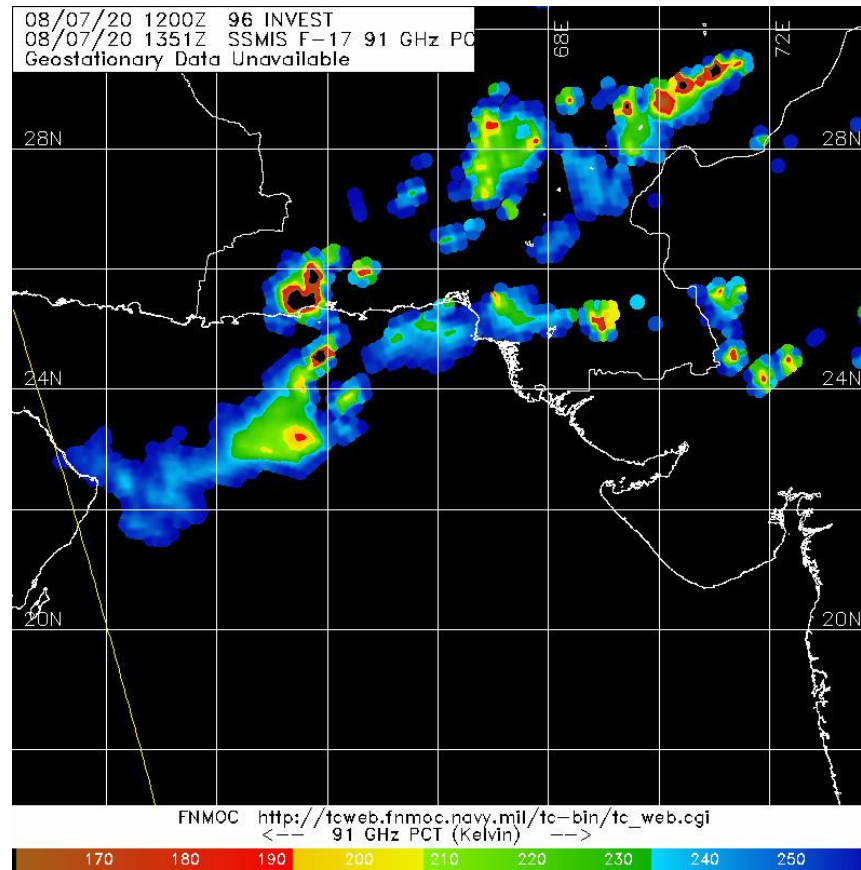
91GHz (H)



37GHz (H)

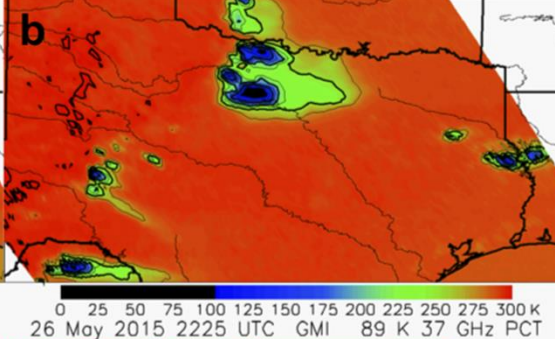
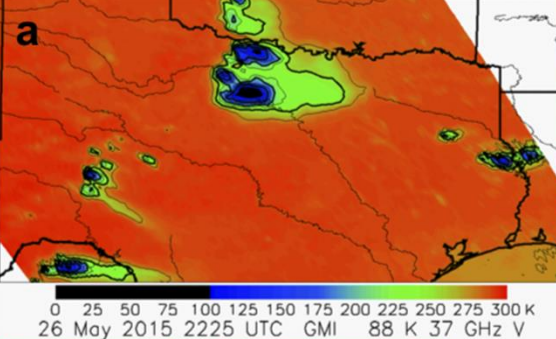


91GHz (PCT)

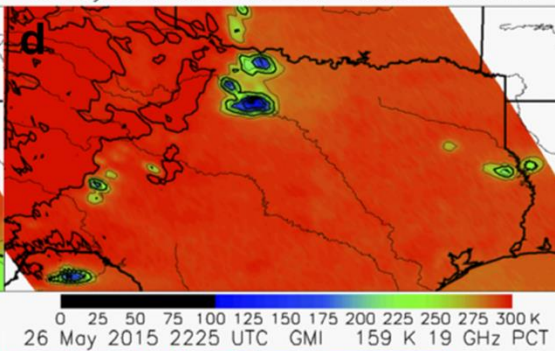
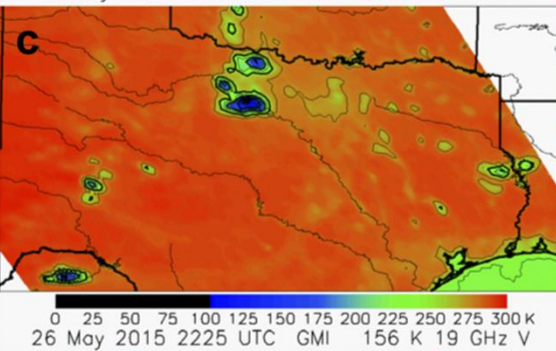


26 May 2015 2225 UTC GMI 62 K 89 GHz V

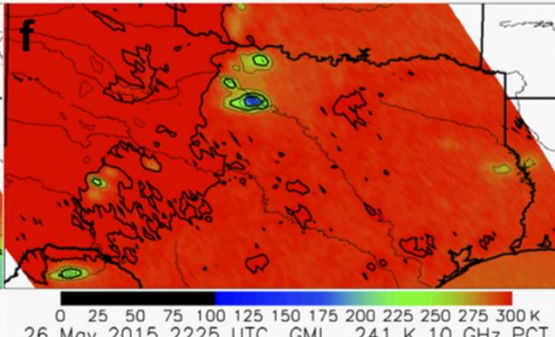
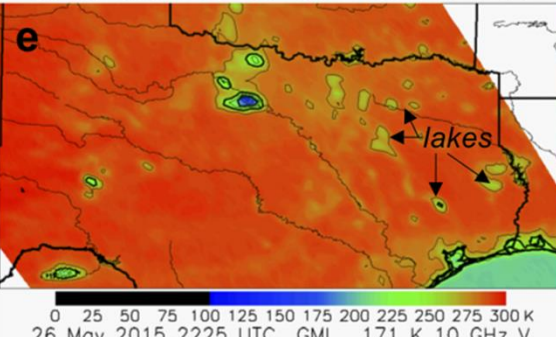
26 May 2015 2225 UTC GMI 62 K 89 GHz PCT



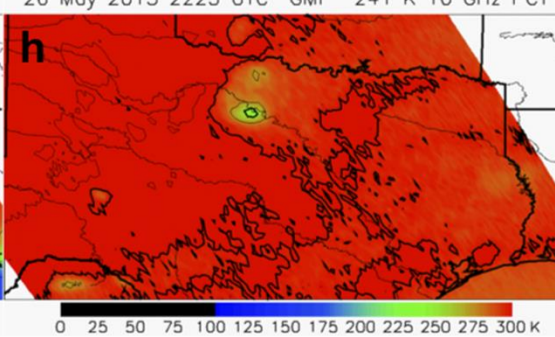
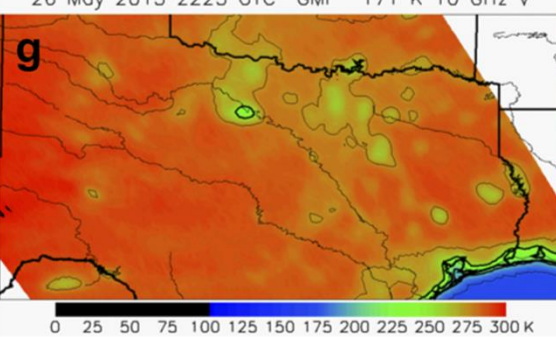
89 GHz



37 GHz



19 GHz



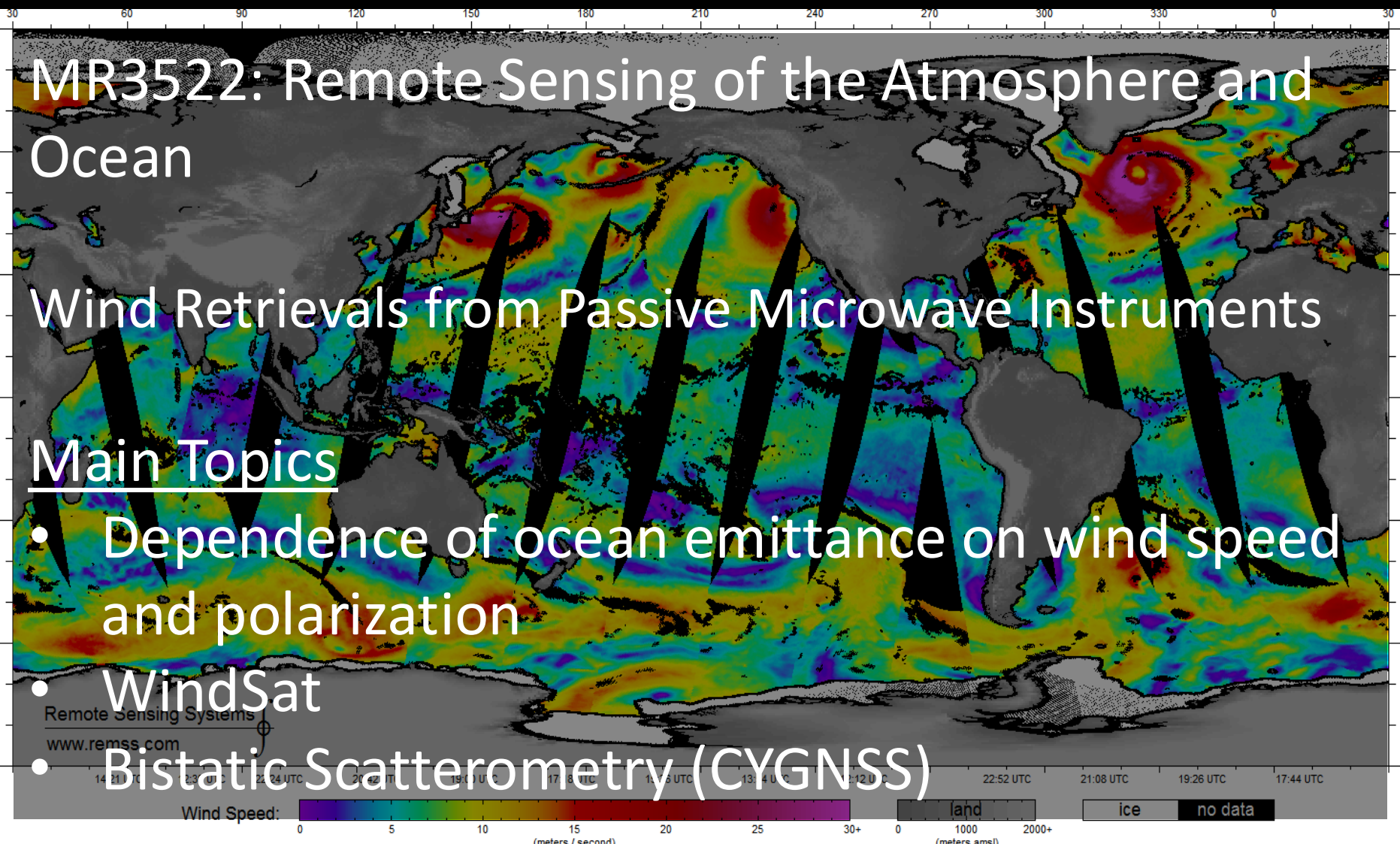
10 GHz

MR3522: Remote Sensing of the Atmosphere and Ocean

Wind Retrievals from Passive Microwave Instruments

Main Topics

- Dependence of ocean emittance on wind speed and polarization
- WindSat
- Bistatic Scatterometry (CYGNSS)



Wind Speed

At MW frequencies,
emittance depends on polarization
(vertical > horizontal)

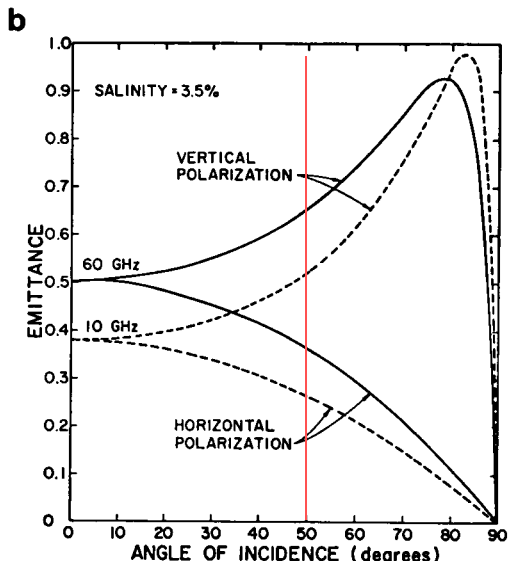


FIGURE 9.17. (a) Nadir emittance of a smooth ocean surface as a function of sea surface temperature.
(b) Emittance of a smooth ocean surface as a function of zenith angle. [After Kidder (1979).]

For a wind roughened ocean at 50° ,
emittance increases with wind speed
for horizontal polarization,

while emittance **does not change** with
wind speed for vertical polarization

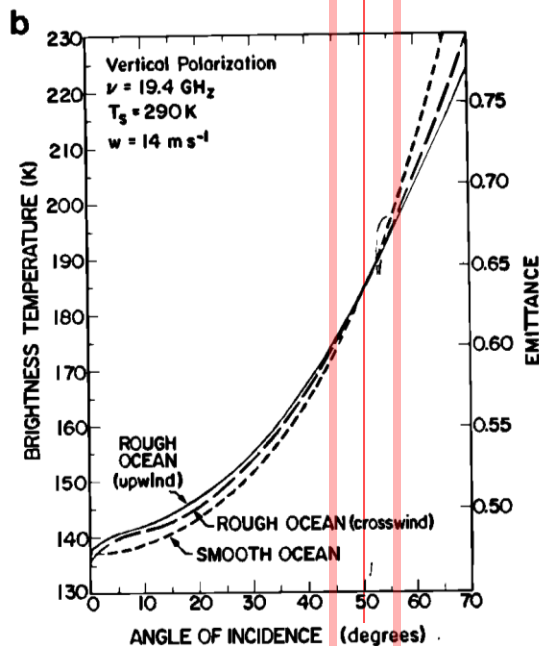
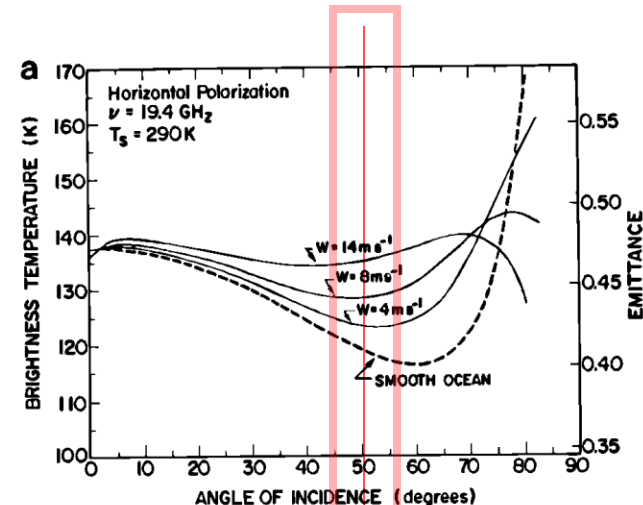


FIGURE 7.7. Calculated emittance at 19.4 GHz of a wind-roughened ocean surface as a function of incidence angle (measured from vertical): (a) horizontal polarization, (b) vertical polarization. [After Stogryn (1967). © 1967 IEEE.]

Passive Wind Speed Retrievals

- Microwave passive sensors can detect wind speed, but they cannot deduce wind direction unless under specific conditions (high wind speed; little cloud cover), and with dual- or multi-polarization.
- SSMI/S for example (see title slide) uses 19 through 37 GHz bands for its wind speed retrieval.
 - Why not 85 or 92 GHz?
- Consider the equation for microwave brightness temperature again:

$$\begin{aligned} T_B(v, \theta, \phi) = & \varepsilon_s(v, \theta, T_s, S) T_s \tau_d(v) + \\ & [1 - \varepsilon_s(v, \theta, T_s, S)] T_a [1 - \tau_d(v)] \tau_d(v) + \\ & T_a [1 - \tau_d(v)] \end{aligned}$$

We only know T_B from the satellite instrument! However, we can use various microwave bands to determine water vapor and liquid water concentration (which affect τ_d), temperature profiles (T_a), and sea surface temperature (T_s). This will permit a unique value of ε_s that can be converted to a wind speed.

Emissivity for this band (in H) increases about 0.08 at 30 m/s wind speed

Ordinate is
 $\Delta\varepsilon_s T_s$ for a
surface at
290K.

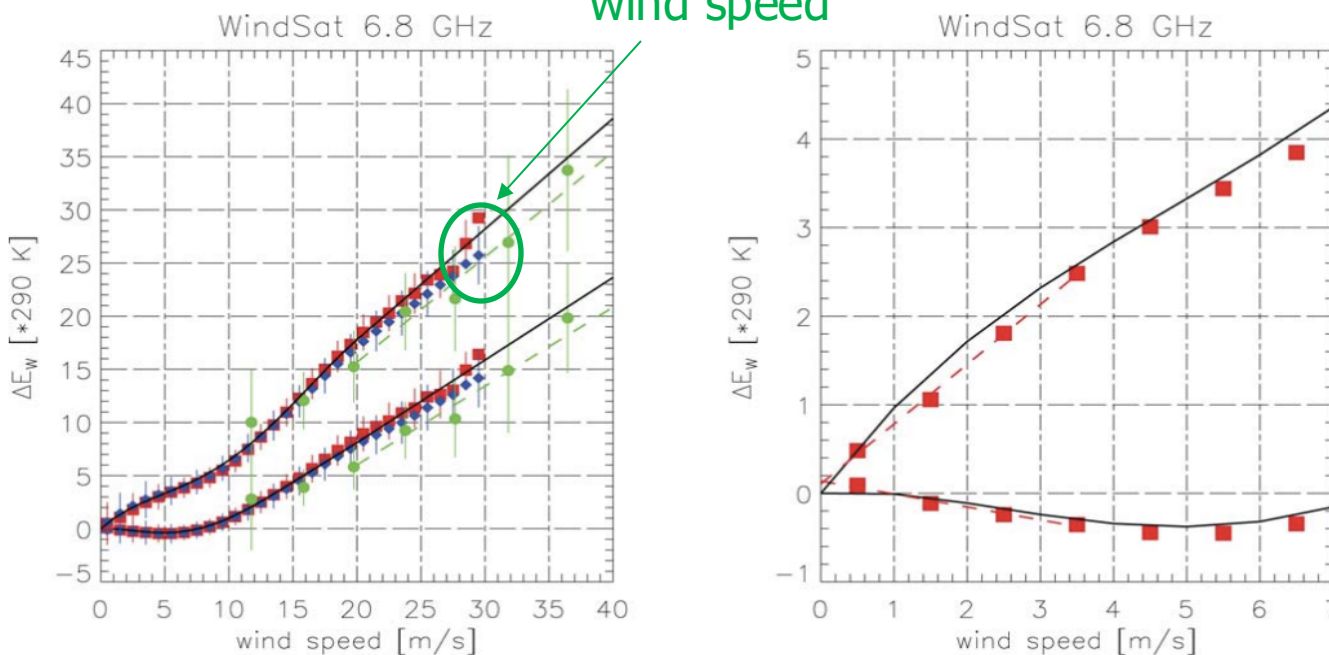
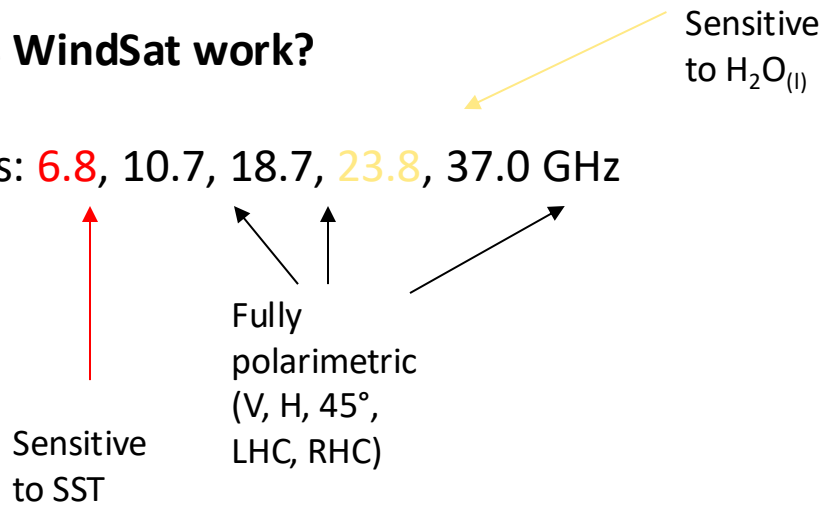


Fig. 3. Wind-induced ocean surface emissivity near the reference temperature $T_{ref} = 20 \text{ }^{\circ}\text{C}$ for the 6.8 GHz v-pol (lower curves) and h-pol (upper curves) channels at EIA 53.8 ° from WindSat TB measurements. The solid lines are the model functions from Section IV of this paper. The red squares/blue diamonds are the results from the analysis of set WS1/set WS2 of Table I, if WindSat (QuikScat) wind speeds are used for binning. For clarity, only every second error bar is displayed. The green circles in the left panel are the results from [13] using HRD wind speeds (set WS3 from Table I). The dashed lines are linear fits to these data above 20 m/s. The right panel magnifies the low wind speed region of data set WS1. The red dashed lines in the right panel are the linear fits to the red squares in the wind sped interval 0–3.5 m/s. The emissivities have been multiplied by a typical surface temperature of 290 K.

How does WindSat work?

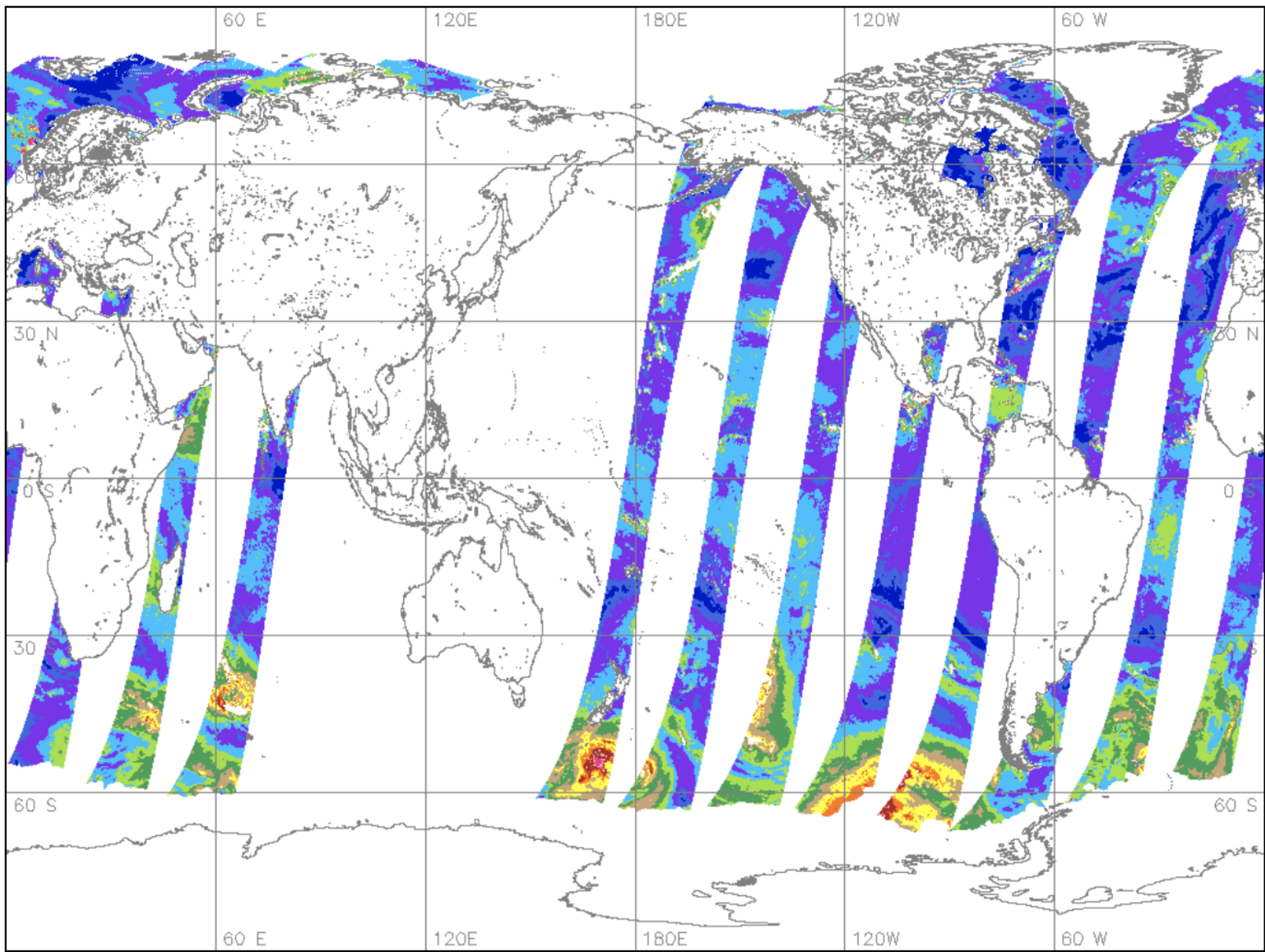
5 channels: 6.8, 10.7, 18.7, 23.8, 37.0 GHz



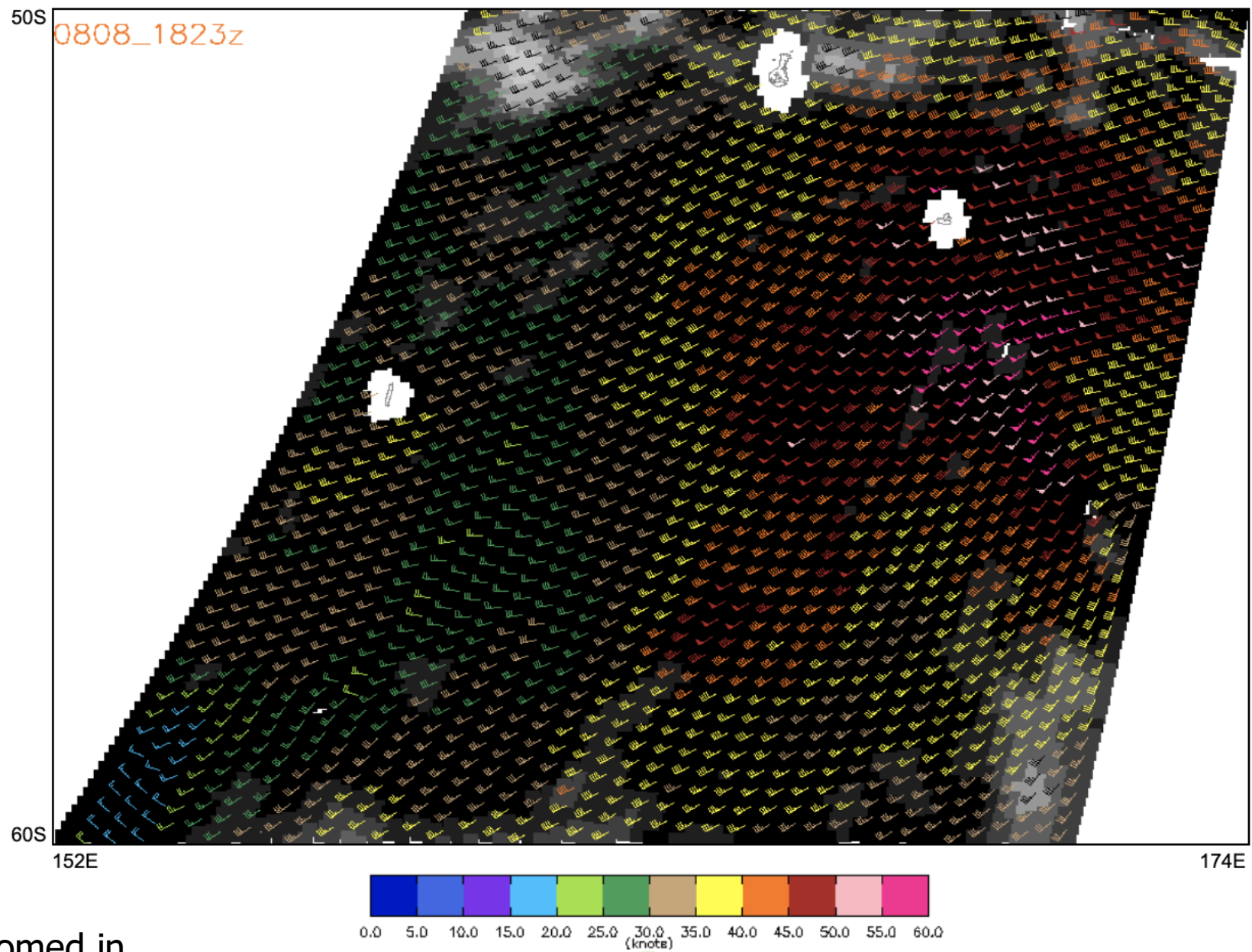
6.8 and 23.8 GHz bands are highly sensitive to SST and water vapor concentration, allowing use of other three channels to deduce wind speed.

Polarimetry used to determine wind direction.

- Use of H and V polarizations from two angles—one ahead and one behind the satellite.
- Single view of scene using H and V polarizations and correlation between their electric field vector (Stokes parameters).
 - Ineffective at light wind speeds

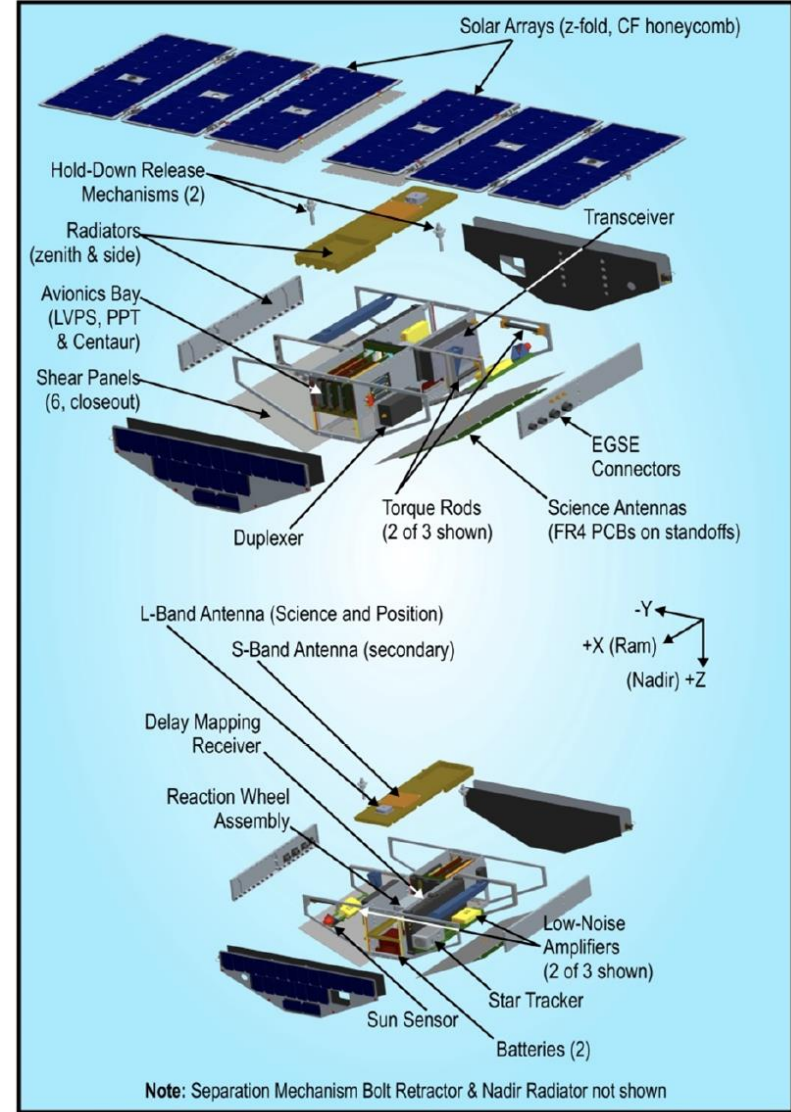
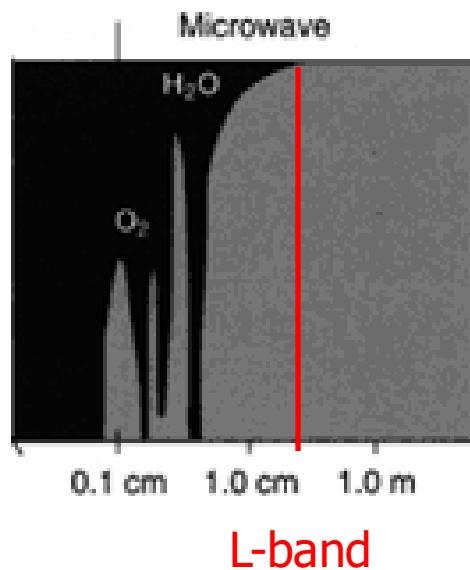


wndmi_fws_d20200808_lon152E_174E_lat60S_50S

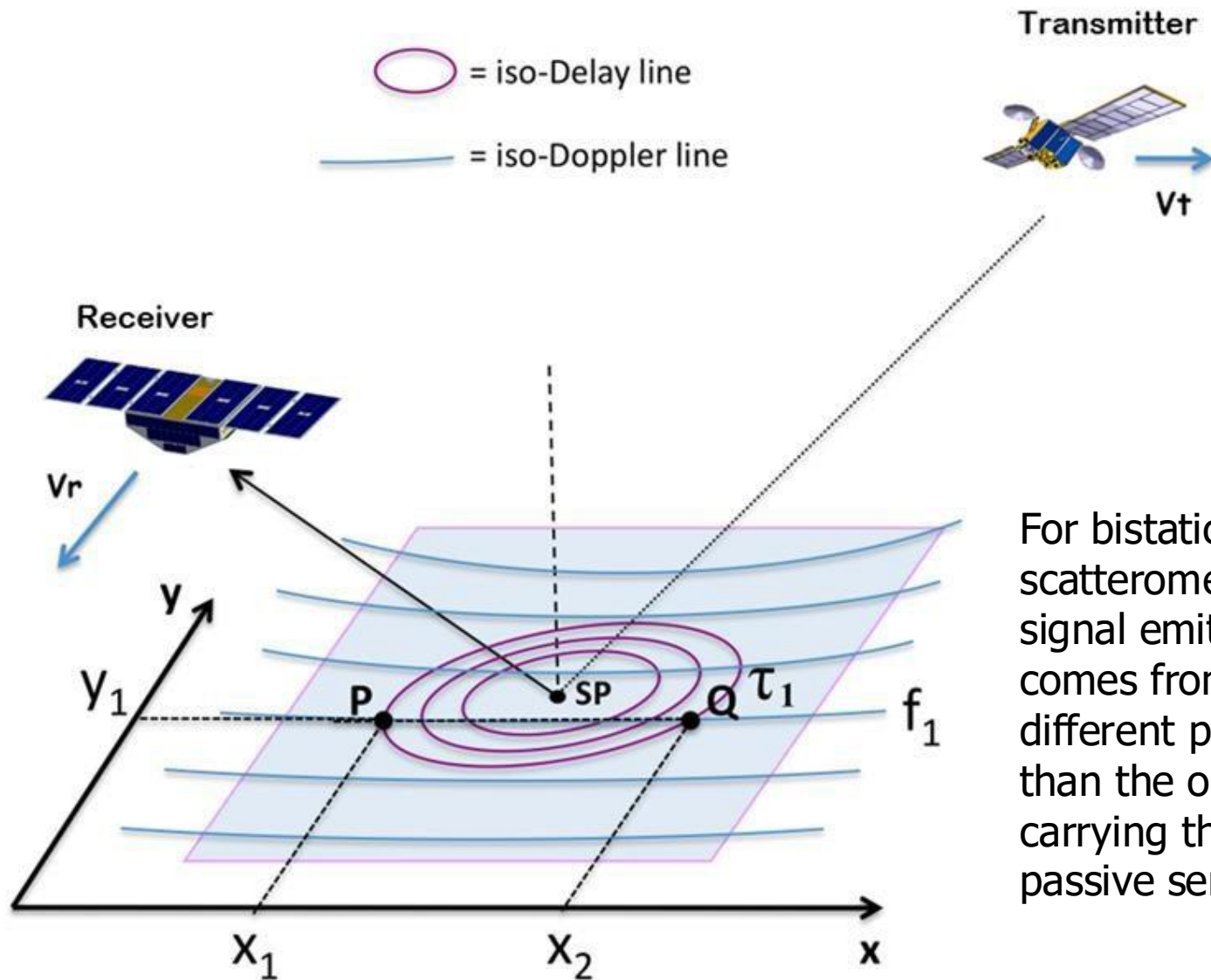


Bistatic scatterometry

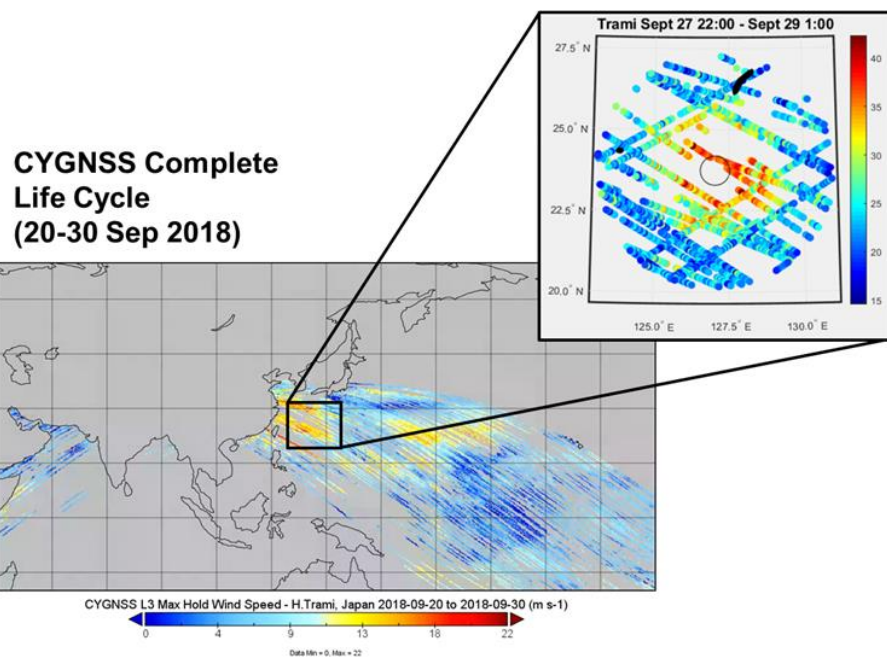
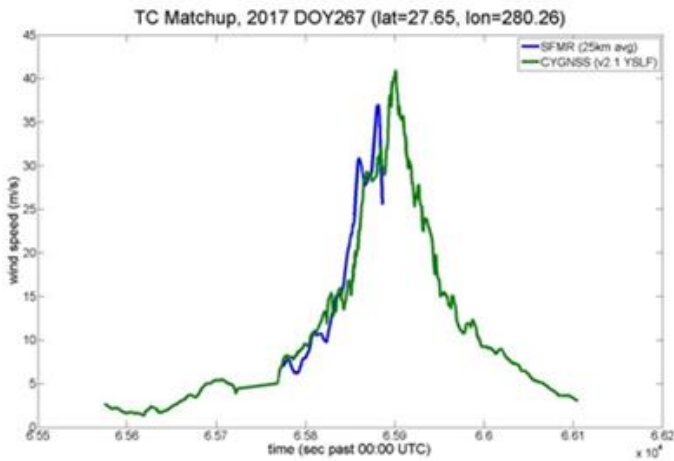
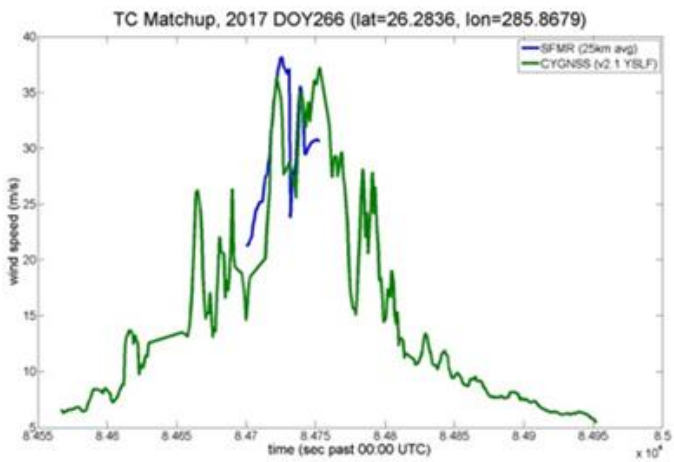
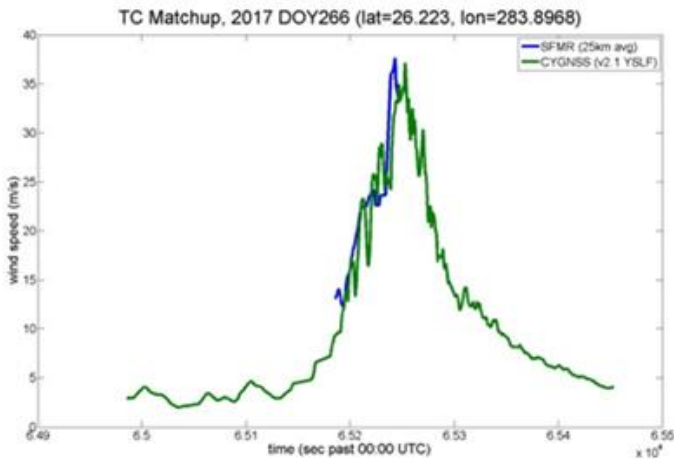
- Scatterometry yields wind speed *and* direction.
- CYGNSS (Cyclone Global Navigation Satellite System); 8 small satellites (<30 kg each in constellation)
- Detects reflection of L-band (1–2 GHz) GPS signal off of Earth's surface.
- L-band not attenuated by water vapor or liquid water.
Can see through clouds!



Bistatic scatterometry



For bistatic scatterometry, the signal emitted comes from a different platform than the one carrying the passive sensor.



CYGNSS Daily Composite (28 Sep 2018)

Accurate measurements of high wind speeds in areas covered in rain.

Multiple satellites (8) allow for high temporal resolution as well!

Why are traditional scatterometers less effective at either of the above?

MR3522: Remote Sensing of the Atmosphere and Ocean

Scatterometers

Main Topics

- Active vs passive sensing
- Bragg scatter
- Ambiguities in determination of wind vectors

Passive sensors detect EM radiation from some observed source.

Active sensors emit EM radiation and observe that scattered toward the sensor.

- Scatterometry works, fundamentally, by measuring the backscatter off of the surface. **We're not looking for emissions from the ocean anymore; instead, we're observing the scattering properties of the ocean surface.**
- The backscatter from the ocean surface changes as a function of surface roughness, which itself depends on wind speed.

Power flux density at a radar antenna:

$$S_r = \frac{\sigma G P_t}{16\pi^2 r^4}$$

Multiply by the effective area of the antenna (A_{eff}) to get the total received power:

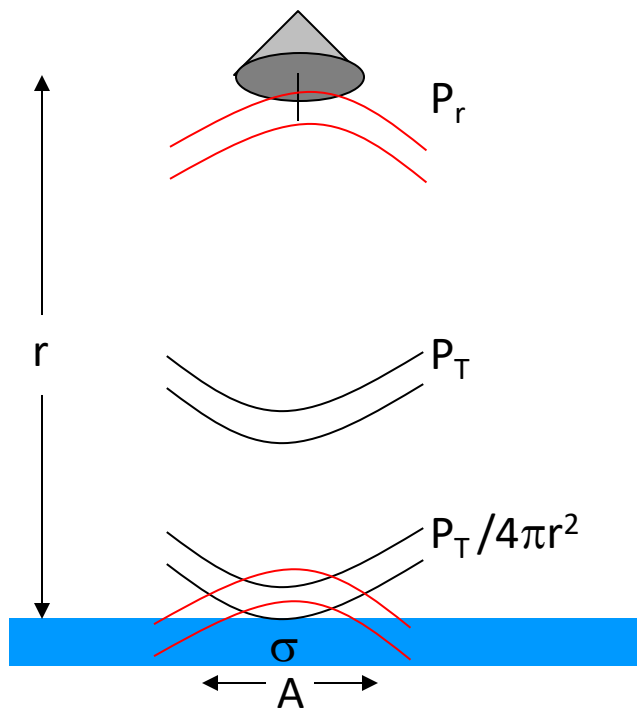
$$P_r = S_r A_{eff} = \frac{\sigma G P_t A_{eff}}{16\pi^2 r^4}$$

For now, we are interested in what effects σ .

σ is the link to the surface properties for scatterometry:

$$\sigma = \int_A \sigma_0 dA$$

σ_0 is the dimensionless cross-section/area and depends on scattering characteristics of the surface



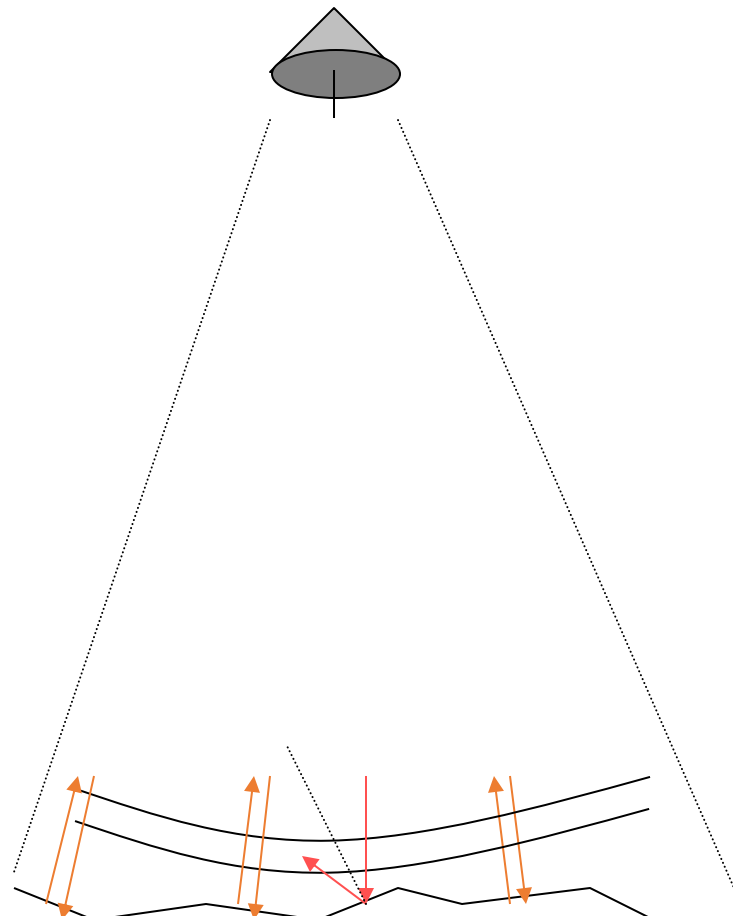
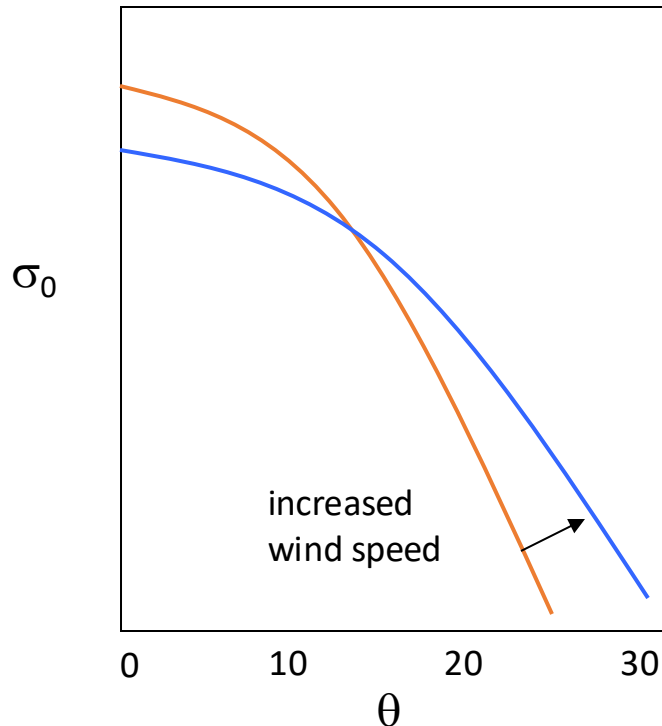
Scattering cross Section, σ_0

There are two primary mechanisms which contribute to σ_0

(1) Specular Reflection

Near vertical incidence

reflection off mirror-like facets

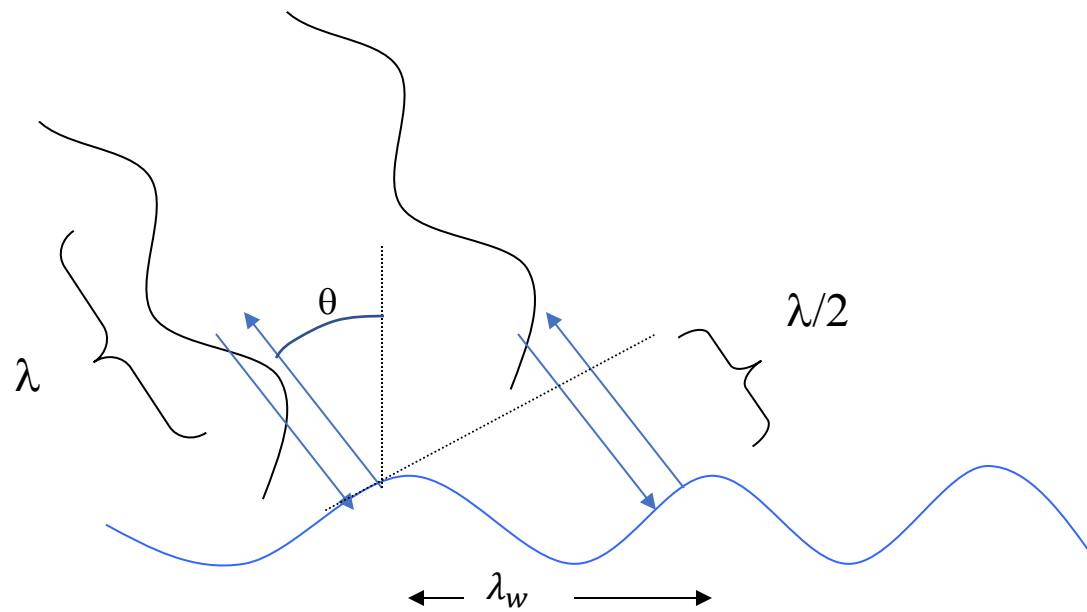


Important for $\theta < 20^\circ$ (there are almost no wave slopes $> 25^\circ$)

(2) Resonant (Bragg) Scatter

$\theta > 20^\circ$ (occurs at all θ but dominates here)
off-nadir so polarization is important
Ocean wave-length of importance:

$$\lambda_w = \frac{n\lambda}{2 \sin \theta}$$



σ_o depends on:

- polarization
- wavelength
- incidence angle
- wave spectrum (are there enough waves with λ_w wavelength?) and wave spectrum in 2-D
- projection of λ_w fronts along line of sight

Specular reflection

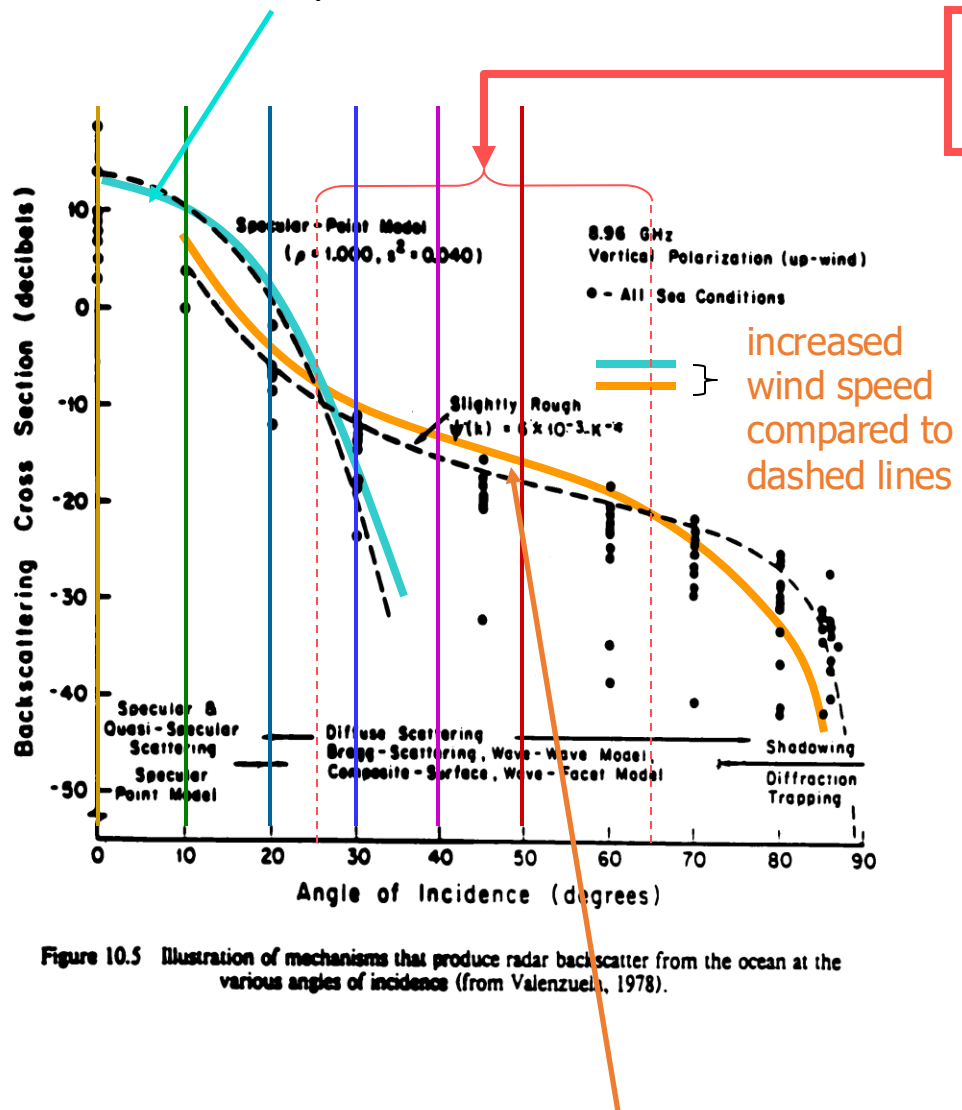


Figure 10.5 Illustration of mechanisms that produce radar backscatter from the ocean at the various angles of incidence (from Valenzuela, 1978).

Bragg scattering

σ_0 increases with increasing wind speed for scatterometer angles

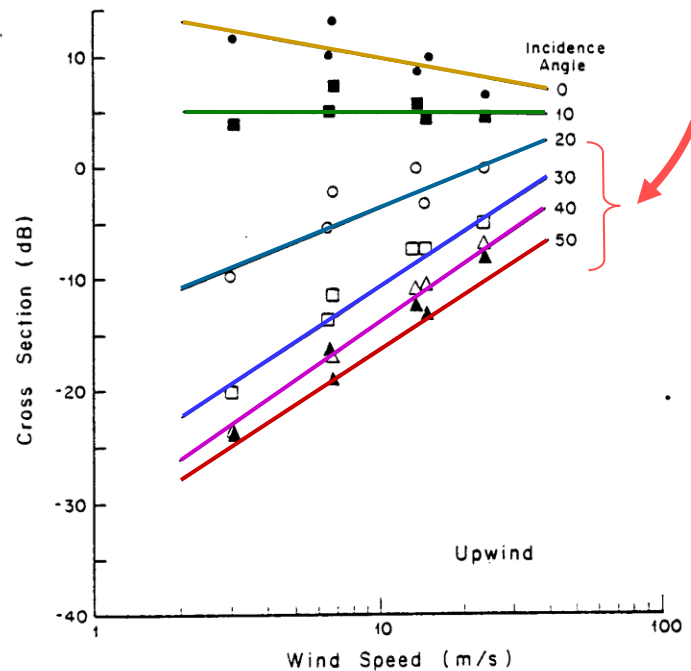
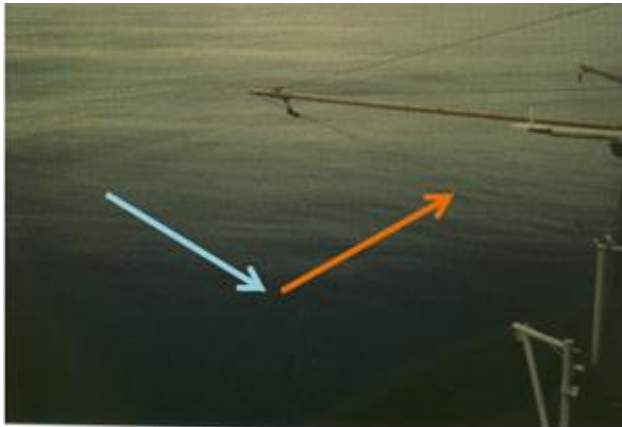


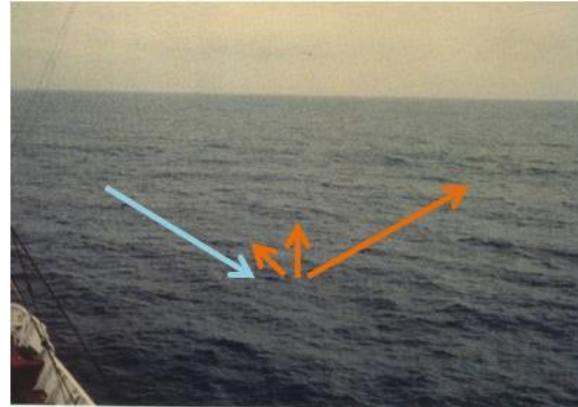
Figure 12.2 Scattering cross section per unit area of the sea for 13.96 GHz vertically polarized signals, as a function of incidence angle and wind speed (from Jones, Wentz, and Schroeder, 1978).



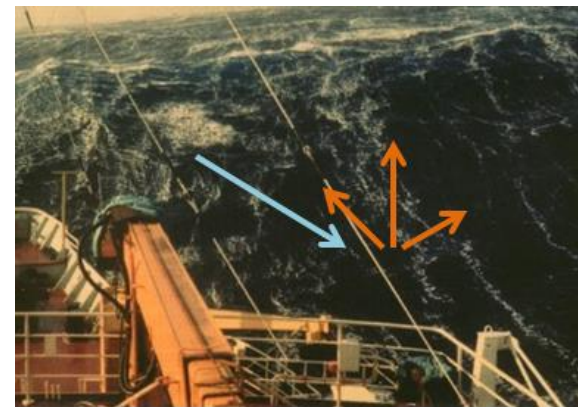
BEAUFORT FORCE 0
WIND SPEED: LESS THAN 1 KNOT
SEA: SEA LIKE A MIRROR



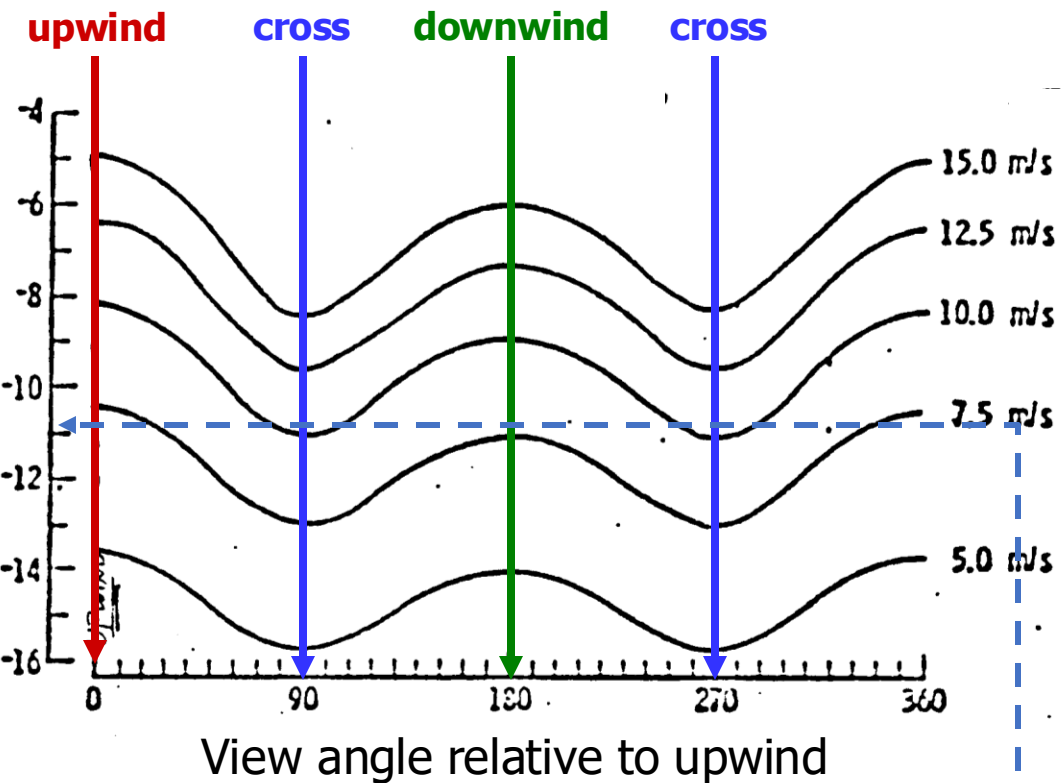
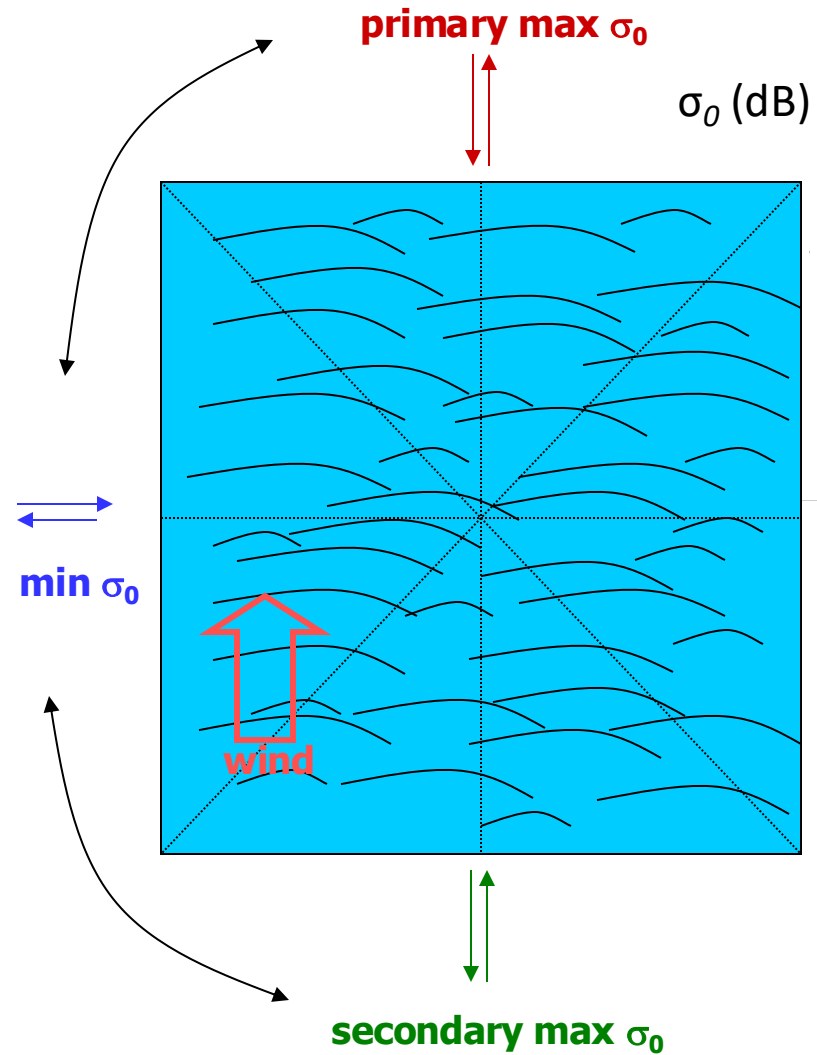
BEAUFORT FORCE 6
WIND SPEED: 22-27 KNOTS
SEA: WAVE HEIGHT 9.5-13 FT, LARGER WAVES BEGIN TO FORM, SPRAY IS PRESENT, WHITE FOAM CRESTS ARE EVERYWHERE



BEAUFORT FORCE 3
WIND SPEED: 7-10 KNOTS
SEA: WAVE HEIGHT 2-3 FT, LARGE WAVELETS, CRESTS BEGIN TO BREAK, ANY FORM HAS GLASSY APPEARANCE, SCATTERED WHITE CAPS

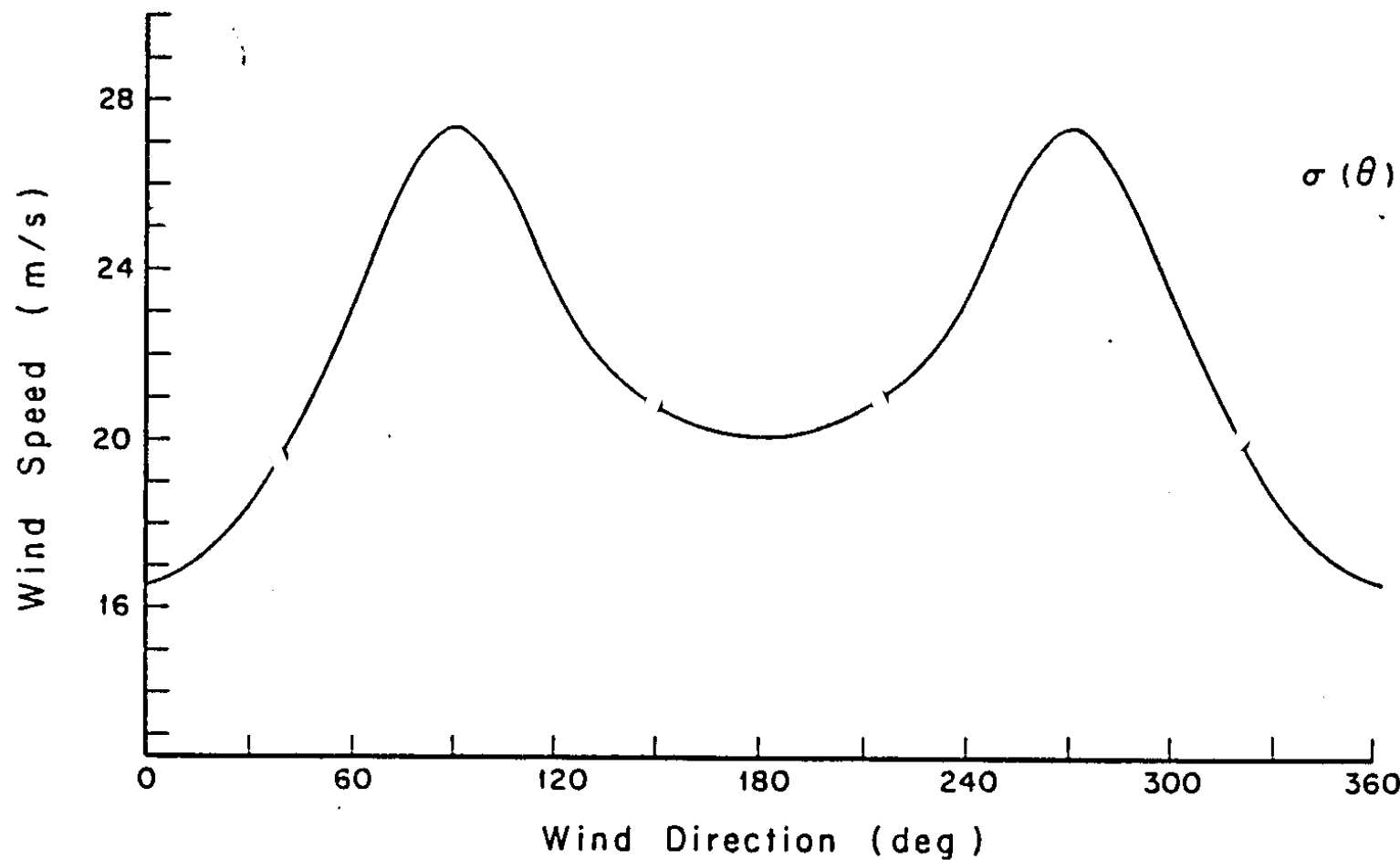


BEAUFORT FORCE 9
WIND SPEED: 41-47 KNOTS
SEA: WAVE HEIGHT 23-32 FT, HIGH WAVES, DENSE STREAKS OF FOAM ALONG DIRECTION OF THE WIND, WAVE CRESTS BEGIN TO TOPPLE, TUMBLE AND ROLL OVER. SPRAY MAY AFFECT VISIBILITY



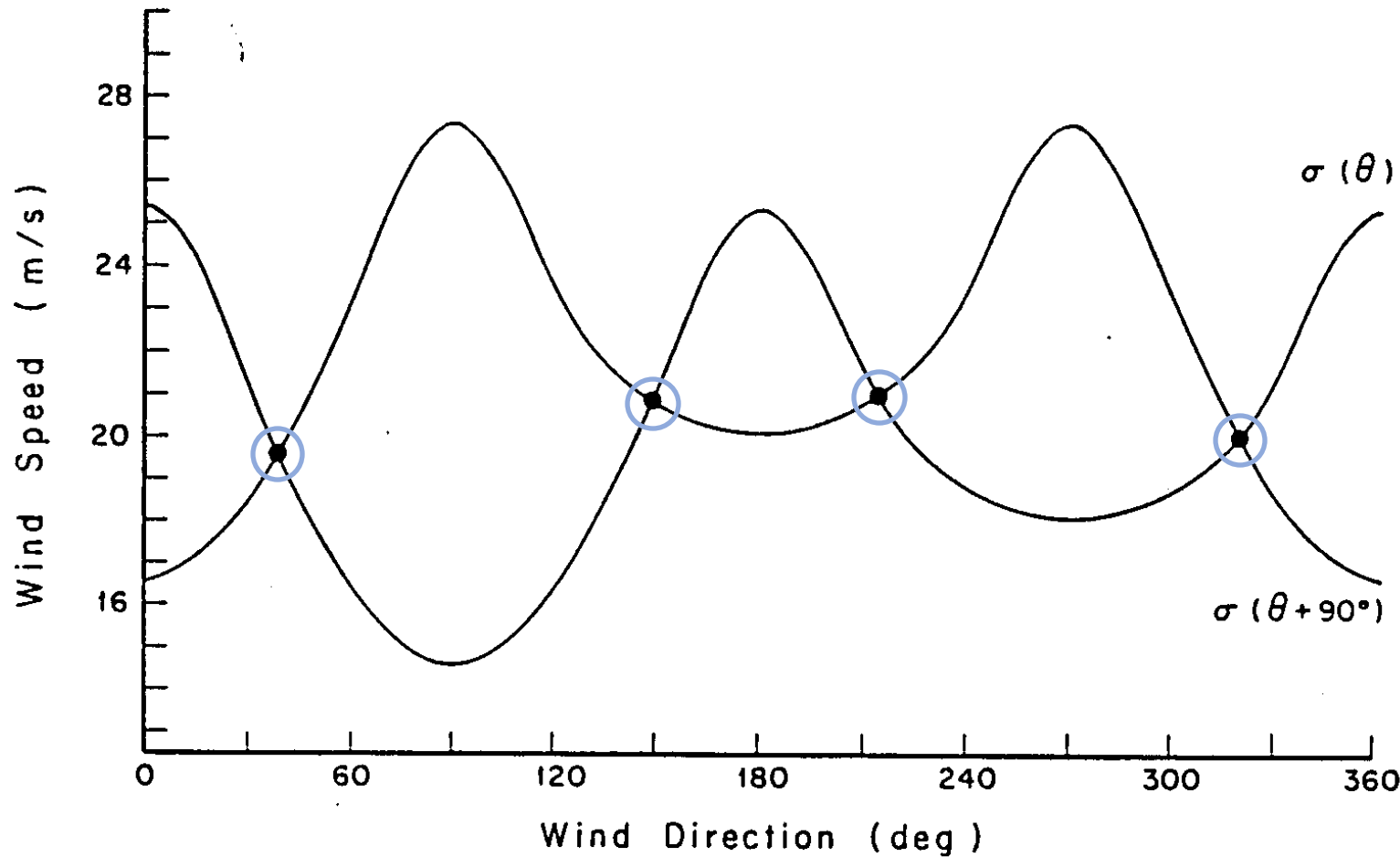
A single measure of σ_0 at some unknown angle relative to the wind direction produces a set of possible speeds and directions

Single View

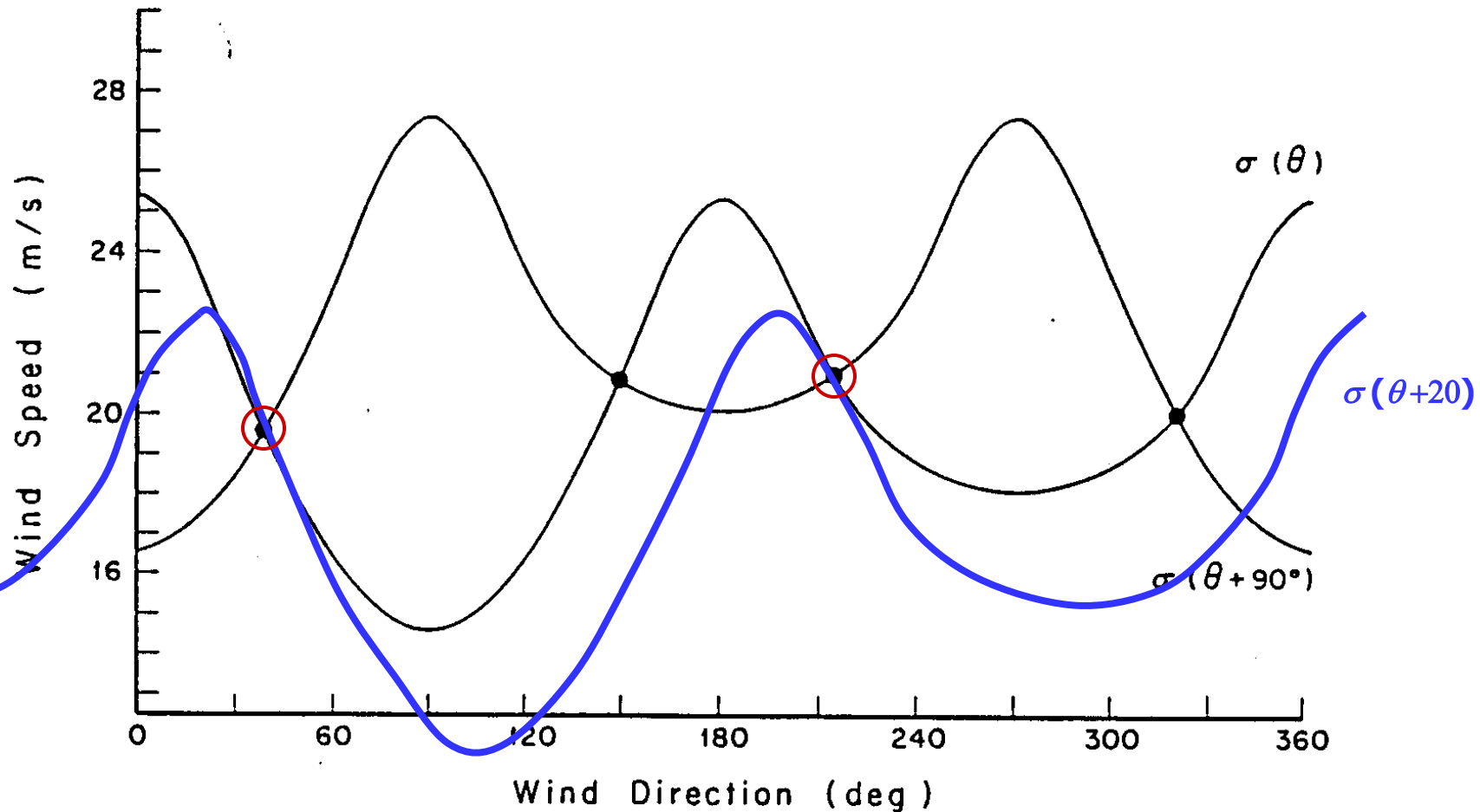


(note here θ is used for azimuth)

Two views

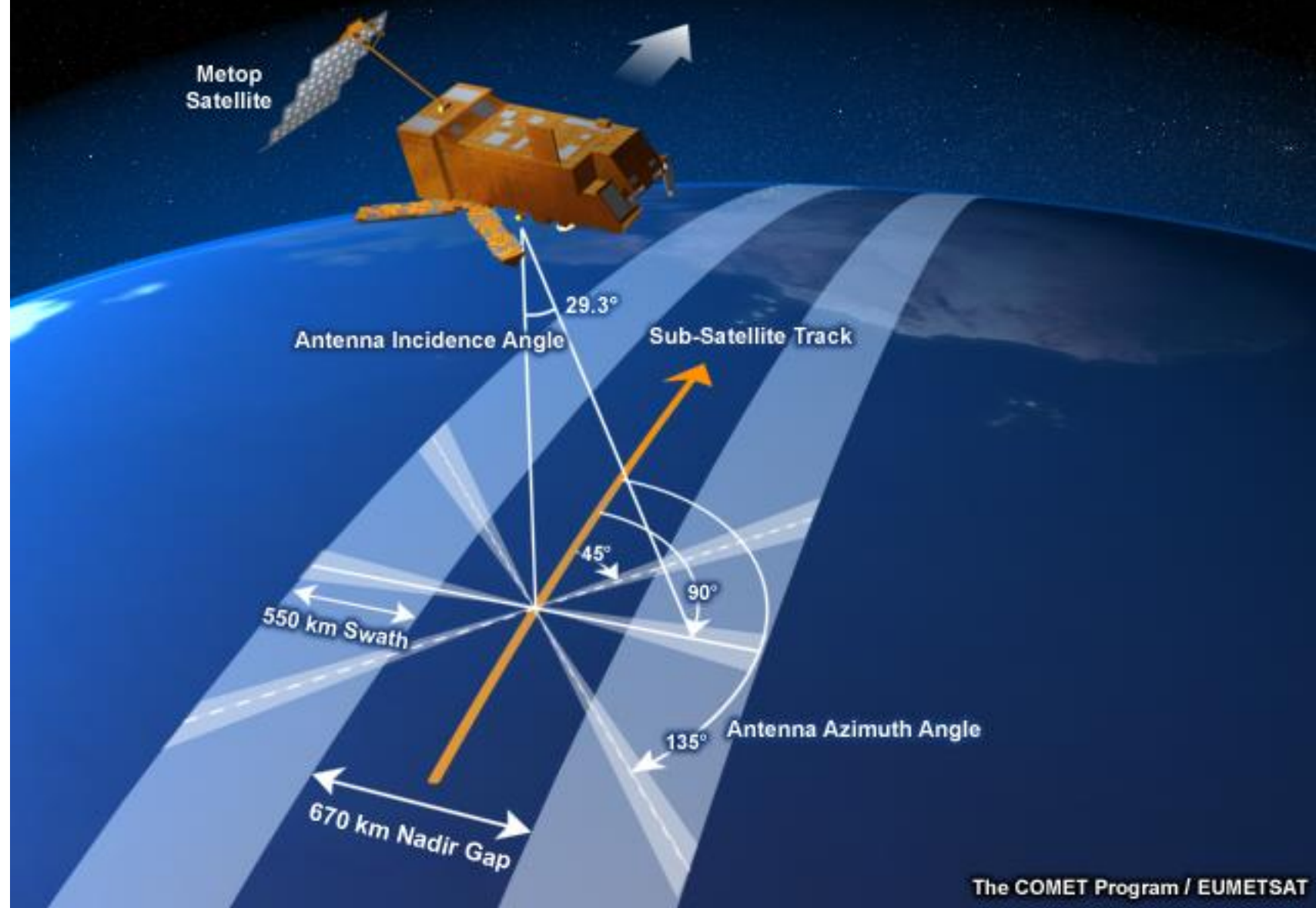


What if a third view direction is added ($\theta+20^\circ$)



Now the solution collapses to **two** possible wind vectors

ASCAT Scatterometer Coverage



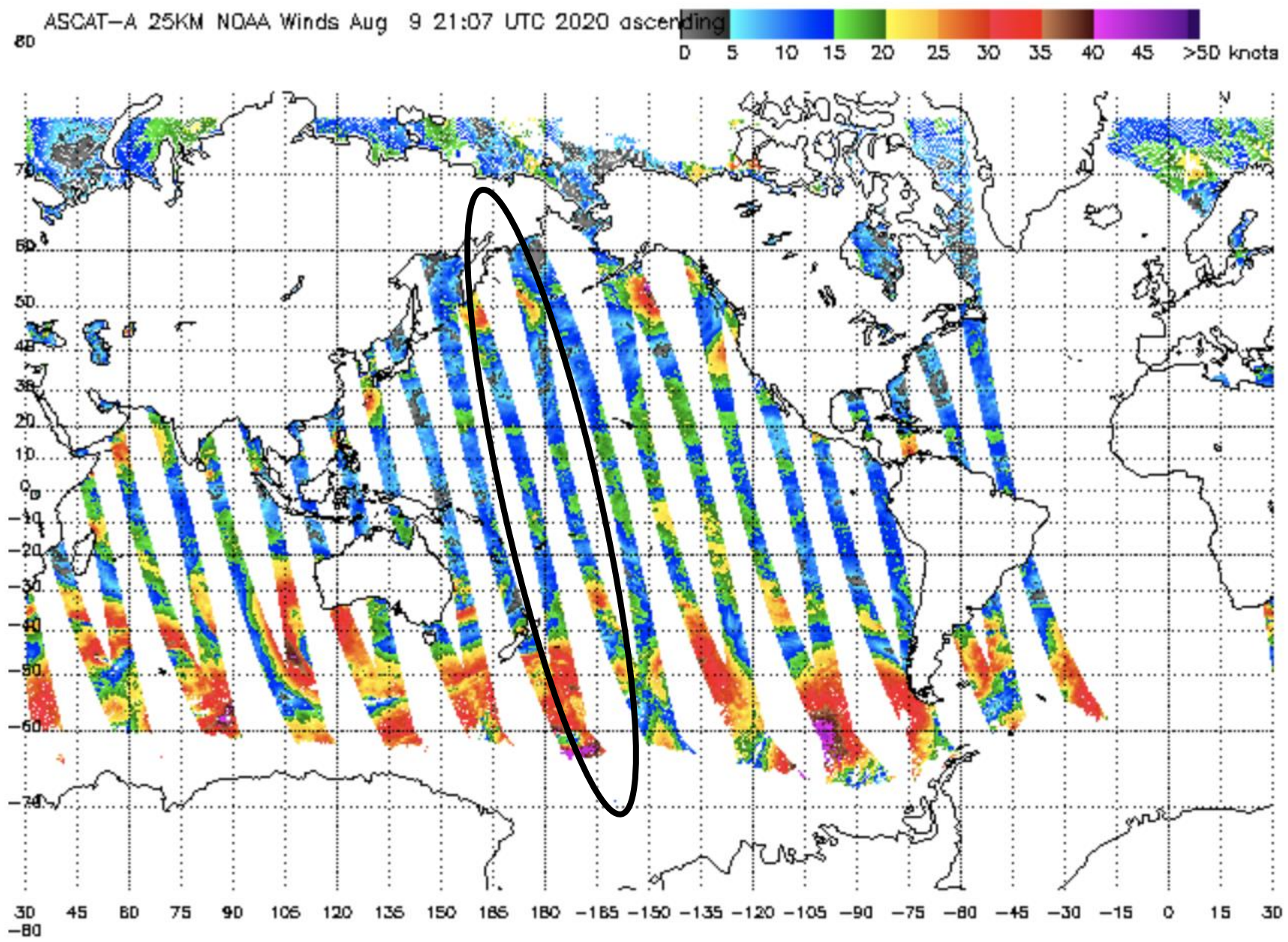
The COMET Program / EUMETSAT

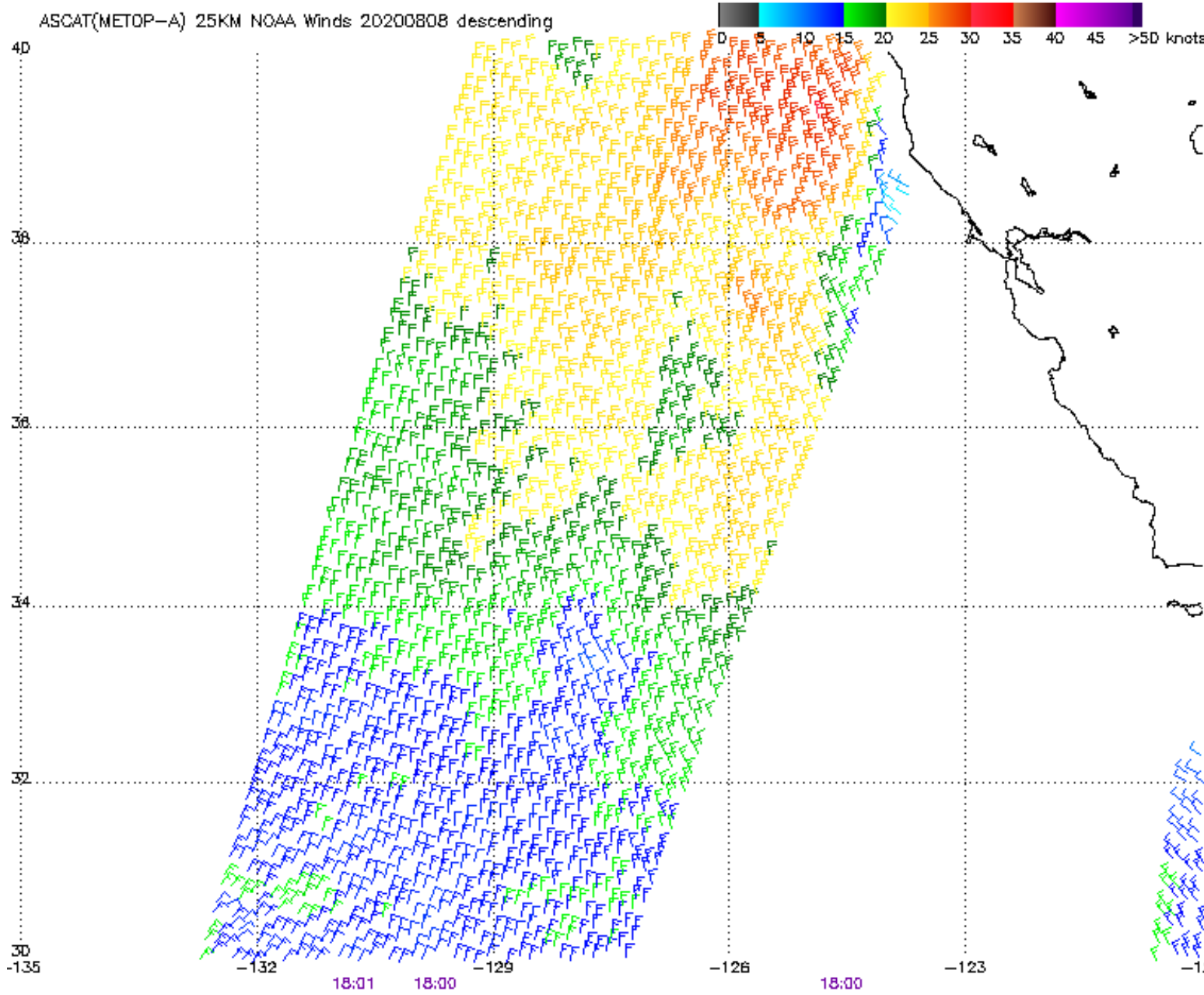
Some images of real-time and archived scatterometer and altimeter data:

<https://manati.star.nesdis.noaa.gov/datasets/WindSATData.php>

More information on scatterometer tracks and scan swaths:

<http://www.eumetrain.org/data/4/438/navmenu.php?tab=2&page=3.0.0>





Note: 1) Times are GMT 2)Times along bottom correspond to measurement at 35N
 3)Data buffer is 22 hrs from 20200808 4) Block wind barbs indicate possible contamination

NOAA/NESDIS/Center for Satellite Applications and Research

MR3522: Remote Sensing of the Atmosphere and Ocean

Altimetry

Main Topics

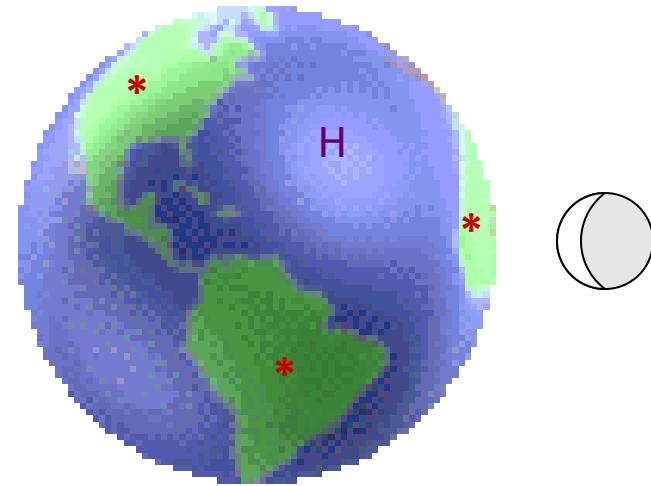
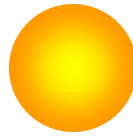
- Use of altimeters (e.g. JASON) to observe sea surface height

Altimetry

$\theta = 0$; looking at nadir

transmit a very short pulse (small fraction of a second measured in microseconds or nanoseconds)

therefore the pulse has some thickness and width (determined by gain, G_T)



speed of light = satellite height above sea surface \div time delay

Signal Processing

Time delay gives satellite-surface distance

Variations in mass concentration in the earth will distort the surface.

an atmosphere will distort the surface

also tides will distort the surface

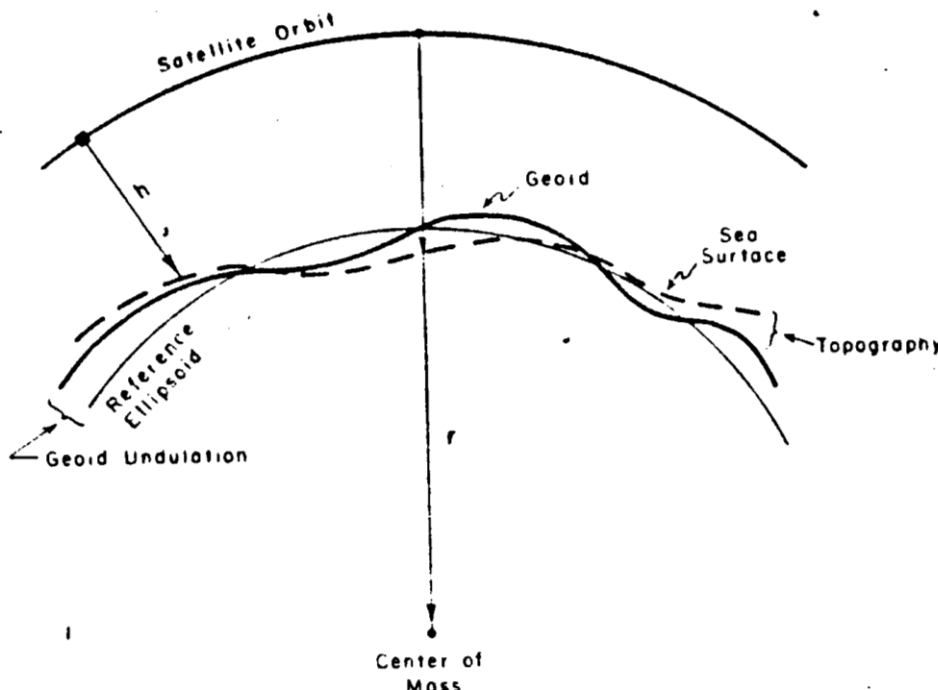
Definitions

geop: equipotential surface

geoid: geop at mean sea level (approximately an ellipsoid); essentially this is the hypothetical height of the ocean surface without tides, wind, etc.

geoid undulation: difference between reference ellipsoid and geoid (~60m)

sea surface topography: difference between sea surface and geoid



contributions to sea surface topography:

tides - 1 meter

currents - 1m/100km

atmospheric pressure - few cm

Figure 14.1 A satellite altimeter measures the height of the satellite above the sea surface. When this is subtracted from the height r of the satellite's orbit, the difference is the height of the sea surface relative to the center of the Earth. The shape of the surface is due to variations in gravity, which produce geoid undulations, and to ocean currents, which produce the oceanic topography, the departure of the sea surface from the geoid. The reference ellipsoid is the best smooth approximation to the geoid.

Jason-3 Orbital Properties

| | |
|------------------------------------|-------------------------------------|
| Semi-major axis | 7,714.43 km |
| Eccentricity | 0.000095 |
| Inclination (non-sun-synchronous) | 66.04° (prograde) |
| Reference altitude (equatorial) | 1,336 km |
| Nodal period | 6,745.72 seconds (112'42" or 1h52') |
| Repeat cycle | 9.9156 days |
| Number of passes per cycle | 254 |
| Ground track separation at Equator | 315 km |
| Acute angle at Equator crossings | 39.5° |
| Longitude at Equator of pass 1 | 99.9242° |
| Orbital velocity | 7.2 km/s |
| Ground scanning velocity | 5.8 km/s |

High orbital altitude (relative to other microwave instruments closer to 500–800 km) limits impacts of atmosphere (e.g. drag), which makes precise determination of orbit possible. This is necessary because very small errors in time delay can cause large errors in surface height!

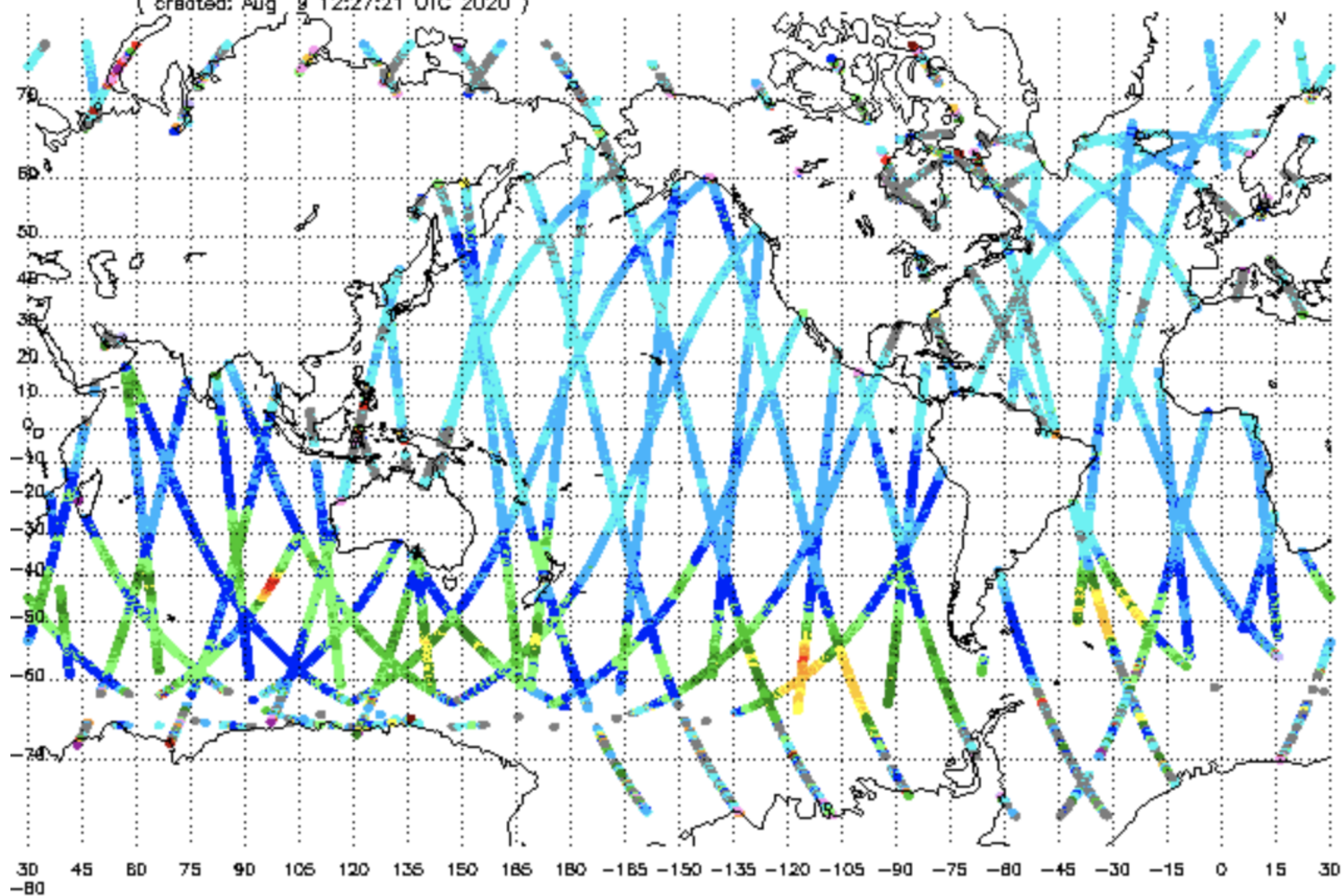
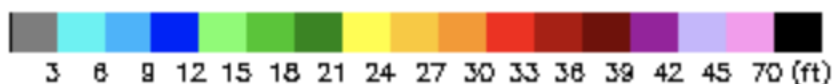
What information do we gain from altimetry?

- Significant wave height
- Ocean floor topography; underwater mountains cause slight bulges in surface topography (although this can be much better resolved with shipboard bathymetry)
- Ocean surface currents deduced from topography (e.g. where is there upwelling?)
- Forecasting of climate events (e.g. ENSO)



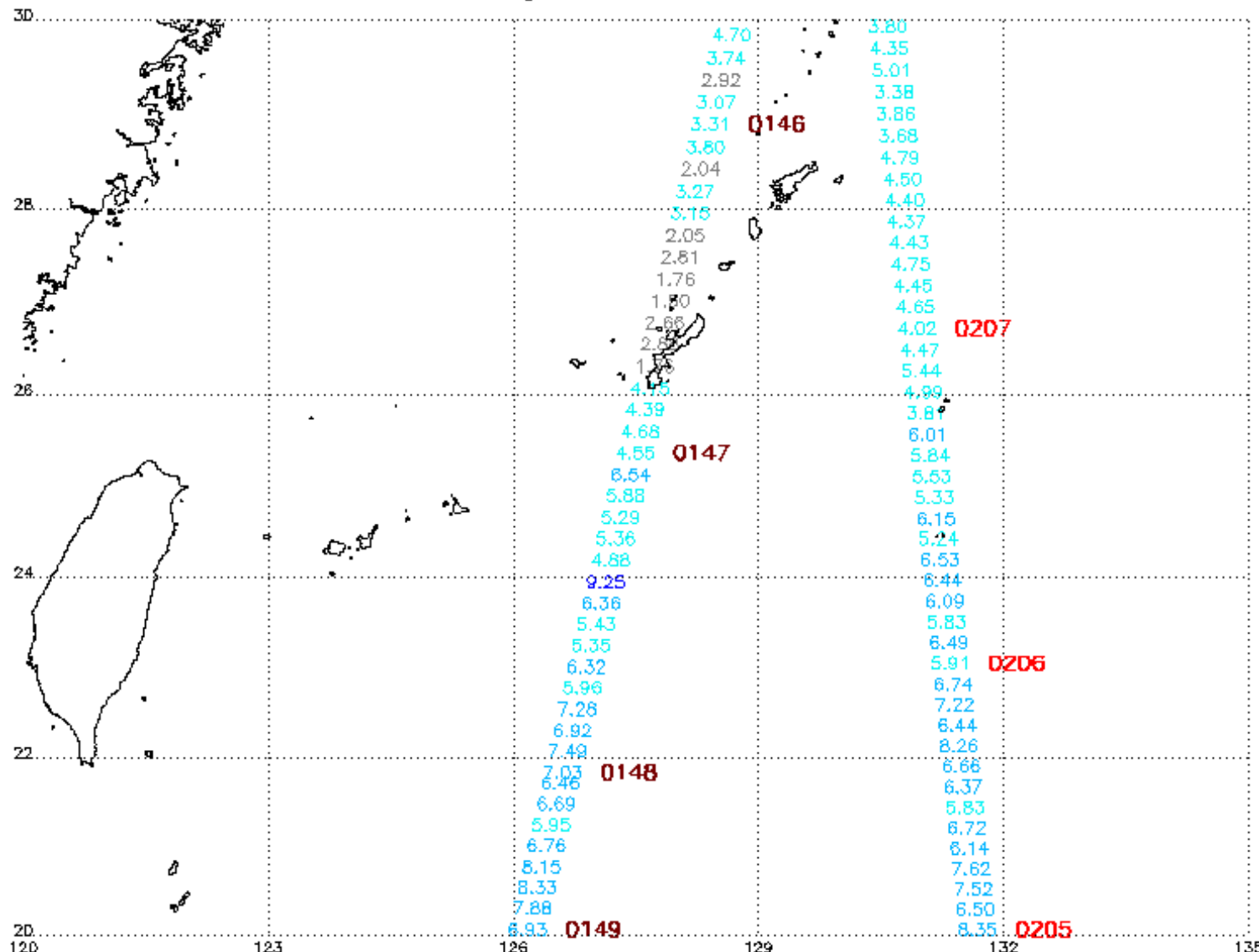
00:00 – 11:59 UTC 08/08/2020

12 hour collection of altimeter wave heights
(created: Aug 9 12:27:21 UTC 2020)



00:00 – 11:59 UTC 08/08/2020

12 hour collection of altimeter wave heights



note: 1) Time is in UTC; 2) SWH is in feet

jason2 jason3 altika cryosat s3a

NOAA/NESDIS Center for Satellite Applications and Research Aug 9 12:27:21 UTC 2020